

Scaling and renormalization in high-dimensional regression

Alexander B. Atanasov,^{1,2,*} Jacob A. Zavatone-Veth,^{1,2,3,†} and Cengiz Pehlevan^{2,3,4,‡}

¹*Department of Physics, Harvard University, Cambridge, MA*

²*Center for Brain Science, Harvard University, Cambridge, MA*

³*John A. Paulson School of Engineering and Applied Sciences, Harvard University, Cambridge, MA*

⁴*Kempner Institute for the Study of Natural and Artificial Intelligence, Harvard University, Cambridge, MA*

(Dated: May 2, 2024)

This paper presents a succinct derivation of the training and generalization performance of a variety of high-dimensional ridge regression models using the basic tools of random matrix theory and free probability. We provide an introduction and review of recent results on these topics, aimed at readers with backgrounds in physics and deep learning. Analytic formulas for the training and generalization errors are obtained in a few lines of algebra directly from the properties of the S -transform of free probability. This allows for a straightforward identification of the sources of power-law scaling in model performance. We compute the generalization error of a broad class of random feature models. We find that in all models, the S -transform corresponds to the train-test generalization gap, and yields an analogue of the generalized-cross-validation estimator. Using these techniques, we derive fine-grained bias-variance decompositions for a very general class of random feature models with structured covariates. These novel results allow us to discover a scaling regime for random feature models where the variance due to the features limits performance in the overparameterized setting. We also demonstrate how anisotropic weight structure in random feature models can limit performance and lead to nontrivial exponents for finite-width corrections in the overparameterized setting. Our results extend and provide a unifying perspective on earlier models of neural scaling laws.

CONTENTS

I. Introduction	3
A. Review of Neural Scaling Laws	4
B. Overview and Contributions	5
C. Code Availability	6
II. Random Matrix Models of Empirical Covariance Matrices	7
A. Motivation: Empirical Covariance Matrices	7
B. Examples of Random Matrices	7
C. The Spectral Density and the Resolvent	8
D. Degrees of freedom	9
E. Addition and Multiplication of Random Matrices	10
1. R -transform	10
2. S -transform	11
F. Application: Empirical Covariances	11
III. Renormalization and Free Probability	14
A. Definition of Freedom	14
B. Diagrammatic Derivations of Subordination Relations	14
1. R -Transform Subordination	15
2. S -Transform Subordination	18
C. Summary of R and S transform identities	19
IV. R and S Transforms of Important Ensembles	21
A. Wigner	21
B. Square Projections	21
C. Rectangular Projections	22
D. White Wishart	22
E. Structured Wishart: Correlated Features	24
F. Structured Wishart: Correlated Samples	25
G. Shifted Wishart	25

* atanasov@g.harvard.edu

† jzavatoneveth@g.harvard.edu

‡ cpehlevan@seas.harvard.edu

H. Deep White Wishart Product	25
I. Deep Structured Wishart Product	26
V. Linear and Kernel Ridge Regression	28
A. Linear Regression with Structured Gaussian Covariates	28
B. Derivation	29
C. Example: Isotropic Linear Regression	30
D. Connection to Kernel Regression via Gaussian Universality	31
E. The S -Transform as a Train-Test Gap	32
F. Double Descent as a Renormalization Effect	33
G. Multiple Descent without Label Noise	33
H. Bias-Variance Decomposition	34
I. Scaling Laws in P	36
1. Normalizable Spectra	36
2. Non-Normalizable Spectra	38
VI. Linear Random Features	39
A. Setup and Motivation	39
B. Averaging Over Data	40
C. Averaging Over Features	40
D. Ridgeless Limits	41
E. Examples	42
1. 1-Layer White Random Feature Model	42
2. Deep White Random Feature Model	43
3. 1-Layer Structured Random Feature Model	44
4. Orthogonal Projections of Structured Covariates	44
5. Deep Structured Random Feature Model	45
F. Training Error	45
G. Implicit Regularization of Ensembles	46
H. Fine-Grained Bias-Variance Decomposition	46
1. Overparameterized Case	47
2. Bottlenecked Case	48
3. Underparameterized Case	48
I. Scaling Laws in P and N	48
1. Target Averaged Results	48
2. General Targets	49
3. Variance-Dominated Scaling	49
4. Effects of Weight Structure	50
5. Characterization of All Scaling Regimes	51
VII. Models with Additive Feature Noise	54
A. Setup and Motivation	54
B. Averaging Over Data	54
C. Averaging Over Isotropic Features	55
D. An Interesting Equivalence	56
E. Example: Nonlinear Random Features with Isotropic Covariates	57
F. Fine-Grained Bias-Variance Decomposition	57
G. Scaling Laws in P and N	59
VIII. Conclusion	61
Acknowledgments	61
References	62

I. INTRODUCTION

The study of scaling laws in deep learning, also known as “neural scaling laws,” has drawn wide attention both from theorists and practitioners. As dataset sizes and compute capabilities have increased in recent years, remarkably regular power law trends have been observed in the performance of large language, vision, and multimodal models [1; 2; 3]. The exponents of these power laws determine how dataset and model size should be jointly scaled in order to achieve optimal performance for a given compute budget [4]. As a result, these scaling laws play an important role in modern deep learning practice, and serve to drive the state of the art performance across a variety of models. Therefore, understanding what determines these exponents is a key question for which one might hope to develop basic theoretical insights.

The observation of scaling laws in deep learning is particularly interesting from the perspective of statistical physics, where the identification of scaling exponents as principal quantities of study led to major breakthroughs in the field [5; 6; 7]. Especially key was the development of renormalization as a central method for the study of scaling properties in complex systems [8; 9].¹

One can ask whether there is simple setting of an information processing system where such power law behavior in performance as a function of dataset size and model size can be studied analytically. Recent papers have shown that high dimensional least squares regression from various feature spaces is one such example. These settings include linear regression [12; 13; 14; 15; 16; 17], kernel regression [18; 19; 20; 21; 22; 23; 24], and random feature models [17; 24; 25; 26; 27; 28; 29; 30; 31; 32; 33; 34; 35]. For these models, sharp asymptotic characterizations of training and generalization performance can be derived in limits where the feature space dimension and number of training data points jointly tend to infinity.

In this paper we pursue an alternative approach to deriving these sharp asymptotics, based in random matrix theory and specifically making use of the S -transform of free probability [36]. This approach makes explicit the central role played by the randomness of sample covariance matrices. Through this lens, a variety of phenomena including sample-wise and model-wise double descent [15; 29; 37; 38], scaling and bottleneck behavior [30; 39], and the analysis of sources of variance for trained networks [28; 40], can be seen as natural consequences of a basic renormalization phenomenon. This approach also yields a simple interpretation of the self-consistent equations that determine the generalization error across a wide variety of solvable models.

We highlight how one can derive these phenomena across a variety of settings from a set of three basic principles:

1. Gaussian Universality

When the number of dimensions in a linear regression problem scales linearly with the number of data points, the covariance matrices of the training and test set are indistinguishable from those of a high-dimensional Gaussian. This phenomenon is also referred to as Gaussian equivalence.

2. Deterministic Equivalence

When calculating average case training and generalization error, one must average over the random choice of finite training set. In particular, this will involve averaging over the empirical covariance matrix of the sample of data. In recent years, several authors have shown how one can replace the (data-dependent, random) sample covariance with the (deterministic) population covariance within relevant algebraic expressions. Such a replacement is known as a **deterministic equivalent**. This allows one to easily perform the necessary averages and precisely characterize average case training and generalization error.

3. The S -transform

The S -transform allows one to characterize the spectral properties of a product of two matrices. An empirical covariance can be viewed as a multiplicative noise applied to the “ground truth” population covariance. In our settings, this noise is usually due to either a finite choice of training set or a finite set of random features that the data is passed through. The S -transform then gives us the method to replace expressions involving the empirical covariance with the deterministic equivalent involving only the population covariance. When this replacement is made, the ridge is rescaled (or more properly *renormalized*) to a new value. The renormalized ridge is given directly by multiplying the original ridge by the S -transform of the noise.

These first two principles have been highlighted by several important recent works, which we review. The primary focus and novelty of our paper is on the third point. By making use of basic properties of the S -transform, one can

¹ See [10] for an early review and [11] for an introduction.

recover the replica, cavity, and linear pencil derivations of prior authors in a few lines of algebra. The appearance of the S -transform also highlights that multiplicative noise on the covariance is at the heart of all overfitting and scaling phenomena in linear models.

A. Review of Neural Scaling Laws

In this section, we will review the phenomenology of neural scaling laws as well as the solvable models that seek to explain how data and task structure determine scaling behavior. For a very recent review of the scaling laws literature in the context of language models, see [41]. Let $\mathcal{L}(N, T)$ be the performance of a model with N parameters trained on T tokens.² We will be interested in characterizing the scaling properties of \mathcal{L} as either N or T increase. For either of the parameters, its scaling law will vary depending on whether it is the bottlenecking parameter or not.

The empirical observation of these scaling laws was highlighted in early work [1; 42] (see also [43] for extremely early work). Kaplan *et al.* [2] performed an extensive empirical study of scaling laws in language modeling tasks and proposed the following form for \mathcal{L} :

$$\mathcal{L}(N, T) = \left[\left(\frac{N_c}{N} \right)^{\alpha_N/\alpha_T} + \frac{T_c}{T} \right]^{\alpha_T}. \quad (1)$$

Here N_c, T_c are constants appropriately fit to the data and α_N, α_T are scaling exponents. As $T \rightarrow \infty$ at fixed N we see a scaling law going as $N^{-\alpha_N}$. Similarly as $N \rightarrow \infty$ at fixed T we get a scaling law going as $T^{-\alpha_T}$. For transformer models on various text datasets, both α_N, α_T are small, of order less than 0.1.

More recently, Hoffmann *et al.* [4] have proposed alternative scaling *Ansätze* that can serve as better fits to data. This accounts for the fact that the entropy of text is nonzero and so the cross-entropy loss should not vanish even in the $N, T \rightarrow \infty$ limit. They write:

$$\mathcal{L}(N, T) = E + N^{-\alpha_N} + T^{-\alpha_T}, \quad (2)$$

where E corresponds to the entropy of natural text. See [44] for details on a replication attempt. Again, as $N \rightarrow \infty$ (resp $T \rightarrow \infty$) this loss has power law scaling with the other parameter. Additional work refining and extending these observations was done in [45; 46; 47; 48; 49]. Scaling laws in the context of vision were studied in [50; 51]. Scaling laws for multi-layer perceptrons (MLPs) were investigated in a recent paper of Bachmann *et al.* [3]. More general parametric fits of the occasionally “broken” power law behavior observed in practice have been investigated in [52].

The vast majority of solvable models of neural network training and generalization focus on learned functions that are linear in the set of trainable weights.³ This means $f(\mathbf{x}) = \mathbf{w} \cdot \phi(\mathbf{x})$ for some N -dimensional vector of features $\phi(\mathbf{x})$, with N possibly infinite. The features themselves may also be random. Such models are called **linear models** and include kernel methods and random feature models. When the weights are learned via ridge regression on a fixed dataset of P examples, one can compute the exact asymptotic behavior for the generalization performance of the model. The crucial simplification which enables precise asymptotic study of these linear models is Gaussian universality, which has been studied both for kernel methods with deterministic kernels [20; 21; 22; 24; 57; 58; 59; 60; 61; 62; 63] and for random feature models [17; 24; 25; 26; 27; 28; 29; 33; 40; 58; 64; 65; 66; 67; 68; 69]. One can adapt these methods to also study the dynamics of a linear model trained with SGD, as in [70; 71].

One motivation for the study of such linear models is that neural networks in the **neural tangent kernel** (NTK) parameterization converge to kernel methods in the infinite width limit [72; 73].⁴ Kernel methods have a long history, as their convex objective function has allowed for a tractable theory to be developed, see [75; 76] for accessible introductions. Even at finite width, networks can be parameterized so that they still behave as linear models by using the output rescaling introduced by Chizat *et al.* in [77]. This is called the **lazy limit** of neural network training. It is also known as the **linearized network**, since the network acts as its linearization in parameter space [78]. Finite-width lazy networks behave like random feature approximations to the infinite-width neural tangent kernel [27; 79]. By developing a better perspective on the kernel regime, one hopes to inform the analysis of feature-learning neural networks [80; 81; 82].

² We will often take N to be the hidden layer width of the random feature models we study. Here it denotes the number of parameters. In deep networks trained end-to-end these quantities do not coincide, but in random feature models they are equal; see Section VI.A for details.

³ There are additional ways of thinking about models of scaling laws that don’t fall into the framework of linear models, including [53; 54; 55; 56].

⁴ See Misiakiewicz and Montanari [74] for a recent review of NTKs and linearized networks.

How does power-law scaling arise in linear models? Significant progress has been made in the limits of $P \gg N$ or $N \gg P$ [20; 22; 30; 34; 39; 71]. Here, Bahri *et al.* [30] provide a useful distinction between the scaling with respect to the bottlenecking parameter (N, P respectively) and the scaling with respect to the non-bottlenecking parameter (P, N respectively). The former type of scaling they term **resolution-limited** and the latter type they term **variance-limited**.

Bahri *et al.* argue that scaling the larger, non-bottleneck parameter (N, P respectively) leads to a trivial exponent of -1 and a power-law decay to an asymptote determined by the bottleneck parameter. In the overparameterized case of large N , one can interpret the $1/N$ corrections as coming from the finite-width variance in the neural tangent kernel, as observed in [83] and calculated in [39; 84; 85; 86; 87; 88; 89]. In the underparameterized case of large P , one can interpret the $1/P$ corrections as coming from the finite-dataset variance of the final predictor as in classical statistics [90; 91]. We will refer to all power laws with exponent -1 as trivial scaling.

The resolution-limited scalings are generally nontrivial. As in [2], when either $N \gg P$ (overparameterized) or $P \gg N$ (underparameterized), the scaling law with respect to the smaller “bottlenecking” parameter exhibits a nontrivial power law scaling. These power-law exponents were calculated in [20; 22; 30] utilizing recent results on kernel regression [20; 21; 22]. We reproduce this analysis in Section V.I. Nontrivial power laws in these calculations arise from a power-law structure in input covariance and teacher weights.

Another version of a single layer linear random feature model with structured input covariates (generalized in Section VI) was studied as a solvable model of neural scaling laws in [34], where they derive similar scaling behavior in P, N . We remark further on these different scaling regimes in Section VII.1 and extend their analysis to more general datasets in Sections VII.2. This analysis was extended to a dynamical setting in work of the first and third author with B. Bordelon [71], where it was demonstrated that one can recover scaling laws for compute-optimal allocation of model size, number of training steps, and dataset size.

It is important to stress that the resolution-limited and variance-limited scalings are *not* different scaling regimes. In both the overparameterized and underparameterized setting, there will always be a bottlenecking parameter with resolution-limited scaling exponents and non-bottlenecking parameters with variance-limited scaling exponents. The resolution-limited scaling exponents will depend on additional details of the dataset and model. These details will determine which **scaling regime** the model is in. We characterize the different scaling regimes for linear and kernel regression using the source and capacity formalism of [63] in Equation (171). We extend the source-capacity analysis to linear random feature models in Equations (251) and (253).

Even when the number of parameters is much greater than the number of data points, one can still observe that the effects of finite model size can limit the scaling of the test error as one increases the number of data points. This worse scaling can occur much earlier than when the number of data points is equal to the number of parameters, or even before it is equal to the width.⁵ This effect was studied by the first and third authors with B. Bordelon and S. Sainathan in [39] and shown to be fully driven by the variance in the predictor due to the randomness over initializations. This was called the “onset of variance”. There, a random feature model with feature noise was shown to exhibit this behavior when the feature space was set to have dimension equal to the number of parameters and the feature noise was set have variance proportional to $1/\text{width}$. In this paper we will show this occurs across a variety of random feature models with and without feature noise, and corresponds to a *variance-dominated* scaling regime.

The goals of this paper are twofold. Firstly, we aim to provide an accessible introduction to the relevant random matrix theory necessary to obtain the results of prior models of neural scaling laws, double descent, and random feature regression [16; 17; 20; 21; 22; 23; 24; 25; 26; 27; 28; 29; 30; 31; 34; 39; 40; 63; 88; 92; 93; 94; 95; 96; 97]. By using the S -transform, the results across a wide variety of the literature can be obtained in a straightforward and parsimonious manner. Secondly, by applying these techniques, we provide novel characterizations of the scaling regimes and the sources of variance that drive them across a wide variety of random feature models.

B. Overview and Contributions

In §II, we give a brief introduction of the key ideas in random matrix theory necessary for the derivations that follow. We motivate this by considering empirical covariance matrices. We highlight that one can view a given empirical covariance as a multiplicatively noised version of the “true” population covariance. We define the resolvent and the Stieltjes transform, and then introduce the R and S -transforms of free probability and their relevant properties.

⁵ $P = \text{width}$ can also be viewed as a separate double descent peak as in [27].

§III is the main technical section, which derives the key R and S transform properties. We do this via a diagrammatic argument, which gives the R and S transforms an interpretation as a self-energy, and highlights their role as cumulant generating functions.

In §IV, we explicitly calculate the R and S transforms for a variety of random matrix ensembles that will be useful for us. By using the basic properties of these transforms, we are able to bootstrap their algebraic form without needing to directly compute any resolvents.

In §V, we apply these results to study learning curves in linear and kernel ridge regression. We efficiently recover the exact asymptotics of training and generalization error as has been studied in [17; 20; 21; 23; 24]. We can understand the key parameter κ (sometimes called the signal capture threshold) as a multiplicatively renormalized ridge parameter λ . The multiplicative constant is precisely given by the S -transform of the multiplicative noise. Through this, double descent can be interpreted as a renormalization effect, as can the multiple descent observed in [21; 95]. We further note that the square of the S -transform gives the ratio between out-of-sample and in-sample errors. By estimating the S -transform using only training data, one can arrive at prior results on out-of-sample risk estimation [72; 92; 98] also known as generalized cross-validation. We then provide exact formulas for the bias-variance decomposition of linear and kernel regression, reproducing the results of [21]. Finally, we derive the resolution-limited scaling exponents in terms of the source and capacity exponents of the dataset as derived in [20; 63; 99; 100]. We highlight how label noise and nonzero ridge can lead to different scaling regimes for the resolution-limited exponents, as explored in [63].

Sections VI and VII contain the main novel technical contributions. In §VI we apply the S -transform to obtain the generalization error of a variety of linear random feature models. This is the simplest setting where both the dataset size and the model size appear jointly in the scaling properties of the model. We derive the training and generalization error for *any class* of random features, as long as the features are relatively free of the empirical covariance. We apply this to recover many previously known formulas for generalization error for specific random feature models, and obtain novel generalization formulas for the case of orthogonal projections. We obtain novel formulas for the fine-grained bias variance decomposition in the case of structured input data. These decompositions yield an equivalence between infinite ensembles of linear random feature models and linear regression with rescaled ridge. Aspects of this have been explored in [101; 102; 103]. We also find that adding structure to the weights can affect the exponents of the finite-width corrections in the overparameterized regime, giving a nontrivial variance-limited scaling. Fast-decaying weight spectra can lead to variance over initializations even when the width is infinite. We recover the target-averaged scaling laws discussed in [30; 34], and extend them to settings where the target labels are more general. Using our fine-grained bias-variance decompositions, we find a new scaling regime where finite-width effects can substantially impact performance even in the overparameterized setting. The bias-variance decomposition further allows us to characterize all scaling regimes of linear random feature models. To our knowledge, a characterization of these scaling regimes has not been previously obtained.

In §VII we extend these results to the setting of a random feature model with additive feature noise. This arises in the study of nonlinear random feature models via Gaussian equivalence, as studied in [24; 25; 26; 27; 28; 29; 33; 40; 58; 64; 65; 66; 67; 68]. There, the effect of nonlinearity can be treated as independent additive noise on the features. Models with feature noise have also been used to study the limiting effects of finite-width fluctuations of the empirical NTK in [39]. We recover results on nonlinear random feature models [26; 27; 94]. The formulas simplify substantially, leading us to note a surprising connection to linear random feature models. We derive novel formulas for the bias-variance decomposition when the input covariates are anisotropic and apply this to provide a characterization of the scaling regimes in this setting as well.

C. Code Availability

The following public repository

https://github.com/Pehlevan-Group/S_transform

contains the code necessary to reproduce all figures in this paper. Readers interested in the numerics may wish to follow along with these interactive Python notebooks.

II. RANDOM MATRIX MODELS OF EMPIRICAL COVARIANCE MATRICES

Here we give a relatively brief overview of the key concepts necessary to understand the derivations that follow. A basic knowledge of probability and linear algebra is sufficient. For a modern introduction to random matrix theory aimed at a broad technical audience, we recommend the recent text of Potters and Bouchaud [104].

A. Motivation: Empirical Covariance Matrices

In many fields involving the analysis of large-scale data, ranging from neuroscience to finance to signal processing, many useful statistical observations depend on the covariance matrix of a given dataset.

Concretely, consider a dataset of P observations $\{\mathbf{x}_\mu\}_{\mu=1}^P$, which we will take to be independent and identically distributed (i.i.d.) throughout this paper. Each $\mathbf{x}_\mu \in \mathbb{R}^N$ consists of N features $[\mathbf{x}_\mu]_{i=1}^N$ and is drawn from the distribution $p(\mathbf{x})$. For simplicity, we will assume all features are mean zero. The Greek μ will label the data points while the Roman i will label the features.

Given this, the **design matrix** $\mathbf{X} \in \mathbb{R}^{P \times N}$ has \mathbf{x}_μ^\top in its μ -th row. The **empirical covariance** (also called the **sample covariance**) of this dataset is given by

$$\hat{\Sigma} \equiv \frac{1}{P} \mathbf{X}^\top \mathbf{X} \in \mathbb{R}^{N \times N}. \quad (3)$$

The matrix $\hat{\Sigma}$ is a random variable. We call this a **random matrix**. A random matrix is a matrix whose entries are random variables distributed according to some probability distribution.

Defining the ground truth covariance of the data (also called the **population covariance**) as $\Sigma \equiv \mathbb{E}_{\mathbf{x} \sim p(\mathbf{x})}[\mathbf{x}\mathbf{x}^\top]$, we get that $\hat{\Sigma} \rightarrow \Sigma$ as $P \rightarrow \infty$ for fixed N . This is the regime of classical statistics (see, e.g. [105] for an overview). In the modern regime of machine learning, however, one frequently encounters situations where P, N are both large and of the same scale, or even where $N \gg P$. For example, in deep learning, the activations of a given layer can exist in a several thousand dimensional space, leading to a covariance where $P \sim N$. In kernel regression, the space of features is often infinite dimensional.

In this work, we will be most interested in problems where a target y , which is a function of \mathbf{x} is to be predicted via linear or ridge regression. Given a training set of $\mathbf{X} \in \mathbb{R}^{P \times N}$ and corresponding set of labels $\{y_\mu\}_{\mu=1}^P$, we will consider finding weights that minimize the least squares error:

$$\hat{\mathbf{w}} = \arg \min_{\mathbf{w}} \frac{1}{P} \sum_{\mu=1}^P (\mathbf{x}_\mu^\top \mathbf{w} - y_\mu)^2 + \lambda \|\mathbf{w}\|^2. \quad (4)$$

The solution to this regression problem is given by:

$$\hat{\mathbf{w}} = (\hat{\Sigma} + \lambda)^{-1} \frac{\mathbf{X}^\top \mathbf{y}}{P}. \quad (5)$$

Both the empirical feature-label correlation $\frac{1}{P} \mathbf{X}^\top \mathbf{y}$ and the empirical covariance $\hat{\Sigma}$ appear in this formula. The role of the empirical covariance will be especially important. Understanding the properties of $\hat{\Sigma}$ in this proportional limit is a rich topic of study that belongs in the field of **random matrix theory** (RMT).

In what follows, we will give some examples of random matrices. When the \mathbf{x}_μ are all drawn from a high-dimensional Gaussian distribution, their empirical covariance will be distributed as a **Wishart** random matrix. Many aspects of these matrices can be easily characterized in the limit where $N, P \rightarrow \infty$ with fixed ratio $q = N/P$, known as the proportional high-dimensional limit. Here, q is called the **overparameterization ratio**. Moreover, a wide variety of covariance matrices that do not come from Gaussian data will have covariances that effectively converge to Wishart matrices in the proportional limit. If one is only interested in properties involving the covariance, one can replace the dataset with a high dimensional Gaussian of matching covariance. This phenomenon is known as **Gaussian universality** or **Gaussian equivalence**.

B. Examples of Random Matrices

Example 1 (White Wishart Matrices). In the case where \mathbf{x}_μ are all drawn i.i.d. from a Gaussian with population covariance Σ equal to the identity, $\mathbf{x}_\mu \sim \mathcal{N}(0, \mathbf{I})$, the empirical covariance is said to be drawn from a **white Wishart**

ensemble. In particular, it is an N -dimensional Wishart matrix with P degrees of freedom and scale matrix $P^{-1}\mathbf{I}$. This is also known as an isotropic or unstructured Wishart matrix .

Example 2 (Structured Wishart Matrices and Multiplicative Noise). When \mathbf{x}_μ are drawn from a Gaussian with population covariance $\Sigma \neq \mathbf{I}$, then Σ is called a structured covariance and $\hat{\Sigma}$ is called a **structured** Wishart. This is also known as the anisotropic or colored case.

Any such \mathbf{X} can be written as $\tilde{\mathbf{X}}\sqrt{\Sigma}$ where the entries of $\tilde{\mathbf{X}}$ are i.i.d. as $\mathcal{N}(0, 1)$ and $\sqrt{\Sigma}$ is the principal square root of Σ . Then $\mathbf{W} = \frac{1}{P}\tilde{\mathbf{X}}^\top\tilde{\mathbf{X}}$ is distributed as a white Wishart, giving that $\hat{\Sigma} = \sqrt{\Sigma}\mathbf{W}\sqrt{\Sigma}$. In this sense, Wishart matrices can be understood as noisy version of the population covariance Σ , where the noise process is given by multiplication with a white Wishart.

Example 3 (Wigner Matrices as Additive Noise). Consider the setting where we are given a symmetric matrix \mathbf{A} (possibly a covariance) that has additive noise applied to each entry. This is usually given by taking \mathbf{A} and adding a symmetric random matrix with Gaussian entries to it. Such additive noise is observed, for example, as a leading-order correction to the empirical covariance $\hat{\Sigma}$ in $1/P$ at large P . This is the regime of classical statistics, which deals with corrections to the empirical covariance due to large but finite P when N is held fixed. For Gaussian data, the central limit theorem implies that at large P one can asymptotically approximate $\hat{\Sigma} = \Sigma + \frac{1}{\sqrt{P}}\sqrt{\Sigma}\mathbf{A}\sqrt{\Sigma} + O(P^{-1})$ [106]. Here \mathbf{A} is an unstructured **Wigner matrix**. We show this at the end of Section IV.D.

An unstructured Wigner matrix can be generated as follows: Take $\mathbf{X} \in \mathbb{R}^{N \times N}$ to be a random matrix with i.i.d. Gaussian entries such that $[\mathbf{X}]_{ij} \sim \mathcal{N}(0, \frac{\sigma^2}{N})$. The symmetrized random matrix $\mathbf{X}^\top + \mathbf{X}$ is known as a **Wigner** random matrix. This construction has the property that because \mathbf{X} is drawn from a rotationally symmetric distribution, so is $\mathbf{X} + \mathbf{X}^\top$. We will not deal with Wigner matrices very often, but they are the most well-known example of random matrices. Their eigenvalue distribution in the large N limit yields the famed **semicircle law**.

Example 4 (Random Projection). Consider a random N -dimensional subspace⁶ of \mathbb{R}^D . The projection operator \mathbf{P} that takes each vector in \mathbb{R}^D and maps it to its orthogonal projection in this N -dimensional subspace is symmetric and satisfies $\mathbf{P}^2 = \mathbf{P}$. It is also a random matrix with the property that its eigenvalues are either zero or one.

C. The Spectral Density and the Resolvent

In what follows, we will consider only symmetric matrices \mathbf{A} . The eigenvalues are therefore real and the eigenvectors form an orthogonal basis by the spectral theorem. It will be convenient to adopt the following shorthand for the normalized trace

$$\text{tr}[\cdot] \equiv \frac{1}{N} \text{Tr}[\cdot], \quad (6)$$

where the matrix being traced over is an $N \times N$ matrix.

We will be principally interested in quantities related to the spectral structure of a given random matrix $\mathbf{A} \in \mathbb{R}^{N \times N}$ in the limit of $N \rightarrow \infty$. At finite N , the **spectral density** of a given random matrix with eigenvalues $\{\lambda_i\}_{i=1}^N$ is given by:

$$\rho_N(\lambda) := \frac{1}{N} \sum_{i=1}^N \delta(\lambda - \lambda_i). \quad (7)$$

In the limit of $N \rightarrow \infty$, ρ_N this tends to a distribution ρ , which can have both a continuous ‘‘bulk’’ and countably many isolated outliers depending on the ensemble from which \mathbf{A} was drawn.

Another quantity of interest is the **matrix resolvent** of a random matrix:

$$\mathbf{G}_\mathbf{A}(z) = (z\mathbf{I} - \mathbf{A})^{-1}. \quad (8)$$

This object has the property that its poles correspond to the eigenvalues of \mathbf{A} , and the residues are the outer products of the corresponding eigenvectors. The normalized trace of this quantity, also known as the **Stieltjes Transform** or

⁶ We get this subspace by starting with the subspace spanned by the first N basis vectors and rotating it by a random orthogonal matrix \mathbf{O} , chosen with respect to Haar measure on the orthogonal group.

sometimes just the **resolvent** of \mathbf{A} is related to the eigenvalue density directly:

$$g_{\mathbf{A}}(z) \equiv \text{tr} [(z\mathbf{I} - \mathbf{A})^{-1}] = \frac{1}{N} \sum_{i=1}^N \frac{1}{z - \lambda_i} = \int \frac{\rho(\lambda)d\lambda}{z - \lambda}. \quad (9)$$

Expanding $g_{\mathbf{A}}(z)$ in a power series in $1/z$, one gets coefficients equal to the normalized traces $\text{tr}[A^k]$. This means $g_{\mathbf{A}}(z)$ behaves like a moment generating function for the spectral distribution of \mathbf{A} .

From this resolvent, one can recover the spectral density using the **inverse Stieltjes transform**:

$$\rho_{\mathbf{A}}(\lambda) = \lim_{\epsilon \rightarrow 0^+} \frac{1}{\pi} \text{Im}[g_{\mathbf{A}}(\lambda - i\epsilon)], \quad (10)$$

where the notation implies that ϵ tends to 0 from above.

Crucially, for all of the random matrices that we will study, the Stieltjes transform $g_{\mathbf{A}}(z)$ **concentrates** over \mathbf{A} as $N \rightarrow \infty$. A quantity $\mathcal{O}_{\mathbf{A}}$ is said to concentrate if it becomes independent of the specific choice of \mathbf{A} in the ensemble. That is, as $N \rightarrow \infty$, $\mathcal{O}_{\mathbf{A}}$ approaches a finite deterministic quantity.⁷ This means that for sufficiently large matrices, we can replace this quantity with its average value. A consequence of this concentration is that the spectral density itself concentrates. That is, the eigenspectrum of a very large random matrix drawn from (e.g. a Wigner or Wishart) ensemble will have an eigenvalue density that is essentially deterministic. For a precise characterization and proof of the conditions under which resolvents and their associated eigenspectra will concentrate, see [107].

A second type of moment-generating function encountered is defined as:

$$\mathbf{T}_{\mathbf{A}}(z) = \mathbf{A}(z\mathbf{I} - \mathbf{A})^{-1}. \quad (11)$$

Its corresponding normalized trace, sometimes called the t -transform, is given by

$$t_{\mathbf{A}}(z) = \text{tr} [\mathbf{A}(z\mathbf{I} - \mathbf{A})^{-1}]. \quad (12)$$

These two quantities are easily related to the resolvent:

$$\begin{aligned} \mathbf{T}_{\mathbf{A}}(z) &= z\mathbf{G}_{\mathbf{A}}(z) - \mathbf{I}, & \mathbf{G}_{\mathbf{A}}(z) &= \frac{1}{z} (\mathbf{T}_{\mathbf{A}}(z) + \mathbf{I}), \\ t_{\mathbf{A}}(z) &= zg_{\mathbf{A}}(z) - 1, & g_{\mathbf{A}}(z) &= \frac{t_{\mathbf{A}}(z) + 1}{z}. \end{aligned} \quad (13)$$

D. Degrees of freedom

Both $g_{\mathbf{A}}$ and $t_{\mathbf{A}}$ enter naturally in the calculations of training and generalization error that we will perform. In all such cases, however, they enter only after being evaluated at a negative value of z , e.g. $z = -\lambda$. This negative value is related to the ridge parameter of the regression. To simplify the final results in this paper, we therefore define the following auxiliary generating functions:

$$\text{df}_{\mathbf{A}}^1(\lambda) \equiv \text{tr} [\mathbf{A}(\mathbf{A} + \lambda\mathbf{I})^{-1}] = -t_{\mathbf{A}}(-\lambda), \quad (14)$$

$$\text{df}_{\mathbf{A}}^2(\lambda) \equiv \text{tr} [\mathbf{A}^2(\mathbf{A} + \lambda\mathbf{I})^{-2}] = \partial_{\lambda}(-\lambda t_{\mathbf{A}}(-\lambda)). \quad (15)$$

These are the the first and second **degrees of freedom** of the matrix \mathbf{A} . When \mathbf{A} is understood from context, they will also be written as df_1 and df_2 . The first of these appears prominently in statistics when defining the effective degrees of freedom of a linear estimator, see for example section 7.6 of [105] and [17]. The notation has also been used extensively in a recent paper by Bach on linear random feature models [35].

For some intuition about what df_1, df_2 measure, we will consider the concrete example of a high-dimensional Gaussian with covariance $\Sigma \in \mathbb{R}^{N \times N}$. The eigenvalues η_k of Σ will appear in the principal component analysis of this Gaussian. Frequently, one is interested in the *effective dimensionality* of such an object. In order to calculate this, we define a scale of resolution λ . Eigenvalues greater than λ will tend to be counted as increasing the dimensionality

⁷ Technically speaking, we only assume that $\mathcal{O}_{\mathbf{A}}$ converges in probability to a deterministic limit.

whereas eigenvalues smaller than λ will tend to be ignored. Rather than a sharp threshold at λ , we instead consider a softer such measure of dimensionality given by:

$$\dim_1(\lambda) \equiv \sum_k \frac{\eta_k}{\lambda + \eta_k}. \quad (16)$$

Here, if $\eta_k \gg \lambda$ then the term will contribute to the sum with a value close to 1. On the other hand, if $\eta_k \ll \lambda$, then the term will enter the sum with a value close to zero, and not contribute substantially. A sharper but still analytic measure of dimensionality would involve raising each term to some power $p > 1$:

$$\dim_p(\lambda) \equiv \sum_k \left(\frac{\eta_k}{\lambda + \eta_k} \right)^p. \quad (17)$$

We see that df_1, df_2 correspond exactly to $\frac{1}{N}\dim_1$ and $\frac{1}{N}\dim_2$. These notions of dimensionality will appear naturally in the context of ridge regression. In fact, they are the only notions of dimensionality that turn out to matter in this context. Given that both df_1, df_2 are bounded to be between 0 and 1, one can also view them as the ‘‘fraction of eigenvalues resolved’’ at a given scale λ .

Similarly, when there is a ‘‘teacher’’ vector $\bar{\mathbf{w}}$ that we want to weight the degrees of freedom by, we will define the following quantities by analogy to df_1, df_2 :

$$\text{tf}_{\mathbf{A}, \bar{\mathbf{w}}}^1(\lambda) = \bar{\mathbf{w}}^\top \mathbf{A}(\mathbf{A} + \lambda \mathbf{I})^{-1} \bar{\mathbf{w}}, \quad (18)$$

$$\text{tf}_{\mathbf{A}, \bar{\mathbf{w}}}^2(\lambda) = \bar{\mathbf{w}}^\top \mathbf{A}^2(\mathbf{A} + \lambda \mathbf{I})^{-2} \bar{\mathbf{w}}. \quad (19)$$

When $\mathbf{A}, \bar{\mathbf{w}}$ are understood, we will similarly write these as just tf_1 and tf_2 . In the case where we average tf_1, tf_2 over $\bar{\mathbf{w}}$ distributed uniformly on the sphere, $\|\bar{\mathbf{w}}\|^2 = 1$, we recover df_1, df_2 respectively. These formulae are also related to quantities used in [17; 31; 35; 94].

The following identities will be particularly useful to us:

$$\frac{d}{d\lambda}(\lambda \text{df}_1) = \text{df}_2, \quad (20)$$

$$\frac{d \text{df}_1}{d \log \lambda} = \lambda \partial_\lambda \text{df}_1 = \text{df}_2 - \text{df}_1, \quad (21)$$

$$\frac{d \log \text{df}_1}{d \log \lambda} = \frac{\lambda}{\text{df}_1} \partial_\lambda \text{df}_1 = \frac{\text{df}_2 - \text{df}_1}{\text{df}_1}. \quad (22)$$

The tf functions satisfy the same relationships between themselves.

Finally we have an upper bound on df_2 by:

$$\begin{aligned} \text{df}_2 &= \text{df}_1 - \lambda \text{tr}[\mathbf{A}(\mathbf{A} + \lambda \mathbf{I})^{-2}] \leq \text{df}_1 - \frac{\lambda}{\|\mathbf{A}\|_{op}} \text{df}_2 \\ \Rightarrow \text{df}_2 &\leq \frac{\text{df}_1}{1 + \lambda/\|\mathbf{A}\|_{op}} \end{aligned} \quad (23)$$

where $\|\mathbf{A}\|_{op}$ is the maximal eigenvalue of \mathbf{A} .

E. Addition and Multiplication of Random Matrices

1. R -transform

Consider two large N -dimensional random matrices \mathbf{A}, \mathbf{B} whose spectra $\rho_{\mathbf{A}}(\lambda), \rho_{\mathbf{B}}(\lambda)$ are known. As discussed, in the $N \rightarrow \infty$ limit these spectra become deterministic. One may ask what can be said about the spectrum of the sum $\mathbf{A} + \mathbf{B}$. It turns out that under certain assumptions on \mathbf{A}, \mathbf{B} , this question can be answered straightforwardly using the R -transform. The R -transform was originally introduced as a tool in free probability theory [36], and finds an important application when dealing with sums of large random matrices.

We define the R -transform of a matrix \mathbf{A} by

$$g_{\mathbf{A}}(z) = \frac{1}{z - R_{\mathbf{A}}(g_{\mathbf{A}})}. \quad (24)$$

Note that, $R_{\mathbf{A}}$ depends explicitly on the the resolvent $g_{\mathbf{A}}$, not on z .

The R -transform satisfies the remarkable property that for two random matrices \mathbf{A}, \mathbf{B} that are **free** of one another:

$$R_{\mathbf{A}+\mathbf{B}}(g) = R_{\mathbf{A}}(g) + R_{\mathbf{B}}(g). \quad (25)$$

We prove this additive property and give the technical definition of freedom in Section III. For now, it is enough to say that \mathbf{A}, \mathbf{B} are free if N is large and \mathbf{A} and \mathbf{B} are “randomly rotated” with respect to one another. The latter condition implies that the spectra of $\mathbf{A} + \mathbf{B}$ and $\mathbf{A} + \mathbf{O}\mathbf{B}\mathbf{O}^\top$ agree in the large N limit for any randomly chosen⁸ rotation \mathbf{O} . We will prove this relationship using diagrammatics in Section III.B.1. See also [104; 107] for several other derivations.

2. S -transform

Just as one is interested in the eigenvalues of a sum of two random matrices $\mathbf{A}, \mathbf{B} \in \mathbb{R}^{N \times N}$, one is also frequently interested in the spectrum of their product. In general, if \mathbf{A} and \mathbf{B} are symmetric, then $\mathbf{A}\mathbf{B}$ will not be symmetric. However both $\mathbf{A}\mathbf{B}$ and $\mathbf{B}\mathbf{A}$ will share the same nonzero eigenspectrum. Further, if we define the symmetrized or **free product** by

$$\mathbf{A} * \mathbf{B} := \mathbf{A}^{1/2} \mathbf{B} \mathbf{A}^{1/2}, \quad (26)$$

we see that $\mathbf{A}\mathbf{B}$, $\mathbf{B}\mathbf{A}$, $\mathbf{A} * \mathbf{B}$, and $\mathbf{B} * \mathbf{A}$ will all share the same non-zero spectrum. We use this symmetrized product to ensure $\mathbf{A} * \mathbf{B}$ remains symmetric.

Just as for sums of matrices, assuming \mathbf{A} and \mathbf{B} are free of one another, there is another transform that allows one to calculate the spectral properties of their product given individual knowledge of the spectra of \mathbf{A} and \mathbf{B} . This is the **S -transform** of free probability theory [36].

The S -transform $S_{\mathbf{A}}(t)$ is defined by the solution of the equation

$$t_{\mathbf{A}}(z) = \frac{1}{z S_{\mathbf{A}}(t_{\mathbf{A}}) - 1}. \quad (27)$$

Equivalently, defining $\zeta_{\mathbf{A}}(t)$ as the functional inverse of $t_{\mathbf{A}}$ satisfying $\zeta_{\mathbf{A}}(t_{\mathbf{A}}(z)) = z$ we get:

$$S_{\mathbf{A}}(t) = \frac{t + 1}{t \zeta_{\mathbf{A}}(t)}. \quad (28)$$

The S -transform has the important property that when \mathbf{A} and \mathbf{B} are free of one another:

$$S_{\mathbf{A} * \mathbf{B}}(t) = S_{\mathbf{A}}(t) S_{\mathbf{B}}(t). \quad (29)$$

This is the main result that we will utilize to derive many of the formulas that follow. We prove this identity in Section III.B.2. Finally, because $\text{df}_{\mathbf{A}}^1(\lambda) = -t_{\mathbf{A}}(-\lambda)$ we will also write $S_{\mathbf{A}}(t) = S_{\mathbf{A}}(-\text{df}_1)$ in many of the applications of this equation.

F. Application: Empirical Covariances

The S -transform is especially useful when studying empirical covariance matrices. When $\hat{\Sigma}$ is drawn from a structured Wishart we have seen that we can write it as the free product of Σ with a white Wishart:

$$\hat{\Sigma} = \Sigma^{1/2} \mathbf{W} \Sigma^{1/2}. \quad (30)$$

The S -transform relation then yields:

$$t_{\hat{\Sigma}}(z) = \frac{1}{z S_{\hat{\Sigma}}(t_{\hat{\Sigma}}) - 1} = \frac{1}{z S_{\mathbf{W}}(t_{\hat{\Sigma}}) S_{\Sigma}(t_{\hat{\Sigma}}) - 1} = t_{\Sigma}(z S_{\mathbf{W}}(t_{\hat{\Sigma}})). \quad (31)$$

⁸ Here by “randomly chosen” we mean with respect to the Haar measure on the orthogonal group of $N \times N$ matrices $O(N)$.

This is sometimes called a **subordination relation** for the S -transform. Taking $\lambda := -z, \kappa := -zS_{\mathbf{W}}(t_{\hat{\Sigma}}(z))$ gives the key relationship:

$$\boxed{\text{df}_{\hat{\Sigma}}^1(\lambda) \simeq \text{df}_{\Sigma}^1(\kappa), \quad \kappa = \lambda S_{\mathbf{W}}(-\text{df}_1)}. \quad (32)$$

The left-hand side is given by the trace of a random matrix and the right-hand side is given by the trace of a deterministic one. For this reason, this equality and its variants go by the name **deterministic equivalence**. We have used the symbol ‘ \simeq ’ to denote that this equality only holds strictly in the limit of $P, N \rightarrow \infty$. Note also that because of the equality (32), one can evaluate $S_{\mathbf{W}} = S_{\mathbf{W}}(-\text{df}_1)$ using either $\text{df}_1 = \text{df}_{\hat{\Sigma}}^1(\lambda)$ or $\text{df}_1 = \text{df}_{\Sigma}^1(\kappa)$.⁹ Because $\text{df}_{\hat{\Sigma}}^1(\lambda)$ enters prominently in all generalization error formulas encountered in this paper, this equation will play a key role in the derivations that follow.

This equation relates the degrees of freedom (as in equation (14)) of the empirical covariance at a given ridge to the degrees of freedom of the true covariance with a **renormalized ridge** κ . Because $S_{\mathbf{W}}$ has a simple analytic form as derived in IV.D, one can write a self-consistent equation for κ , giving,

$$\kappa = \lambda S_{\mathbf{W}}(-\text{df}_1) = \frac{\lambda}{1 - \frac{N}{P} \text{df}_1}. \quad (33)$$

Again, one can evaluate df_1 either as $\text{df}_{\hat{\Sigma}}^1(\lambda)$ or $\text{df}_{\Sigma}^1(\kappa)$. The first way gives an estimate of κ from the empirical data of $\hat{\Sigma}$ alone, while the second way yields an analytic self-consistent equation for κ in terms of the true population covariance Σ .

As an aside: the use of the term *renormalized* here is intentional, as this is an exact example of a renormalization procedure. For one, the diagrammatic picture as discussed in Section III.B as well as [34; 108] mirrors the treatment of self-energy diagrams in renormalized perturbation theory. More generally, the change from λ to κ is exactly due to κ absorbing the contributions of the statistical fluctuations when we go from $\hat{\Sigma}$ to Σ . This is analogous to how a renormalized mass term absorbs the quantum or thermal fluctuations in standard field theory. The S -transform exactly accounts for the multiplicative rescaling of λ due to these fluctuations. In this setting the resolvents \mathbf{T}, \mathbf{G} play the roles of Green’s functions.

Equation (32) extends to the following equality of matrices. This is known as **strong deterministic equivalence**. It will follow from the relation (43) proved in the next section.

$$\boxed{\hat{\Sigma}(\hat{\Sigma} + \lambda \mathbf{I})^{-1} \simeq \Sigma(\Sigma + \kappa \mathbf{I})^{-1}}. \quad (34)$$

Here, for sequences of (possibly random) $N \times N$ matrices \mathbf{A} and \mathbf{B} , we write $\mathbf{A} \simeq \mathbf{B}$ if $\text{tr}(\mathbf{A}\mathbf{M}) \rightarrow \text{tr}(\mathbf{B}\mathbf{M})$ in probability as $N \rightarrow \infty$ for any test matrix \mathbf{M} of bounded operator norm, as in [35].

Using the relationship (13) between the t -transform and the resolvent, (32) and (34) extend to deterministic equivalents for the resolvents:

$$\text{tr}((\hat{\Sigma} + \lambda \mathbf{I})^{-1}) \simeq \frac{\kappa}{\lambda} \text{tr}((\Sigma + \kappa \mathbf{I})^{-1}), \quad (35)$$

$$(\hat{\Sigma} + \lambda \mathbf{I})^{-1} \simeq \frac{\kappa}{\lambda} (\Sigma + \kappa \mathbf{I})^{-1}. \quad (36)$$

Equations (34) and (36) are true when $\hat{\Sigma}$ is the free product of Σ with *any* multiplicative noise matrix \mathbf{M} , not just a white Wishart, as long as \mathbf{M} is relatively free of Σ . In particular, writing $\hat{\Sigma} = \Sigma^{1/2} \mathbf{M} \Sigma^{1/2}$

$$\hat{\Sigma}(\hat{\Sigma} + \lambda \mathbf{I})^{-1} = \Sigma(\Sigma + \kappa \mathbf{I})^{-1}, \quad (\hat{\Sigma} + \lambda \mathbf{I})^{-1} = \frac{\kappa}{\lambda} \Sigma(\Sigma + \kappa \mathbf{I})^{-1}, \quad \kappa = S_{\mathbf{M}} \lambda. \quad (37)$$

In all of the above equations, κ can be interpreted in several ways:

1. It is the original ridge λ , renormalized by $S_{\mathbf{W}}$ coming from the multiplicative noise of the high-dimensional covariance. Even in the ridgeless limit, κ remains nonzero provided that $S_{\mathbf{W}}$ picks up a pole. We will study this in Sections V.C and V.F; see also [17; 109; 110] for some early discussions of this effect. In fact, the poles of the S -transform will be in correspondence with the different ridgeless regimes of a given model, as we show in Section VI.D.

⁹ Throughout this paper, we use the shorthand df_1 . Because of Equation (32), in the large N, P limit that we work in, there is no confusion as to whether this is $\text{df}_{\hat{\Sigma}}^1(\lambda)$ or $\text{df}_{\Sigma}^1(\kappa)$. Both of these quantities are asymptotically equal in this limit.

2. It is the **signal capture threshold**, or equivalently the **resolution**. Eigenvalues larger than κ will correspond to modes that are all learned, while eigenvalues smaller than κ will not be learned. We will demonstrate this in Equation (128) in Section V.B.

As P gets larger, the fluctuations of the high dimensional covariance are suppressed and $S_{\mathbf{W}}$ becomes smaller. Consequently, κ becomes smaller and the resolution improves. We will see in V.I that for covariances with power law structure, where the k th eigenvalue of Σ decays $k^{-\alpha}$ that the resolution improves as $\kappa \sim P^{-\alpha}$. α is called the **capacity** exponent of the data manifold [63; 96; 99; 100; 111]. Large α implies most of the spread of the data is in the first few principal components, leading to effective low dimensionality. Smaller α imply the data is higher dimensional and thus the curse of dimensionality has a stronger effect. Consequently, the resolution κ gets finer-grained at a slower rate in P . This is at the heart of all resolution-limited scalings.

Next, in Section III, we give a technical derivation of the R and S properties given in Equations (25) and (29). In fact we will prove a more general property known as a **subordination relation** of matrices in each case. From this, the matrix equalities of (34), (36), (37) will follow. If the reader is more interested in directly applying the S -transform to calculating training and generalization errors of various models, they can safely skip this section on first reading.

III. RENORMALIZATION AND FREE PROBABILITY

In this section, we give a brief overview of the aspects of free probability theory as applied to random matrices that we will use in this paper, including a self-contained derivation of the key identities we require. For the interested reader, there are many more extensive introductory texts, including [104; 112; 113; 114]. The key results are Equations (41), (42), (43). If the reader is not interested in their derivation, this section can be safely skipped.

A. Definition of Freedom

Free probability studies non-commutative random variables. The simplest statistic that distinguishes free probability from commutative probability is the joint fourth moment of two random variables. Consider two random matrices $\mathbf{A}_1, \mathbf{A}_2$ with $\text{tr}[\mathbf{A}_i] \simeq 0$ in the limit $N \rightarrow \infty$. If $\mathbf{A}_1, \mathbf{A}_2$ are **free** of one another, one consequence is that

$$\mathbb{E}_{\mathbf{A}_1, \mathbf{A}_2} \text{tr}[\mathbf{A}_1 \mathbf{A}_2 \mathbf{A}_1 \mathbf{A}_2] \simeq 0. \quad (38)$$

Note that this fourth moment certainly would not vanish for nonzero commutative random variables. In free probability, when two mean zero random variables \mathbf{A}, \mathbf{B} are free of one another, their alternating moments will vanish. One consequence of this is that a sum of free random variables has lower kurtosis. This is a reason why the Wigner semicircle law (the analog of the Gaussian in free random matrix theory; see §IV.A) has lower kurtosis than the Gaussian and is in fact compactly supported.

We now formally define what it means for a collection of random variables to be **jointly free**. Though the theory of free probability extends to more general algebras [112], here we will focus only on the case of **asymptotically free random matrices**,¹⁰ i.e., $N \times N$ matrices which behave as free random variables in the limit $N \rightarrow \infty$, as that is the setting which is relevant for the present work [114]. As we work in the $N \rightarrow \infty$ limit throughout, we will frequently drop the qualifier ‘‘asymptotic’’ and simply state that certain random matrices are free.

Joint (asymptotic) freedom of a set of n random matrices $\{\mathbf{A}_i\}_{i=1}^n$ of size $N \times N$ is defined by considering all mixed moments of these random variables in the limit $N \rightarrow \infty$. Take a set of m polynomials $\{p_k\}_{k=1}^m$ and a labeling $\{i_k\}_{k=1}^m$ with each $i_k \in \{1, \dots, n\}$ so that $i_k \neq i_{k+1}$ for all k . Let each p_k have the property that

$$\text{tr}[p_k(\mathbf{A}_{i_k})] \simeq 0. \quad (39)$$

Then $\{\mathbf{A}_i\}_{i=1}^n$ are jointly asymptotically free if and only if

$$\text{tr}[p_1(\mathbf{A}_{i_1}) \cdots p_m(\mathbf{A}_{i_m})] \simeq 0 \quad (40)$$

for any m and labeling $\{i_k\}$ and set of polynomials $\{p_k\}_{k=1}^m$ satisfying the mean zero property above. Independent draws from the classical random matrix ensembles we consider are all jointly asymptotically free. The normalized traces concentrate to deterministic values for all ensembles we consider.

B. Diagrammatic Derivations of Subordination Relations

We now give a derivation of the following two important relationships. We will take \mathbf{A} to be deterministic and take \mathbf{B} free of \mathbf{A} :

$$\mathbb{E}_{\mathbf{B}} \mathbf{G}_{\mathbf{A}+\mathbf{B}}(z) \simeq \mathbf{G}_{\mathbf{A}}(z - R_{\mathbf{B}}(g_{\mathbf{A}+\mathbf{B}}(z))) \quad (41)$$

$$\mathbb{E}_{\mathbf{B}} \mathbf{T}_{\mathbf{A}\mathbf{B}}(z) \simeq \mathbf{T}_{\mathbf{A}}(z S_{\mathbf{B}}(t_{\mathbf{A}\mathbf{B}}(z))). \quad (42)$$

These are called **subordination relations** for the R and S transforms respectively. Viewing \mathbf{B} as additive or multiplicative noise respectively, one can directly interpret these equations. Equation (41) states that the resolvent of an additively noised matrix is equal to the resolvent of the clean matrix with a shifted value of z . The shift is given by the R -transform. Equation (42) states that \mathbf{T} of a multiplicatively noised matrix is equal to \mathbf{T} of the clean matrix with a rescaled value of z . This rescaling is given by the S -transform.

¹⁰ The reader should distinguish this from the notion of asymptotic freedom in gauge theory.

Note that after multiplying Equation (42) by $\mathbf{A}^{-1/2}$ and $\mathbf{A}^{1/2}$ on the left and right respectively and making use of the pushthrough identity, (174), we obtain its symmetrized analogue:

$$\mathbb{E}_{\mathbf{B}} \mathbf{T}_{\mathbf{A} * \mathbf{B}}(z) \simeq \mathbf{T}_{\mathbf{A}}(z S_{\mathbf{B}}(t_{\mathbf{A}\mathbf{B}}(z))). \quad (43)$$

Here, $t_{\mathbf{A} * \mathbf{B}} = t_{\mathbf{A}\mathbf{B}}$ since the nonzero eigenvalues are the same for both matrices. In the setting of $\mathbf{A} = \Sigma$ a population covariance and $\mathbf{B} = \mathbf{W}$ a white Wishart, equation (43) gives exactly the strong deterministic equivalence (34). Note on the right hand side there is no need to take an expectation over \mathbf{B} because $R_{\mathbf{B}}, S_{\mathbf{B}}, g_{\mathbf{A}+\mathbf{B}}, t_{\mathbf{A}\mathbf{B}}$ all concentrate.

If we take the trace of Equations (41) and (42) and use that $g_{\mathbf{A}+\mathbf{B}} = (z - R_{\mathbf{A}+\mathbf{B}}(g_{\mathbf{A}+\mathbf{B}}(z)))^{-1}$ and $t_{\mathbf{A}\mathbf{B}} = (z S_{\mathbf{A}\mathbf{B}} - 1)^{-1}$ we get:

$$\begin{aligned} R_{\mathbf{A}+\mathbf{B}}(g_{\mathbf{A}+\mathbf{B}}(z)) &= R_{\mathbf{B}}(g_{\mathbf{A}+\mathbf{B}}(z)) + R_{\mathbf{A}}(g_{\mathbf{A}}(z - R_{\mathbf{B}}(g_{\mathbf{A}}(z)))) \\ &= R_{\mathbf{A}}(g_{\mathbf{A}+\mathbf{B}}) + R_{\mathbf{B}}(g_{\mathbf{A}+\mathbf{B}}(z)), \end{aligned} \quad (44)$$

$$\begin{aligned} S_{\mathbf{A}\mathbf{B}}(t(z)) &= S_{\mathbf{B}}(t_{\mathbf{A}\mathbf{B}}(z)) S_{\mathbf{A}}(t_{\mathbf{A}}(z S_{\mathbf{B}}(t(z)))) \\ &= S_{\mathbf{A}}(t_{\mathbf{A}\mathbf{B}}(z)) S_{\mathbf{B}}(t_{\mathbf{A}\mathbf{B}}(z)). \end{aligned} \quad (45)$$

These are the familiar R and S transform properties. We thus see that Equations (41) and (42) are stronger forms of these two properties.

Here, we will derive these subordination relations diagrammatically. For a derivation using the replica trick and the Harish-Chandra-Itzhakson-Zuber integral, we direct the interested reader to Appendix B of the work of Bun, Allez, Bouchaud, and Potters [115]. For a slightly different diagrammatic approach based on viewing the random matrices as perturbative corrections to a Wigner matrix, see [108].

1. R -Transform Subordination

We will consider the case where \mathbf{A} is deterministic and \mathbf{B} is random and drawn from an isotropic distribution. In the large N limit, the spectra of both \mathbf{A}, \mathbf{B} will be deterministic. We then have $\mathbf{B} = \mathbf{O}\mathbf{B}'\mathbf{O}^\top$ where \mathbf{B}' is a deterministic diagonal matrix. Then, to average over \mathbf{B} , we only need to evaluate the average over the relative rotation matrix \mathbf{O} .

We perform the following expansion of $\mathbf{G}_{\mathbf{A}+\mathbf{B}}$:

$$\mathbb{E}_{\mathbf{O}} \mathbf{G}_{\mathbf{A}+\mathbf{O}\mathbf{B}'\mathbf{O}^\top}(z) = \mathbb{E}_{\mathbf{O}} [\mathbf{G}_{\mathbf{A}}(z) + \mathbf{G}_{\mathbf{A}}(z)\mathbf{O}\mathbf{B}'\mathbf{O}^\top\mathbf{G}_{\mathbf{A}}(z) + \dots]. \quad (46)$$

We use solid dots to denote insertions of $\mathbf{O}\mathbf{B}'\mathbf{O}^\top$ and solid lines to denote contraction with $\mathbf{G}_{\mathbf{A}}(z)$. A general term in this series will look like:



We now perform the average over \mathbf{O} . We will not have to do any explicit calculations. Rather, we observe the following facts:

1. Because the entries of an orthogonal matrix have average size $N^{-1/2}$, a correlator of $2n$ \mathbf{O} matrices has the scaling:

$$\mathbb{E}_{\mathbf{O}}[\mathbf{O}_{i_1 j_1} \dots \mathbf{O}_{i_{2n} j_{2n}}] \sim O(N^{-n}). \quad (47)$$

2. At leading order in N , the \mathbf{O} behave like matrices with independent Gaussian entries. This allows us to compute averages by Wick contractions, also known as Isserlis' theorem:

$$\mathbb{E}[\mathbf{O}_{i_1 j_1} \dots \mathbf{O}_{i_{2n} j_{2n}}] = N^{-n} \sum_{\text{pairings } P} \prod_{(k, k') \in P} \delta_{i_k i_{k'}} \delta_{j_k j_{k'}} + \text{subleading terms}. \quad (48)$$

Here the i and j indices have the same pairing in each term. The subleading terms contributing to higher cumulants are known as Weingarten contributions, and have been studied in [116; 117; 118; 119]. Although they will enter into our calculations, we will not need to know precise details about their forms. See Chapter 12 of [104] for details.

We will denote the expectation of this over \mathbf{O} by dashed lines. Consider first the quantity $\mathbf{OB}'\mathbf{O}^\top$:

$$\mathbb{E}_{\mathbf{O}}[\mathbf{OB}'\mathbf{O}^\top] \equiv \begin{array}{c} \text{---} \\ \bullet \\ \text{---} \\ \mathbf{OB}'\mathbf{O}^\top \end{array} \quad (49)$$

One can evaluate this expectation by appeal to symmetry alone. First, because the distribution of \mathbf{O} is invariant under an orthogonal transformation $\mathbf{O} \mapsto \mathbf{U}_L \mathbf{O}$ for any orthogonal matrix \mathbf{U}_L , the final result must be rotationally invariant, and therefore proportional to the identity matrix \mathbf{I} . Second, because the distribution of \mathbf{O} is invariant under an orthogonal transformation $\mathbf{O} \mapsto \mathbf{O} \mathbf{U}_R$ for any orthogonal matrix \mathbf{U}_R , the expectation must depend only on the eigenvalues of \mathbf{B}' , and the dependence must be linear. Finally, when $\mathbf{B}' = \mathbf{I}$, it is equal to \mathbf{I} . This uniquely determines this quantity to be:

$$\mathbf{C}_1 \equiv \mathbb{E}_{\mathbf{O}}[\mathbf{OB}'\mathbf{O}^\top] = \text{tr}[\mathbf{B}]\mathbf{I}. \quad (50)$$

This agrees with just directly applying Equation (48). However, the above argument is true for all N , not just at leading order. We now make an observation about traces:

- Each loop in the diagrams corresponds to a free index that is traced over. Converting from a trace to a normalized trace (which is order 1) leaves over a factor of N .

Thus, to get an $O(1)$ contribution from a correlator of $2n$ matrices \mathbf{O} , we need diagrams with n loops to contribute n factors of N to cancel out the N^{-n} scaling. Diagrams with fewer loops will be suppressed in the large N limit. This will mean that crossing diagrams are not counted.

Next, using shorthand $\mathbf{B} = \mathbf{OB}'\mathbf{O}^\top$, consider the second moment $\mathbb{E}_{\mathbf{O}}[\mathbf{BG}_A\mathbf{B}]$. We can write this as two pieces:

$$\mathbb{E}_{\mathbf{O}}[\mathbf{BG}_A\mathbf{B}] = (\mathbb{E}_{\mathbf{O}}[\mathbf{BG}_A\mathbf{B}] - \mathbb{E}_{\mathbf{O}}[\mathbf{B}]\mathbf{G}_A\mathbb{E}_{\mathbf{O}}[\mathbf{B}]) + \mathbb{E}_{\mathbf{O}}[\mathbf{B}]\mathbf{G}_A\mathbb{E}_{\mathbf{O}}[\mathbf{B}] \quad (51)$$

We call the first term this **connected** term and the second term the **disconnected** term. Graphically, we will write this as

$$\mathbb{E}_{\mathbf{O}}[\mathbf{BG}_A\mathbf{B}] = \begin{array}{c} \text{---} \\ \bullet \\ \text{---} \\ \mathbf{OB}'\mathbf{O}^\top \end{array} \mathbf{G}_A \begin{array}{c} \text{---} \\ \bullet \\ \text{---} \\ \mathbf{OB}'\mathbf{O}^\top \end{array} + \begin{array}{c} \text{---} \\ \bullet \\ \text{---} \\ \mathbf{OB}'\mathbf{O}^\top \end{array} \mathbf{G}_A \begin{array}{c} \text{---} \\ \bullet \\ \text{---} \\ \mathbf{OB}'\mathbf{O}^\top \end{array} \quad (52)$$

This is analogous to how a moment is equal to a given cumulant plus contributions from lower order cumulants. Here, we have shaded the first diagram to highlight that it includes both the Wick contraction as well as a potential contribution from the fourth cumulant of orthogonal matrices:

$$C_2[\mathbf{G}_A] \equiv \begin{array}{c} \text{---} \\ \bullet \\ \text{---} \\ \mathbf{OB}'\mathbf{O}^\top \end{array} \mathbf{G}_A \begin{array}{c} \text{---} \\ \bullet \\ \text{---} \\ \mathbf{OB}'\mathbf{O}^\top \end{array} = \begin{array}{c} \text{---} \\ \bullet \\ \text{---} \\ \mathbf{OB}'\mathbf{O}^\top \end{array} \mathbf{G}_A \begin{array}{c} \text{---} \\ \bullet \\ \text{---} \\ \mathbf{OB}'\mathbf{O}^\top \end{array} + \begin{array}{c} \text{---} \\ \bullet \\ \text{---} \\ \mathbf{OB}'\mathbf{O}^\top \end{array} \mathbf{G}_A \begin{array}{c} \text{---} \\ \bullet \\ \text{---} \\ \mathbf{OB}'\mathbf{O}^\top \end{array} \quad (53)$$

Here, the first term is a Wick contraction, giving a term proportional to $\text{tr}[\mathbf{G}_A] \text{tr}[\mathbf{B}^2]$. We have not included the crossing Wick contraction because it will not contribute at large N , as discussed above. The second term corresponds the fourth cumulant of the \mathbf{O} s. This is a subleading Weingarten term in Equation (48). The only way that it might contribute is if it has at least 3 traces. Thus, if it enters, it must enter as $\text{tr}[\mathbf{G}_A] \text{tr}[\mathbf{B}]^2$.

At third order we will have several terms involving connected and disconnected components. One such term is:

$$C_2[\mathbf{G}_A]\mathbf{G}_A\mathbf{C}_1 = \begin{array}{c} \text{---} \\ \bullet \\ \text{---} \\ \mathbf{OB}'\mathbf{O}^\top \end{array} \mathbf{G}_A \begin{array}{c} \text{---} \\ \bullet \\ \text{---} \\ \mathbf{OB}'\mathbf{O}^\top \end{array} \mathbf{G}_A \begin{array}{c} \text{---} \\ \bullet \\ \text{---} \\ \mathbf{OB}'\mathbf{O}^\top \end{array} \quad (54)$$

Another such term is

$$C_2[\mathbf{G}_A C_1 \mathbf{G}_A] = \text{OBO}^\top \mathbf{G}_A \text{OBO}^\top \mathbf{G}_A \text{OBO}^\top \quad (55)$$

The fully connected term is denoted by $C_3[\mathbf{G}_A, \mathbf{G}_A]$ with

$$C_3[\mathbf{A}_1, \mathbf{A}_2] \equiv \text{OB}'\text{O}^\top \mathbf{A}_1 \text{OB}'\text{O}^\top \mathbf{A}_2 \text{OB}'\text{O}^\top \quad (56)$$

This will be the sum of the Wick contractions, plus the fourth cumulant contributions that correlate together at least one \mathbf{O} from each $\text{OB}'\text{O}^\top$ insertion, plus the potential sixth cumulant contributions. Again, because the only way these subleading cumulants can contribute is by introducing additional traces, we'll have that this quantity will depend on $\mathbf{A}_1, \mathbf{A}_2$ only through $\text{tr}[\mathbf{A}_1] \text{tr}[\mathbf{A}_2]$.

We will call diagrams that cannot be reduced to two independently-taken averages **irreducible**. Diagrams (53), (55), (56) are all irreducible while (54) is not. We will call the diagrams corresponding to C_1, C_2, C_3 etc **fully connected**. Diagram (55) is irreducible but not fully connected. We denote n -point fully connected diagram by $C_n[\mathbf{A}_1, \dots, \mathbf{A}_{n-1}]$. The \mathbf{A}_i are the matrices that appear below the arcs. For our purposes, it is enough to know the following facts:

4. The n -point fully connected diagram depends on the \mathbf{A}_i only through the product of their traces $\prod_{i=1}^{n-1} \text{tr}[\mathbf{A}_i]$. At the level of Wick contractions this is clear, where C_n goes as $\text{tr}[\mathbf{B}^n] \prod_{i=1}^{n-1} \text{tr}[\mathbf{A}_i]$. Subleading terms will only serve to further split $\text{tr}[\mathbf{B}^n]$ into additional traces over \mathbf{B} .
5. Dually, by tracing C_n against a test matrix \mathbf{A}_n , we have that this can depend only on \mathbf{A}_n through $\text{tr}[\mathbf{A}_n]$. This implies that $C_n \propto \mathbf{I}$. Together with iv), this implies:

$$C_n[\mathbf{A}_1, \dots, \mathbf{A}_{n-1}] = \kappa_{\mathbf{B}}^{(n)} \text{tr}[\mathbf{A}_1] \cdots \text{tr}[\mathbf{A}_{n-1}] \mathbf{I} \quad (57)$$

for some constant $\kappa_{\mathbf{B}}^{(n)}$ that depends only on \mathbf{B} which we call the n th **free cumulant** of \mathbf{B} . The reasons for this will become clear shortly.

Because crossing diagrams do not contribute, we can notice a pattern. Each term in the series can be broken up into a string of irreducible diagrams connected together by \mathbf{G}_A .



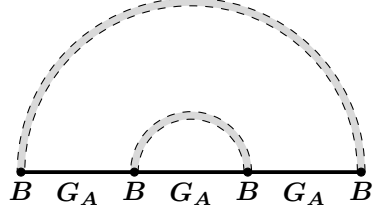
The matrix \mathbf{R} is analogous to the **1 Particle Irreducible** diagrams or **Self-Energy** in physics that contribute to a mass shift. We can then resum this series:

$$\begin{aligned} \mathbb{E}_O \mathbf{G}_{A+O\text{B}'\text{O}^\top}(z) &\simeq \mathbf{G}_A(z) + \mathbf{G}_A(z) \mathbf{R} \mathbf{G}_A(z) + \mathbf{G}_A(z) \mathbf{R} \mathbf{G}_A(z) \mathbf{R} \mathbf{G}_A(z) + \dots \\ &= (z\mathbf{I} - \mathbf{A} - \mathbf{R})^{-1}. \end{aligned} \quad (58)$$

It remains to compute \mathbf{R} . We get the following sum over fully-connected diagrams:

$$\mathbf{R} = \begin{array}{c} \text{---} \\ \bullet \\ \text{---} \\ \text{OB}'\text{O}^\top \end{array} + \begin{array}{c} \text{---} \\ \text{---} \\ \text{---} \\ \text{OB}'\text{O}^\top \quad \mathbf{G}_{A+B} \quad \text{OB}'\text{O}^\top \end{array} + \begin{array}{c} \text{---} \\ \text{---} \\ \text{---} \\ \text{OB}'\text{O}^\top \quad \mathbf{G}_{A+B} \quad \text{OB}'\text{O}^\top \quad \mathbf{G}_{A+B} \quad \text{OB}'\text{O}^\top \end{array} + \dots \quad (59)$$

Note we are using \mathbf{G}_{A+B} rather than \mathbf{G}_A to perform the contractions beneath each arc. Because of that, we don't need to include terms corresponding to configurations of "arcs within arcs", as they are already accounted for. That is, we don't need to explicitly include irreducible diagrams that aren't fully-connected. For example, the following contribution is already included for in the second term of Equation (59) above.



When we average over \mathbf{O} in Equation (59), all the appearances of $\mathbf{G}_{A+B}(z)$ will be traced over. Using Equation (57) together with the fact that g_{A+B} concentrates over \mathbf{O} we can write:

$$\mathbf{R} \simeq \sum_{n=0}^{\infty} \kappa_B^{(n)} g_{A+B}(z)^{n-1} \mathbf{I}. \quad (60)$$

We now define R_B by

$$R_B(g) = \sum_{n=0}^{\infty} \kappa_B^{(n)} g^{n-1}. \quad (61)$$

We thus arrive at the desired subordination relation:

$$\mathbb{E}_O \mathbf{G}_{A+B'}(z) \simeq \mathbf{G}_A(z - R_B(g_{A+B}(z))). \quad (62)$$

As discussed at the start of Section III.B, from this relation, one obtains the additivity of the R -transform. This further implies that

$$\kappa_{A+B}^{(n)} \simeq \kappa_A^{(n)} + \kappa_B^{(n)}. \quad (63)$$

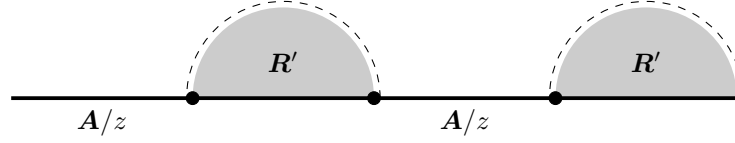
This justifies the term "free cumulants" for the $\kappa_A^{(n)}$. The free cumulants of a sum of two relatively free random matrices just add. This is analogous to how cumulants of independent random variables are additive in classical probability.

2. S -Transform Subordination

The proof for the S -transform is very similar. We again take \mathbf{A} , \mathbf{B} deterministic and perform the \mathbf{O} average. This time, we expand in powers of \mathbf{B}/z :

$$\mathbb{E}_O \mathbf{T}_{A O B' O^\top}(z) = \mathbf{A} \mathbb{E}_O \left[\frac{1}{z} \text{OB}'\text{O}^\top + \frac{1}{z^2} \text{OB}'\text{O}^\top \mathbf{A} \text{OB}'\text{O}^\top + \dots \right]. \quad (64)$$

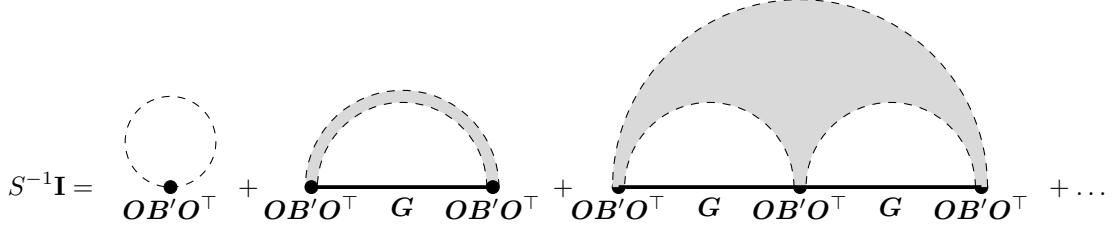
We again resum in terms of irreducible diagrams:



As before, because of the outer orthogonal average, \mathbf{R}' is proportional to the identity. Calling the constant of proportionality S^{-1} gives:¹¹

$$\begin{aligned}\mathbb{E}_O \mathbf{T}_{\mathbf{A}O\mathbf{B}'O^\top}(z) &\simeq \frac{1}{z} \mathbf{A} S^{-1} + \frac{1}{z^2} \mathbf{A} S^{-1} \mathbf{A} S^{-1} + \dots \\ &= \mathbf{A}(z\mathbf{S}\mathbf{I} - \mathbf{A})^{-1} = \mathbf{T}_{\mathbf{A}}(z\mathbf{S}).\end{aligned}\quad (65)$$

It remains to evaluate S . Expanding \mathbf{R}' give the following terms



Here, the lines beneath each arc are:

$$\mathbf{G} = \frac{1}{z} \mathbf{A} + \frac{1}{z^2} \mathbf{A} O\mathbf{B}'O^\top \mathbf{A} + \dots = \mathbf{G}_{\mathbf{A}\mathbf{B}'} \mathbf{A} = \frac{1}{z} (\mathbf{I} + \mathbf{T}_{\mathbf{A}\mathbf{B}}) \mathbf{A}. \quad (66)$$

Where we have related the resolvent $\mathbf{G}_{\mathbf{A}\mathbf{B}}$ to $\mathbf{T}_{\mathbf{A}\mathbf{B}}$ using Equation (13). As before, by Equation (57), S^{-1} is equal to:

$$S^{-1} \simeq \sum_{n=0}^{\infty} \frac{\kappa_{\mathbf{B}}^{(n)}}{z^{n-1}} \text{tr} [(\mathbf{I} + \mathbf{T}_{\mathbf{A}\mathbf{B}}(z)) \mathbf{A}]^{n-1} \simeq \sum_{n=0}^{\infty} \kappa_{\mathbf{B}}^{(n)} [St_{\mathbf{A}}(z\mathbf{S})]^{n-1} = R_{\mathbf{B}}(St_{\mathbf{A}\mathbf{B}}(z)). \quad (67)$$

Here we have used the \mathbf{A}, \mathbf{B} are free of one another and that $t_{\mathbf{A}\mathbf{B}}$ concentrates. Defining $S_{\mathbf{B}}$ through the self-consistent equation $1/S_{\mathbf{B}}(t) = R_{\mathbf{B}}(S_{\mathbf{B}}(t)t)$ gives us the desired subordination relation:

$$\mathbb{E}_O \mathbf{T}_{\mathbf{A}O\mathbf{B}O^\top}(z) = \mathbf{T}_{\mathbf{A}}(zS_{\mathbf{B}}(t_{\mathbf{A}\mathbf{B}}(z))). \quad (68)$$

As discussed at the start of Section III.B, from this relation, one obtains the multiplicative property of the S -transform.

C. Summary of R and S transform identities

There are a few identities that will be helpful for us in our derivations. Firstly, a trivial consequence of the additivity of R is that

$$R_{\mathbf{A}+\mathbf{J}\mathbf{I}}(g) = J + R_{\mathbf{A}}(g). \quad (69)$$

Further we can get a multiplicative identity for R by noting that for a fixed constant α

$$g_{\alpha\mathbf{A}}(z) = \alpha^{-1} g_{\mathbf{A}}(z/\alpha) \Rightarrow z_{\alpha\mathbf{A}}(g) = \alpha z_{\mathbf{A}}(\alpha g) \Rightarrow R_{\alpha\mathbf{A}}(g) = \alpha R_{\mathbf{A}}(\alpha g). \quad (70)$$

Here we have let $z_{\mathbf{A}}(g)$ be the functional inverse of $g_{\mathbf{A}}(z)$.

We can also get a multiplicative identity for S . Consider $t_{\alpha\mathbf{A}}(z)$. We see that

$$t_{\alpha\mathbf{A}}(z) = t_{\mathbf{A}}(z/\alpha) \Rightarrow \zeta_{\alpha\mathbf{A}}(t) = \alpha \zeta_{\mathbf{A}}(t) \Rightarrow S_{\alpha\mathbf{A}}(t) = \frac{t+1}{t\alpha\zeta_{\mathbf{A}}(t)} = \alpha^{-1} S_{\mathbf{A}}(t). \quad (71)$$

¹¹ It is because of historical convention that this is denoted by S^{-1} rather than S .

One can relate $g_{\mathbf{A}}, t_{\mathbf{A}}, R_{\mathbf{A}}, S_{\mathbf{A}}$ in the following two equations:

$$g_{\mathbf{A}}(z) = \frac{t_{\mathbf{A}}(z) + 1}{z} = t_{\mathbf{A}}(z)S_{\mathbf{A}}(t_{\mathbf{A}}(z)), \quad (72)$$

$$t_{\mathbf{A}}(z) = zg_{\mathbf{A}} - 1 = g_{\mathbf{A}}(z)R_{\mathbf{A}}(g_{\mathbf{A}}(z)). \quad (73)$$

Combining the above two equations also gives a relationship between the R and S transforms:

$$S_{\mathbf{A}}(t) = \frac{1}{R_{\mathbf{A}}(tS_{\mathbf{A}}(t))}, \quad (74)$$

$$R_{\mathbf{A}}(g) = \frac{1}{S_{\mathbf{A}}(gR_{\mathbf{A}}(g))}. \quad (75)$$

IV. R AND S TRANSFORMS OF IMPORTANT ENSEMBLES

In this section we derive the S -transforms of a variety of useful random matrix ensembles. For a random matrix \mathbf{A} we will write $S_{\mathbf{A}}(t)$ as a function of the t -transform to connect to the standard literature. In future sections, the results will be much more clearly expressible in terms of the degrees of freedom $\text{df}_1(\lambda) \equiv -t(-\lambda)$. There, we will have $S_{\mathbf{A}}(t) = -S(-\text{df}_1)$.

A. Wigner

As their elements are Gaussian, the sum of two matrices $\mathbf{M}_1, \mathbf{M}_2$ taken from Wigner distributions of variance σ_1^2, σ_2^2 will be a Wigner matrix of variance $\sigma_1^2 + \sigma_2^2$. Because the R -transform is additive, we get that $R_{\mathbf{M}_i}(g)$ must be proportional to σ_i^2 . Further, by writing $R_{\mathbf{M}} = \sigma^2 f(g)$ and noting that $\alpha \mathbf{M}$ is a Wigner matrix with variance $\alpha^2 \sigma^2$, the scaling property in Equation (70) gives that $\alpha^2 \sigma^2 f(g) = \alpha \sigma^2 f(\alpha g)$ from which we conclude that $f(g)$ must be linear.

The constant can be fixed by considering the Laurent series expansion of $g_{\mathbf{M}}$:

$$g_{\mathbf{M}}(z) = \frac{1}{z} + \frac{1}{z^3} \text{tr}[\mathbf{M}^2] + O(z^{-4}) = \frac{1}{z - \frac{\text{tr}[\mathbf{M}^2]}{z}} + O(z^{-4}), \quad (76)$$

which gives at leading order that $R_{\mathbf{M}}(g) = \text{tr}[\mathbf{M}^2]g$. Because we've shown $R_{\mathbf{M}}$ is linear, this is exact. Using the fact that $\text{tr}[\mathbf{M}^2] = \sigma^2$, we get that

$$R_{\mathbf{M}}(g) = \sigma^2 g \quad (77)$$

More generally, the above equality follows immediately from the fact that the R -transform is the free cumulant generating function and the only nonzero free cumulant of a Wigner matrix is its second. As a consequence of Equation (76), we get that

$$g_{\mathbf{M}}(z) = \frac{1}{z - \sigma^2 g_{\mathbf{M}}(z)}. \quad (78)$$

We can solve for g as a function of z . We take the branch so that $g(z) \sim 1/z$ as $z \rightarrow \infty$ to obtain:

$$g(z) = \frac{1}{2\sigma^2} (z - \sqrt{z^2 - 4\sigma^2}), \quad (79)$$

from which we can extract the density using equation (10), yielding the famous **Wigner Semicircle Law**:

$$\rho(\lambda) = \frac{\sqrt{4\sigma^2 - \lambda^2}}{2\pi\sigma^2}, \quad -2\sigma \leq \lambda \leq 2\sigma. \quad (80)$$

We illustrate the semicircle law in Fig. 1. The Wigner distribution plays the role in free probability theory that the Gaussian distribution plays in ordinary probability theory: the spectral measure of properly normalized sums of free random matrices with independent and identically distributed elements converges to the Wigner distribution [120].

B. Square Projections

We consider symmetric square projection matrices $\mathbf{P} \in \mathbb{R}^{D \times D}$ onto N -dimensional subspaces of \mathbb{R}^D . \mathbf{P} satisfies $\mathbf{P} = \mathbf{P}^2$. \mathbf{P} thus has all eigenvalues either 0 or 1. We take N out of D eigenvalues to be unity and the rest to be zero. Defining the parameter $q = N/D$ we have that

$$t_{\mathbf{P}}(z) = qt_{\mathbf{I}}(z) \Rightarrow \zeta_{\mathbf{P}}(t) = \zeta_{\mathbf{I}}(t/q) = \frac{t/q}{t/q + 1}. \quad (81)$$

This directly yields the S -transform:

$$S_{\mathbf{P}}(t) = \frac{t+1}{t} \frac{t/q}{t/q + 1} = \frac{t+1}{t+q}. \quad (82)$$

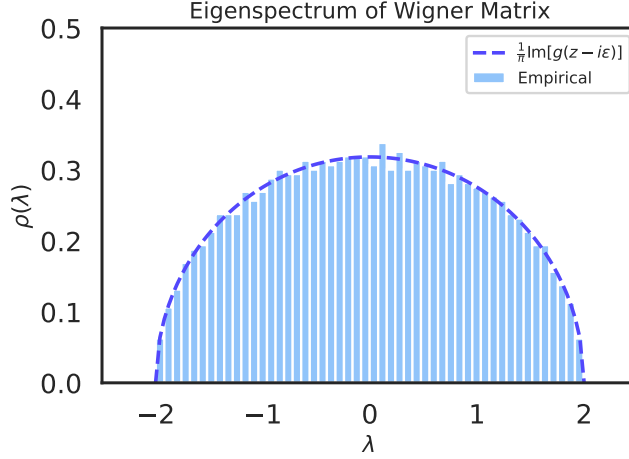


FIG. 1 Empirical eigenspectrum of an $N \times N$ Wigner matrix when $N = 2000$ (blue). Overlaid is the prediction of random matrix theory (dashed blue).

C. Rectangular Projections

Often, one will encounter a projection matrix $\mathbf{\Pi} \in \mathbb{R}^{D \times N}$ mapping from $\mathbb{R}^D \rightarrow \mathbb{R}^N$. We call this a rectangular projection because $\mathbf{\Pi}$ is a rectangular matrix. Here, the directions in the null space are not included in the codomain of $\mathbf{\Pi}$. One can still calculate $S_{\mathbf{\Pi}^\top \mathbf{A} \mathbf{\Pi}}(t)$ in terms of $S_{\mathbf{P}^* \mathbf{A}}(t) = S_{\mathbf{P}}(t) S_{\mathbf{A}}(t)$.

Let $\mathbf{P} \in \mathbb{R}^{D \times D}$ be the square form of $\mathbf{P}i$. The trick is to relate $t_{\mathbf{P}^* \mathbf{A}}(z)$ in D -dimensional space to $t_{\mathbf{\Pi}^\top \mathbf{A} \mathbf{\Pi}}(z)$ in N -dimensional space. Since we are keeping all the dimensions with nonzero eigenvalues, the unnormalized traces are the same, and we just need to account for the different normalizations. This means

$$\begin{aligned} N t_{\mathbf{\Pi}^\top \mathbf{A} \mathbf{\Pi}}(z) &= D t_{\mathbf{P}^* \mathbf{A}}(z) \\ \Rightarrow t_{\mathbf{\Pi}^\top \mathbf{A} \mathbf{\Pi}}(z) &= q^{-1} t_{\mathbf{P}^* \mathbf{A}}(z) \\ \Rightarrow \zeta_{\mathbf{\Pi}^\top \mathbf{A} \mathbf{\Pi}}(t) &= \zeta_{\mathbf{P}^* \mathbf{A}}(qt). \end{aligned} \quad (83)$$

In terms of S -transforms, using Equation (82) this yields:

$$S_{\mathbf{\Pi}^\top \mathbf{A} \mathbf{\Pi}}(t) = \frac{(t+1)qt}{t(qt+1)} S_{\mathbf{P}}(qt) S_{\mathbf{A}}(qt) = S_{\mathbf{A}}(qt). \quad (84)$$

D. White Wishart

The formula for the S -transform of a large Wishart matrix can be obtained by direct computation of $t_{\mathbf{A}}$, which is possible through a variety of methods (cavity, replica, etc). However, to demonstrate the manipulations that can be performed via the S -transform, we will derive this solely from knowing the S -transform of a projection as calculated in the preceding section.

In the large- N limit, it will turn out that the spectral properties of a Wishart matrix depend only on the ratio of the number of dimensions to the number of data points. We therefore will view Wishart matrices as a one-parameter family of distributions. Concretely, for $\mathbf{X} \in \mathbb{R}^{P \times D}$ a data matrix with i.i.d. standard Gaussian entries, we therefore write $\mathbf{W}_q = \frac{1}{P} \mathbf{X}^\top \mathbf{X}$ for the corresponding empirical covariance, where $q = N/P$.

Consider a $q = 1$ Wishart matrix $\mathbf{W}_1 \in \mathbb{R}^{D \times D}$. The act of subsampling from D down to P points corresponds to taking a free product of \mathbf{W}_1 with $\frac{D}{P} \mathbf{P}$ where $\mathbf{P} \in \mathbb{R}^{D \times D}$ is a square projection onto a random P -dimensional space. Applying Equation (82) this for any ratio D/P and using the fact that the resulting matrix has a Wishart distribution with P degrees of freedom yields

$$S_{\mathbf{W}_{D/P}}(t) = S_{\frac{D}{P} \mathbf{P}}(t) S_{\mathbf{W}_1}(t) = \frac{1+t}{1+\frac{D}{P}t} S_{\mathbf{W}_1}(t). \quad (85)$$

Here, we have applied equation (71) and recognized \mathbf{P} as a projection with parameter $\frac{P}{D}$.

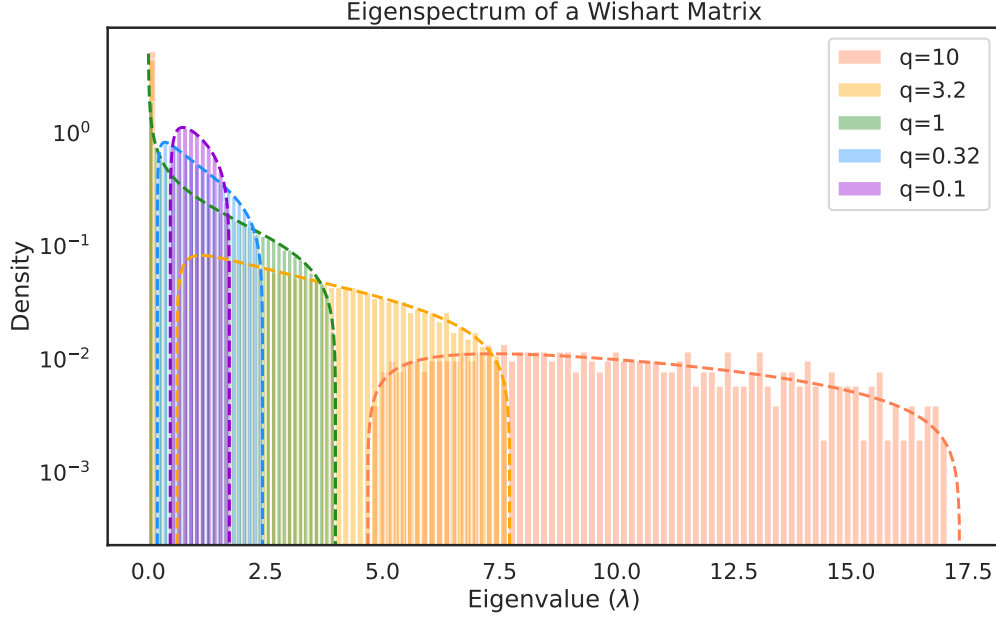


FIG. 2 A series of empirical eigenspectra of unstructured Wishart matrices across different values of the overparameterization ratio $q = D/P$. In all cases we have chosen $D = 1000$. The population covariance corresponds to a dirac delta function spike at $\lambda = 1$. The dashed lines are the prediction of random matrix theory, given by $\frac{1}{\pi} \text{Im } g_{\mathbf{W}}(\lambda - i\epsilon)$ as $\epsilon \rightarrow 0$. We see as $q \rightarrow 0$ we get close to a delta function at 1. For $q > 1$ we have some component that is a delta function at 0 with weight $q - 1$, separated from a bulk of eigenvalues. As q increases above q , this gap grows. At $q = 1$ we have no gap. This is the key effect leading to double descent in linear regression, as was observed in [16].

In addition to subsampling, we can also project out features from D to N . This involves multiplying by a *rectangular* projection with parameter N/D . Using equation (84) we get:

$$S_{\mathbf{W}_{N/P}}(t) = S_{\mathbf{W}_{D/P}}(tN/D) = \frac{1 + \frac{N}{D}t}{1 + \frac{N}{P}t} S_{\mathbf{W}_1}(tN/D). \quad (86)$$

We now take D much larger than N, P so that $N/D \rightarrow 0$ and write $q = N/P$. By considering the $P \rightarrow \infty$ limit and noting that there, $\mathbf{W}_q \rightarrow \mathbf{I}$ and $S_{\mathbf{I}}(t) = 1$ we fix the normalization and obtain:

$$S_{\mathbf{W}_q}(t) = \frac{1}{1 + qt}. \quad (87)$$

This is the most important S -transform for what follows.

A consequence of this is that via equation (75), we get

$$R_{\mathbf{W}}(g) = \frac{1}{1 - qg} \Rightarrow g_{\mathbf{W}}(z) = \frac{1}{z - \frac{1}{1 - qg_{\mathbf{W}}(z)}}. \quad (88)$$

This is a quadratic equation for $g_{\mathbf{W}}$, which can be solved exactly. Recalling that $g_{\mathbf{W}}(z)$ is the moment generating function in powers of $1/z$ and that $\text{tr}[\mathbf{W}^0] = 1$, we must have $g_{\mathbf{W}}(z) \sim 1/z$ at large z . This fixes the root and yields:

$$g_{\mathbf{W}}(z) = \frac{z + q - 1 - \sqrt{(z - \lambda_+)(z - \lambda_-)}}{2qz}, \quad \lambda_{\pm} = (1 \pm \sqrt{q})^2. \quad (89)$$

We can extract the spectrum using the equation (10). This time we must be careful as $g_{\mathbf{W}}(z)$ has a pole with residue $q - 1$ at 0 if $q > 1$. This is due to $q > 1$ Wishart matrices being non-invertible. We get:

$$\rho(\lambda) = \frac{q-1}{q} \delta(\lambda) \mathbf{1}_{q>1} + \frac{\sqrt{(\lambda_+ - \lambda)(\lambda - \lambda_-)}}{2\pi q \lambda}. \quad (90)$$

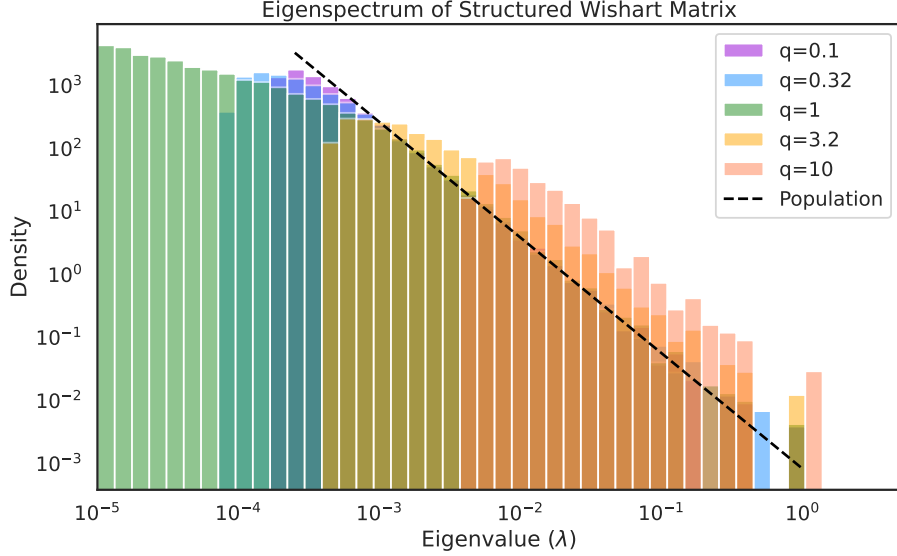


FIG. 3 The eigenspectra of structured Wishart matrices as one varies the overparameterization parameter $q = D/P$. In all cases $D = 1000$. The dashed black line is the eigenspectrum of the population covariance Σ . Here Σ is chosen to have structure $\lambda_k = k^{-\alpha}$ for $k = \{1, \dots, D\}$ and $\alpha = 1.2$.

Here $\mathbf{1}_{q>1}$ is the indicator function that is 1 when $q > 1$ and 0 otherwise. The result is the well-known **Marčenko-Pastur** eigenvalue distribution [121]. See Figure 2 for details.

We note at small q that this looks like a semicircle law of the identity matrix plus a Wigner matrix with entry noise having a standard deviation of \sqrt{q} . We noted that this is the leading order correction to covariance matrices in classical statistics in Section II.B Example 3.

We can also calculate the S -transform of the Gram matrix $\frac{1}{P}\mathbf{X}\mathbf{X}^\top \in \mathbb{R}^{P \times P}$ by recognizing it as $\frac{N}{P}$ times a Wishart with parameter $1/q$. Then using equation (71), we obtain another important S -transform:

$$S_{\frac{1}{P}\mathbf{X}\mathbf{X}^\top}(t) = \frac{1}{q} \frac{1}{1+t/q} = \frac{1}{q+t}. \quad (91)$$

E. Structured Wishart: Correlated Features

We have considered the case where the features are not identically drawn from an isotropic distribution in Section II.F, to motivate an application of the S -transform. Let us take $\hat{\Sigma} = \frac{1}{P}\mathbf{X}^\top\mathbf{X}$ where the rows of \mathbf{X} are i.i.d. but drawn from a Gaussian with nontrivial covariance $\mathbf{x}_\mu \sim \mathcal{N}(\mathbf{0}, \Sigma)$. Having explicitly calculated the S -transform for a white Wishart matrix \mathbf{W} with parameter $q = N/P$, we can now write:

$$S_{\hat{\Sigma}}(t) = \frac{S_{\Sigma}(t)}{1+qt}. \quad (92)$$

This lets us write

$$\begin{aligned} t_{\hat{\Sigma}}(z) &= t_{\Sigma}(\tilde{z}) \\ \tilde{z} &= \frac{z}{1+qt_{\Sigma}(\tilde{z})}. \end{aligned} \quad (93)$$

Given the spectrum of Σ , this gives a self-consistent equation for \tilde{z} . We will use this equation (with $z = -\lambda$, $\tilde{z} = -\kappa$, $t = -df_1$) very often in later sections.

F. Structured Wishart: Correlated Samples

The converse problem is for the rows to be drawn from an isotropic (unstructured) Gaussian $x_\mu \sim \mathcal{N}(\mathbf{0}, \mathbf{I})$ but for different datapoints to be correlated. This corresponds to a matrix of the form

$$\hat{\Sigma} = \frac{1}{P} \mathbf{X}^\top \mathbf{K} \mathbf{X}. \quad (94)$$

We can calculate the S transform of this as a rectangular projection with parameter N/P of the free product $\mathbf{K} * \mathbf{W}_1$ where $\mathbf{W}_1 \in \mathbb{R}^{P \times P}$ is a white Wishart. This gives

$$S_{\hat{\Sigma}}(t) = \frac{S_{\mathbf{K}}(qt)}{1+qt} \Rightarrow \zeta_{\hat{\Sigma}}(t) = q(1+t)\zeta_{\mathbf{K}}(qt) \quad (95)$$

This implies that

$$\begin{aligned} z &= \zeta_{\hat{\Sigma}}(t_{\hat{\Sigma}}(z)) = q(1+t_{\hat{\Sigma}}(z))\zeta_{\mathbf{K}}(qt_{\hat{\Sigma}}(z)) \\ &\Rightarrow qt_{\hat{\Sigma}}(z) = t_{\mathbf{K}}\left(\frac{z}{q(1+t_{\hat{\Sigma}}(z))}\right). \end{aligned} \quad (96)$$

Equivalently we can write this as

$$t_{\hat{\Sigma}}(z) = q^{-1}t_{\mathbf{K}}(\tilde{z}), \quad \tilde{z} = \frac{z}{q+t_{\mathbf{K}}(\tilde{z})}. \quad (97)$$

G. Shifted Wishart

Consider a white Wishart matrix \mathbf{W} shifted by the identity, $\mathbf{W} + \mathbf{J}\mathbf{I}$. Calculating the S -transform of this will be very helpful in the derivations that follow. One of the easiest ways to obtain this is to use equation (74) to relate the S transform to the R transform and then use equation (69) to perform the shift. This gives:

$$S_{\mathbf{W}+\mathbf{J}\mathbf{I}}(t) = \frac{1}{R_{\mathbf{W}+\mathbf{J}\mathbf{I}}(tS_{\mathbf{W}+\mathbf{J}\mathbf{I}})} = \frac{1}{J + \frac{1}{1-qtS_{\mathbf{W}+\mathbf{J}\mathbf{I}}(t)}}. \quad (98)$$

This can be solved exactly to give

$$S_{\mathbf{W}+\mathbf{J}\mathbf{I}}(t) = \frac{2}{1+J+qt + \sqrt{(1+J+qt)^2 - 4Jqt}}. \quad (99)$$

This is related to the generalization error of additively noised random features studied in Section VII. For our purposes in Section V, we will only care about the leading order behavior in J , which can be written as:

$$S_{\mathbf{W}+\mathbf{J}\mathbf{I}} = \frac{1}{1+qt + \frac{J}{1+qt}} + O(J^2) \quad (100)$$

H. Deep White Wishart Product

Consider a series of white Wishart matrices $\mathbf{W}_\ell = \frac{1}{N_{\ell-1}} \mathbf{X}_\ell^\top \mathbf{X}_\ell$ with $\mathbf{X}_\ell \in \mathbb{R}^{N_{\ell-1} \times N_\ell}$ having rows drawn i.i.d. from $\mathcal{N}(\mathbf{0}, \mathbf{I})$. Consider the following matrix product, which we will call a deep Wishart product:

$$\mathbf{C}_L = \frac{\mathbf{X}_L^\top \dots \mathbf{X}_1^\top \mathbf{X}_1 \dots \mathbf{X}_L, \mathbf{X}_L}{N_0 \dots N_{L-1}}. \quad (101)$$

By Equations (87) and (91), we have

$$\begin{aligned} S_{\frac{1}{N_{\ell-1}} \mathbf{X}_\ell^\top \mathbf{X}_\ell}(t) &= \frac{1}{1 + \frac{N_\ell}{N_{\ell-1}} t}, \\ S_{\frac{1}{N_{\ell-1}} \mathbf{X}_\ell \mathbf{X}_\ell^\top}(t) &= \frac{1}{\frac{N_\ell}{N_{\ell-1}} + t}. \end{aligned} \quad (102)$$

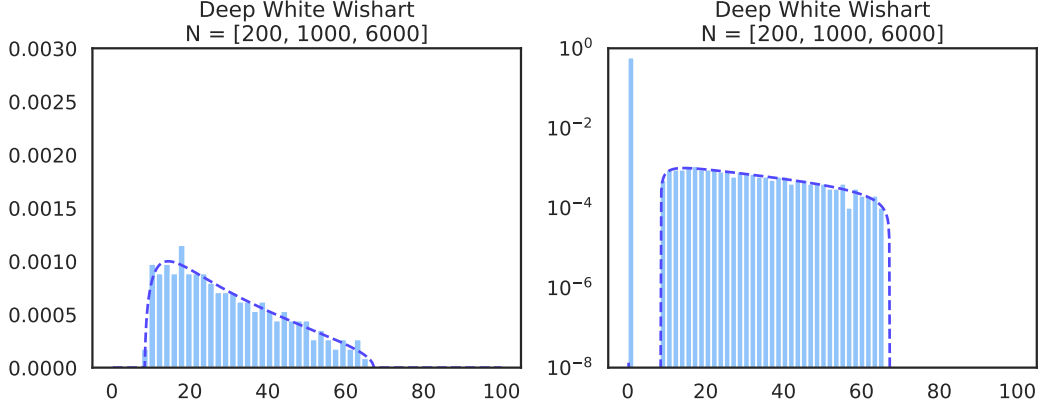


FIG. 4 The eigenspectrum of a depth-2 Wishart product $\frac{1}{N_0 N_1} \mathbf{X}_2^\top \mathbf{X}_1^\top \mathbf{X}_1 \mathbf{X}_2$, where $\mathbf{X}_\ell \in \mathbb{R}^{N_{\ell-1} \times N_\ell}$. Here, $N_0 = 200$, $N_1 = 1000$, and $N_2 = 6000$, as indicated by the list of dimensions in the title of each panel. The dashed solid lines are given by the predictions of (105) The left panel is linearly spaced on the y-axis while the right is logarithmically spaced.

At each step we look first at the free product

$$\begin{aligned} \tilde{\mathcal{C}}_\ell &\equiv \mathcal{C}_{\ell-1} * \left(\frac{1}{N_{\ell-1}} \mathbf{X}_\ell \mathbf{X}_\ell^\top \right) \in \mathbb{R}^{N_{\ell-1} \times N_{\ell-1}} \\ \Rightarrow S_{\tilde{\mathcal{C}}_\ell}(t) &= S_{\mathcal{C}_{\ell-1}}(t) \frac{1}{\frac{N_\ell}{N_{\ell-1}} + t}. \end{aligned} \quad (103)$$

Again, because the nonzero spectra of these matrices agree, their unnormalized traces are equal. Accounting for the different normalizations, we have $t_{\mathcal{C}_\ell} = \frac{N_{\ell-1}}{N_\ell} t_{\tilde{\mathcal{C}}_\ell} \Rightarrow \zeta_{\mathcal{C}_\ell}(t) = \zeta_{\tilde{\mathcal{C}}_\ell}(t N_\ell / N_{\ell-1})$. That means

$$\begin{aligned} S_{\mathcal{C}_\ell}(t) &= \frac{t+1}{t + \frac{N_{\ell-1}}{N_\ell}} S_{\tilde{\mathcal{C}}_\ell}(t N_\ell / N_{\ell-1}) \\ &= \frac{1}{1 + \frac{N_\ell}{N_{\ell-1}} t} S_{\mathcal{C}_{\ell-1}}(t N_\ell / N_{\ell-1}). \end{aligned} \quad (104)$$

Expanding this full product recursively yields:

$$S_{\mathcal{C}_L}(t) = \prod_{\ell=0}^{L-1} \frac{1}{1 + \frac{N_\ell}{N_\ell} t}, \quad (105)$$

consistent with the self-consistent equation derived in previous works [122; 123; 124]. As shown in Figure 4, numerical solution of the resulting self-consistent equation yields an excellent match to numerical experiment.

One can apply the same recursive argument to the Gram matrices:

$$\mathbf{K}_L = \frac{\mathbf{X}_1 \cdots \mathbf{X}_L \mathbf{X}_L^\top \cdots \mathbf{X}_1^\top}{N_0 \cdots N_{L-1}}. \quad (106)$$

This yields:

$$S_{\mathbf{K}_L}(t) = \prod_{\ell=1}^L \frac{1}{\frac{N_\ell}{N_0} + t}. \quad (107)$$

I. Deep Structured Wishart Product

Now, let us allow for arbitrary structure in the features of each Wishart matrix in the deep product. We write $\frac{1}{N_{\ell-1}} \mathbf{M}_\ell^\top \mathbf{M}_\ell = \mathbf{W}_\ell * \boldsymbol{\Sigma}_\ell$ for \mathbf{W}_ℓ a white Wishart and $\boldsymbol{\Sigma}_\ell$ the population covariance of the ℓ -th Wishart matrix. We

then get

$$S_{\tilde{C}_\ell}(t) = S_{C_{\ell-1}}(t) \frac{1+t}{\frac{N_\ell}{N_{\ell-1}} + t} S_{W_\ell}(tN_{\ell-1}/N_\ell) S_{\Sigma_\ell}(tN_{\ell-1}/N_\ell) \quad (108)$$

$$\begin{aligned} \Rightarrow S_{C_\ell}(t) &= \frac{1+t}{\frac{N_{\ell-1}}{N_\ell} + t} S_{\tilde{C}_\ell}(tN_\ell/N_{\ell-1}) \\ &= \frac{1+t}{\frac{N_{\ell-1}}{N_\ell} + t} \frac{1+t \frac{N_\ell}{N_{\ell-1}}}{\frac{N_\ell}{N_{\ell-1}} + t \frac{N_\ell}{N_{\ell-1}}} S_{W_\ell}(t) S_{\Sigma_\ell}(t) S_{C_{\ell-1}}(tN_\ell/N_{\ell-1}) \\ &= \frac{S_{\Sigma_\ell}(t)}{1 + \frac{N_\ell}{N_{\ell-1}} t} S_{C_{\ell-1}}(tN_\ell/N_{\ell-1}). \end{aligned} \quad (109)$$

Expanding this recursively gives

$$S_{C_L}(t) = \prod_{\ell=0}^{L-1} \frac{S_{\Sigma_\ell}(\frac{N_L}{N_\ell} t)}{1 + \frac{N_L}{N_\ell} t}. \quad (110)$$

In terms of the inverse functions ζ_{Σ_ℓ} we get:

$$\frac{1}{S_{C_L}(t)} = \prod_{\ell=0}^{L-1} \frac{N_L}{N_\ell} t \zeta_{\Sigma_\ell} \left(\frac{N_L}{N_\ell} t \right). \quad (111)$$

Similarly one gets:

$$\frac{1}{S_{K_L}(t)} = \prod_{\ell=1}^L t \zeta_{\Sigma_\ell} \left(\frac{N_0}{N_L} t \right). \quad (112)$$

This is consistent with the self-consistent equation derived in [123], where it was shown that the resulting prediction for the spectral density gives good matches with numerical experiment.

V. LINEAR AND KERNEL RIDGE REGRESSION

In this section, we will use the random matrix technology developed thus far to compute sharp asymptotics for the training and generalization error in linear ridge regression in the limit of dataset size P and input dimension N going to infinity jointly with fixed ratio, as in [12; 13; 14; 16; 17]. We will assume that the data is distributed according to a high-dimensional Gaussian. In the proportional limit, this assumption is not restrictive due to the phenomenon of Gaussian equivalence, which states that the generalization error for models with suitably-distributed non-Gaussian covariates will coincide with that of a Gaussian model with matched first and second moments. We will provide a more detailed discussion of Gaussian equivalence in Section V.D. We will further show how these results naturally give the formulae for the generalization error of kernel ridge regression as studied in [20; 21; 22].

As a technical note: Although the formulas that will be presented hold only in the limit of $N, P \rightarrow \infty$ with fixed ratio, we will keep P, N explicit in all of the formulas that we present in this and subsequent sections. We will view all expressions as the leading order term in an asymptotic series in $1/P, 1/N$. The subleading finite N, P contributions can in principle be calculated through finite N, P corrections to the spectrum of the covariance together with adding crossing diagrams in the derivation of Section III. The latter is given by the genus expansion in the full Weingarten formula [116]. In this sense, the deterministic equivalence \simeq will be taken to mean that these quantities are equal after neglecting the higher order terms in the series. In practice, we find excellent agreement from just the leading term.

A. Linear Regression with Structured Gaussian Covariates

We begin by defining our statistical model for training data, along the way fixing notation that will be used throughout the paper. We consider P data points $\mathbf{x}_\mu \in \mathbb{R}^N$, which we assume to be drawn i.i.d. from a N -dimensional Gaussian distribution with zero mean and covariance Σ :

$$\mathbf{x}_\mu \underset{\text{i.i.d.}}{\sim} \mathcal{N}(\mathbf{0}, \Sigma). \quad (113)$$

We generate labels y_μ corresponding to each \mathbf{x}_μ by

$$y_\mu = \bar{\mathbf{w}} \cdot \mathbf{x}_\mu + \epsilon_\mu, \quad (114)$$

where $\bar{\mathbf{w}} \in \mathbb{R}^N$ is the **signal** or **teacher weights** and ϵ_μ is **label noise** which models variability in y_μ conditional on \mathbf{x}_μ . Unless stated otherwise, we assume that $\bar{\mathbf{w}}$ is deterministic. We take the noise to be independent and Gaussian:

$$\epsilon_\mu \underset{\text{i.i.d.}}{\sim} \mathcal{N}(0, \sigma_\epsilon^2). \quad (115)$$

Collecting the covariates into a design matrix $\mathbf{X} \in \mathbb{R}^{P \times N}$ with $\mathbf{X}_{\mu i} = [\mathbf{x}_\mu]_i$, the labels into a vector $\mathbf{y} \in \mathbb{R}^P$, and the label noises into a vector $\boldsymbol{\epsilon} \in \mathbb{R}^P$, our statistical model can therefore be summarized as

$$\mathbf{y} = \mathbf{X} \bar{\mathbf{w}} + \boldsymbol{\epsilon}. \quad (116)$$

For brevity, we denote our data model by \mathcal{D} , and write $\mathbb{E}_{\mathcal{D}}[\cdot] = \mathbb{E}_{\mathbf{X}, \boldsymbol{\epsilon}}[\cdot]$. We will take the eigenvalues of Σ and the norm of $\bar{\mathbf{w}}$ to be of order unity with respect to N .

We will consider ridge regression with as in Equation (4). The weights of the ridge regression estimator are then given by

$$\begin{aligned} \hat{\mathbf{w}} &= (\mathbf{X}^\top \mathbf{X} + P\lambda \mathbf{I})^{-1} \mathbf{X}^\top \mathbf{y} \\ \Rightarrow \bar{\mathbf{w}} - \hat{\mathbf{w}} &= P\lambda (\mathbf{X}^\top \mathbf{X} + P\lambda \mathbf{I})^{-1} \bar{\mathbf{w}} - (\mathbf{X}^\top \mathbf{X} + P\lambda \mathbf{I})^{-1} \mathbf{X}^\top \boldsymbol{\epsilon} \\ &= \lambda (\hat{\Sigma} + \lambda \mathbf{I})^{-1} \bar{\mathbf{w}} - \frac{1}{P} (\hat{\Sigma} + \lambda \mathbf{I})^{-1} \mathbf{X}^\top \boldsymbol{\epsilon}. \end{aligned} \quad (117)$$

Here, we have taken $\hat{\Sigma} := \frac{1}{P} \mathbf{X}^\top \mathbf{X} \in \mathbb{R}^{N \times N}$ to be the empirical covariance obtained from sampling P datapoints. As $P \rightarrow \infty$ we have $\hat{\Sigma} \rightarrow \Sigma$ and $\mathbb{E}_{\hat{\Sigma} \sim \mathcal{N}} \hat{\Sigma} = \Sigma$. On a held out identically distributed test point \mathbf{x}' (i.e. $\mathbb{E}[\mathbf{x}' \mathbf{x}'^\top] = \Sigma$) we

calculate the average generalization error.

$$\begin{aligned}
E_g &= \mathbb{E}_{\mathcal{D}, \mathbf{x}'} \|\mathbf{x}'^\top \hat{\mathbf{w}} - \mathbf{x}'^\top \bar{\mathbf{w}}\|^2 \\
&= \mathbb{E}_{\hat{\Sigma}, \epsilon} [(\bar{\mathbf{w}} - \hat{\mathbf{w}})^\top \Sigma (\bar{\mathbf{w}} - \hat{\mathbf{w}})] \\
&= \lambda^2 \mathbb{E}_{\hat{\Sigma}} [\bar{\mathbf{w}}^\top (\hat{\Sigma} + \lambda \mathbf{I})^{-1} \Sigma (\hat{\Sigma} + \lambda \mathbf{I})^{-1} \bar{\mathbf{w}}] + \frac{\sigma_\epsilon^2}{P} \mathbb{E}_{\hat{\Sigma}} \text{Tr} [\hat{\Sigma} (\hat{\Sigma} + \lambda \mathbf{I})^{-1} \Sigma (\hat{\Sigma} + \lambda \mathbf{I})^{-1}] \\
&= \underbrace{-\lambda^2 \partial_J \bar{\mathbf{w}}^\top \mathbb{E}_{\hat{\Sigma}} [(\hat{\Sigma} + J \Sigma + \lambda \mathbf{I})^{-1}] \bar{\mathbf{w}}}_{\text{Signal}} \Big|_{J=0} + \underbrace{\frac{\sigma_\epsilon^2}{P} \partial_\lambda \mathbb{E}_{\hat{\Sigma}} [\lambda \text{Tr} [\Sigma (\hat{\Sigma} + \lambda \mathbf{I})^{-1}]]}_{\text{Noise}}.
\end{aligned} \tag{118}$$

We get two terms. The first, which we call the *signal* term, involves $\bar{\mathbf{w}}$ directly. The other, which we call the *noise* term is proportional to σ_ϵ^2 and independent of $\bar{\mathbf{w}}$. Both of these terms have been written in terms of matrix resolvents in the last line. We will now perform the average over the data in both of these terms using the methods developed in the prior section.

To evaluate the noise term, we will simply need the deterministic equivalence stated in Equation (36). For the signal term, we need the equation for the S -transform of a shifted Wishart matrix obtained in Section IV.G as well as the deterministic equivalence between resolvents for general noise structure given by Equation (37).

B. Derivation

We evaluate the noise term first. There, using the deterministic equivalence (36) of the resolvent we have that

$$\text{Noise} \simeq \frac{\sigma_\epsilon^2}{P} \partial_\lambda [\kappa \text{Tr} [\Sigma (\Sigma + \kappa \mathbf{I})^{-1}]] = \sigma_\epsilon^2 \frac{d\kappa}{d\lambda} \frac{N}{P} \partial_\kappa [\kappa \text{df}_1(\kappa)] = \sigma_\epsilon^2 \frac{d\kappa}{d\lambda} \frac{N}{P} \text{df}_2(\kappa) \tag{119}$$

where we have used Equation (20) in the last equality to relate df_1 to df_2 . Recalling that $t_{\mathbf{A}} = -\text{df}_{\mathbf{A}}^1$ for any matrix \mathbf{A} we can write $\kappa = S_{\mathbf{W}} \lambda$ as:

$$\kappa = \frac{\lambda}{1 - \frac{N}{P} \text{df}_{\Sigma}^1(\kappa)}. \tag{120}$$

Adopting the shorthand $\text{df}_1 = \text{df}_{\Sigma}^1(\kappa)$, This lets us evaluate κ and its derivative:

$$\kappa \left(1 - \frac{N}{P} \text{df}_1(\kappa)\right) = \lambda \Rightarrow \frac{d\lambda}{d\kappa} = 1 - \frac{N}{P} \text{df}_2(\kappa). \tag{121}$$

By defining the quantity

$$\gamma \equiv \frac{N}{P} \text{df}_2(\kappa) = \frac{1}{P} \text{Tr} [\Sigma^2 (\Sigma + \kappa \mathbf{I})^{-2}] \tag{122}$$

we get that

$$\text{Noise} = \sigma_\epsilon^2 \frac{\gamma}{1 - \gamma}. \tag{123}$$

For the signal term, we need to calculate a deterministic equivalent for the resolvent $(\lambda + \hat{\Sigma} + J \Sigma)^{-1}$. The trick is to realize that $\hat{\Sigma} + J \Sigma$ can be written as the free product of Σ with a shifted white Wishart matrix. That is, $\hat{\Sigma} + J \Sigma = \Sigma^{1/2} (\mathbf{W} + J \mathbf{I}) \Sigma^{1/2}$. Then, using Equation (37):

$$(\hat{\Sigma} + J \Sigma + \lambda)^{-1} \simeq \frac{\kappa_J}{\lambda} (\Sigma + \kappa_J \mathbf{I})^{-1}, \quad \kappa_J = S_{\mathbf{W} + J \mathbf{I}} \lambda. \tag{124}$$

The signal term then becomes:

$$\text{Signal} \simeq -\lambda \partial_J [\kappa_J \bar{\mathbf{w}}^\top (\Sigma + \kappa_J \mathbf{I})^{-1} \bar{\mathbf{w}}] \Big|_{J=0} = -\lambda \frac{d\kappa_J}{dJ} \Big|_{J=0} \bar{\mathbf{w}}^\top \Sigma (\Sigma + \kappa \mathbf{I})^{-2} \bar{\mathbf{w}}. \tag{125}$$

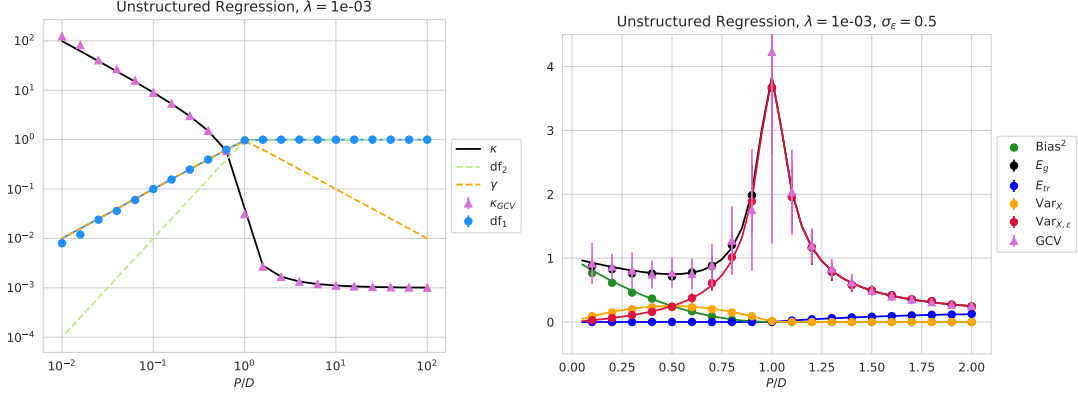


FIG. 5 Linear regression on unstructured covariates, i.e. $\Sigma = \mathbf{I}$. Left: we plot theory (solid lines) for the various quantities of interest $\kappa, \gamma, df_1, df_2$. We also plot the empirical estimate of df_1 , namely $df_{\Sigma}(\lambda)$. Using this, we estimate of κ_1 using the training set and find excellent agreement. Right: We plot the training and generalization (blue, black respectively) as well as the bias (green) and variances (orange, red) due to the dataset and label noise. Dots and error bars indicate empirical simulations over 20 seeds over the training set. Solid curves show theory. We find excellent agreement for all relevant quantities. The GCV estimator is plotted as orchid triangles and again we find strong agreement with the generalization error.

We have calculated the shifted Wishart S -transform $S_{\mathbf{W}+J\mathbf{I}}$ in Section IV.G. There, using Equation (100), we have at leading order in J that

$$\kappa_J \left(1 - \frac{N}{P} df_1(\kappa_J) + J \frac{\kappa_J}{\lambda} \right) = \lambda \Rightarrow - \frac{d\kappa_J}{dJ} \Big|_{J=0} = \frac{\kappa^2/\lambda}{1-\gamma}. \quad (126)$$

This gives the full generalization error:

$$E_g \simeq - \frac{\kappa^2 \text{tf}'_{\Sigma, \bar{\mathbf{w}}}(\kappa_2)}{1-\gamma} + \sigma_\epsilon^2 \frac{\gamma}{1-\gamma}. \quad (127)$$

Letting η_i be the eigenvalues of the covariance matrix Σ , this can be written as:

$$E_g \simeq \frac{\kappa^2}{1-\gamma} \sum_{k=1}^N \frac{\eta_k \bar{w}_k^2}{(\kappa + \eta_k)^2} + \sigma_\epsilon^2 \frac{\gamma}{1-\gamma}. \quad (128)$$

This result recovers the sharp asymptotics for linear ridge regression obtained with various methods in prior works, including [17; 20; 21]. As noted in Section II.F, modes with $\eta_k \gg \kappa$ are learned while modes with $\eta_k \ll \kappa$ are not yet learned.

Equation (128) is sometimes referred to as an **omniscient risk estimate**. This is because it requires exact knowledge of the spectrum of Σ , the scale of σ_ϵ^2 , and the form of $\bar{\mathbf{w}}$ in order to calculate this. In statistical learning, it is strongly preferable to be able to build such an estimator out of the training data alone, without having to know all the details of the distribution of \mathbf{x} and the data generating process for y .

As we will show in Section V.E, one can estimate the out-of-sample risk from *only* the training error and S . Because of the key property that S can be calculated solely in terms of the sample covariance and the original “bare” ridge λ , namely $S = (1 - qdf_{\Sigma}^1(\lambda))^{-1}$, we obtain a way to estimate the out-of-sample risk using in-sample data alone. This has been obtained in prior works [72; 92; 98; 125] under the name of **kernel alignment risk estimator** (KARE) or **generalized cross-validation** (GCV).

C. Example: Isotropic Linear Regression

In the case where $\Sigma = \mathbf{I}$, the formulas simplify. This setting has been studied in [12; 16]. Here, $df_{\Sigma}^1(\kappa) = (1 + \kappa)^{-1}$ and the self-consistent equation for the renormalized ridge κ can be solved exactly:

$$\kappa = \frac{\lambda}{1 - \frac{N}{P} \frac{1}{1+\kappa}} \Rightarrow \kappa = \frac{1}{2} \left(\lambda + \frac{N}{P} - 1 + \sqrt{\left(\lambda + \frac{N}{P} - 1 \right)^2 + 4 \frac{N}{P} \lambda} \right). \quad (129)$$

The equations for the generalization of ridge regression can then be written down explicitly in terms of κ .

$$E_g = \frac{1}{1-\gamma} \frac{\kappa^2}{(1+\kappa)^2} + \sigma_\epsilon^2 \frac{\gamma}{1-\gamma}, \quad \gamma = \frac{N}{P} \frac{1}{(1+\kappa)^2}. \quad (130)$$

In the limit of $\lambda \rightarrow 0$ we get $\kappa = \max(0, \frac{N}{P} - 1)$. Thus, in the underparameterized ridgeless limit where $P > N$, $\kappa = 0$ and the ridge is not renormalized. However, in the overparameterized setting where $P < N$, even at zero ridge κ has the finite value $\frac{N}{P} - 1$. Similarly we have $\gamma = \min(\frac{P}{N}, \frac{N}{P})$. Thus,

$$E_g \simeq \begin{cases} \sigma_\epsilon^2 \frac{N/P}{1 - N/P} & \text{underparameterized} \\ \left(1 - \frac{P}{N}\right) + \sigma_\epsilon^2 \frac{P/N}{1 - P/N} & \text{overparameterized.} \end{cases} \quad (131)$$

We plot this in Figure 5.

D. Connection to Kernel Regression via Gaussian Universality

So far, we have focused on linear regression directly from the space in which the covariates live. However, both in machine learning at large and in the specific setting of linearized neural networks as outlined in §I.A, one is often interested in the case in which the covariates are transformed into some higher-dimensional feature space via a fixed mapping, i.e., in **kernel regression**.

Concretely, consider a case in which we have P datapoints $\mathbf{x}_\mu \in \mathbb{R}^D$ sampled i.i.d. from some probability measure $\rho(\mathbf{x})$. Then, choose some kernel $K(\mathbf{x}, \mathbf{x}')$ with which to measure similarities. Then, under suitable conditions, the kernel has a Mercer decomposition

$$K(\mathbf{x}, \mathbf{x}') = \sum_{i=1}^N \eta_i \phi_i(\mathbf{x}) \phi_i(\mathbf{x}') \quad (132)$$

with eigenvalues $\eta_i \geq 0$ and eigenfunctions ϕ_i , which satisfy

$$\begin{aligned} \int \phi_i(\mathbf{x}) K(\mathbf{x}, \mathbf{x}') \phi_j(\mathbf{x}') d\rho(\mathbf{x}) d\rho(\mathbf{x}') &= \Sigma_{ij} = \delta_{ij} \eta_i, \\ \mathbb{E}[\phi_i \phi_j] &= \int \phi_i(\mathbf{x}) \phi_j(\mathbf{x}) d\rho(\mathbf{x}) = \delta_{ij}, \quad \mathbb{E}[\phi_i] = \int \phi_i(\mathbf{x}) d\rho(\mathbf{x}) = 0. \end{aligned} \quad (133)$$

We can write $K(\mathbf{x}, \mathbf{x}') = \sum_i \eta_i \phi_i(\mathbf{x}) \phi_i(\mathbf{x}') = \sum_i \psi_i(\mathbf{x}) \psi_i(\mathbf{x}')$ for features $\psi_i(\mathbf{x}) := \sqrt{\eta_i} \phi_i(\mathbf{x})$. In this setting, we are performing linear regression from a feature space spanned by the functions ψ_i . We take y to be generated from a linear combination of the features ψ together with additive noise ϵ :

$$y_\mu = \bar{\mathbf{w}} \cdot \psi(\mathbf{x}_\mu) + \epsilon_\mu. \quad (134)$$

Here, we have assumed that the dimension N of the kernel’s Hilbert space is finite. We will comment on how to relax this assumption and take $N \rightarrow \infty$ faster than P at the end. We remark that very recent works show how one can work directly in an infinite-dimensional Hilbert space using “dimension-free” techniques [126; 127].

Let $\Psi \in \mathbb{R}^{P \times N}$ be the design matrix, with $\Psi_{\mu i} = \psi_i(\mathbf{x}^\mu)$. To apply our earlier results, we would like to claim that in the limit $P, N \rightarrow \infty$ with N/P fixed we can replace the empirical covariance matrix $\hat{\Sigma} = \frac{1}{P} \Psi^\top \Psi$ with one where the features are drawn from a Gaussian distribution with matching population covariance. For certain combinations of data distribution and kernel—most simply for the case where $\rho(\mathbf{x})$ is the uniform measure on the sphere and $K(\mathbf{x}, \mathbf{x}') = k(\mathbf{x}^\top \mathbf{x}')$ is a dot-product kernel and if the input dimension D is taken to infinity proportionally with some power of the dataset size—this Gaussian equivalence can be rigorously justified [58; 59; 60; 61; 62; 127].

Then, using (127) and redefining $\kappa \rightarrow \kappa/P$, we recover the results of [20; 21]:

$$E_g = \frac{1}{1-\gamma} \sum_{k=1}^N \frac{\eta_k \bar{w}_k^2 \kappa^2}{(\kappa + P\eta_k)^2} + \sigma_\epsilon^2 \frac{\gamma}{1-\gamma}, \quad \gamma = \sum_{k=1}^N \frac{P\eta_k^2}{(\kappa + P\eta_k)^2}. \quad (135)$$

Although this calculation was performed at finite N , assuming that the spectrum of Σ decays quickly enough (as $\eta \sim k^{-b}$ for $b > 1$), one can justify taking $N \rightarrow \infty$ at finite λ . This is because df_1 , df_2 , and tf_1 will become independent

of the cutoff N at this spectral decay, as shown in §V.I. However, when $\lambda \rightarrow 0$ it is not clear that one can interchange the ridgeless limit with the large N limit. It is not obvious when Gaussian equivalence should hold for general kernel methods; some sufficient conditions are obtained in very recent work of Misiakiewicz and Saeed [127], who obtain dimension-free results with non-asymptotic error bounds in P . Indeed, one can consider low-dimensional settings in which this theory breaks; see [128] for examples.

E. The S -Transform as a Train-Test Gap

Using the same tools, one can also efficiently calculate the training error:

$$\begin{aligned}
E_{tr} &= \frac{1}{P} \|\mathbf{y} - \hat{\mathbf{y}}\|^2 \\
&= \frac{\lambda^2}{P} \|(\frac{1}{P} \mathbf{X} \mathbf{X}^\top + \lambda \mathbf{I})^{-1} (\mathbf{X} \bar{\mathbf{w}} + \boldsymbol{\epsilon})\|^2 \\
&= \lambda^2 \bar{\mathbf{w}}^\top \hat{\boldsymbol{\Sigma}} (\hat{\boldsymbol{\Sigma}} + \lambda \mathbf{I})^{-2} \bar{\mathbf{w}} - \frac{\sigma_\epsilon^2 \lambda^2}{P} \text{Tr} \left[(\hat{\boldsymbol{\Sigma}} + \lambda \mathbf{I})^{-2} \right] \\
&= -\lambda^2 \partial_\lambda \bar{\mathbf{w}}^\top \hat{\boldsymbol{\Sigma}} (\hat{\boldsymbol{\Sigma}} + \lambda \mathbf{I})^{-1} \bar{\mathbf{w}} - \sigma_\epsilon^2 \lambda^2 \frac{N}{P} \partial_\lambda \left[-g_{\frac{1}{P} \mathbf{X} \mathbf{X}^\top}(-\lambda) \right].
\end{aligned} \tag{136}$$

Using relationship (13), we can write the second term as a derivative on:

$$-g_{\frac{1}{P} \mathbf{X} \mathbf{X}^\top}(-\lambda) = \frac{1 - \text{df}_{\frac{1}{P} \mathbf{X} \mathbf{X}^\top}^1(\lambda)}{\lambda} = \frac{1 - \frac{N}{P} \text{df}_{\hat{\boldsymbol{\Sigma}}}^1(\lambda)}{\lambda} \simeq \frac{1}{\kappa}. \tag{137}$$

We now apply strong deterministic equivalence, giving:

$$\begin{aligned}
E_{tr} &\simeq \frac{\lambda^2}{1 - \gamma} \bar{\mathbf{w}}^\top \boldsymbol{\Sigma} (\boldsymbol{\Sigma} + \kappa \mathbf{I})^{-2} \bar{\mathbf{w}} + \frac{\sigma_\epsilon^2}{1 - \gamma} \frac{\lambda^2}{\kappa^2} \\
&= \frac{\lambda^2}{\kappa^2} [E_g + \sigma_\epsilon^2].
\end{aligned} \tag{138}$$

This relationship was studied in [72; 92] and also derived in [21]. If we include noise at test time, the out-of-sample risk is $E_{out} = E_g + \sigma_\epsilon^2$. Recognizing $\lambda^2/\kappa^2 = S_{\mathbf{W}}(t)^{-2}$ we get:

$$E_{out} \simeq E_{tr} S_{\mathbf{W}}^2(t) = \frac{E_{tr}}{(1 - \frac{N}{P} \text{df}_{\hat{\boldsymbol{\Sigma}}}^1(\kappa))^2} \simeq \frac{E_{tr}}{(1 - \frac{N}{P} \text{df}_{\hat{\boldsymbol{\Sigma}}}^1(\lambda))^2} \equiv E_{GCV}. \tag{139}$$

Here, we have recognized the definition of the GCV risk estimator E_{GCV} [98; 125], which can be estimated *from the training data alone*. Estimating the S -transform in this way is also equivalent to the **kernel alignment risk estimator** (KARE) defined in [72]. By writing

$$E_{tr} = \frac{\lambda^2}{P} \mathbf{y}^\top (\frac{1}{P} \mathbf{X} \mathbf{X}^\top + \lambda \mathbf{I})^{-2} \mathbf{y}, \quad 1 - \frac{N}{P} \text{df}_{\hat{\boldsymbol{\Sigma}}}^1(\lambda) = \lambda \frac{1}{P} \text{Tr}[(\frac{1}{P} \mathbf{X} \mathbf{X}^\top + \lambda \mathbf{I})^{-1}] \tag{140}$$

we get the KARE:

$$E_{out} \simeq \frac{\frac{1}{P} \mathbf{y}^\top (\frac{1}{P} \mathbf{X} \mathbf{X}^\top + \lambda \mathbf{I})^{-2} \mathbf{y}}{(\frac{1}{P} \text{Tr}[(\frac{1}{P} \mathbf{X} \mathbf{X}^\top + \lambda \mathbf{I})^{-1}])^2}. \tag{141}$$

Wei *et al.* [92] have found that this accurately predicts neural scaling laws for kernel regression with the (finite width) neural tangent kernel of a pretrained neural network.

The S transform also allows us to also estimate κ directly from a given training set, without full knowledge of the data distribution of data generating process. This estimate comes from the relationship:

$$\kappa \simeq \frac{\lambda}{1 - \frac{N}{P} \text{df}_{\hat{\boldsymbol{\Sigma}}}^1(\lambda)}. \tag{142}$$

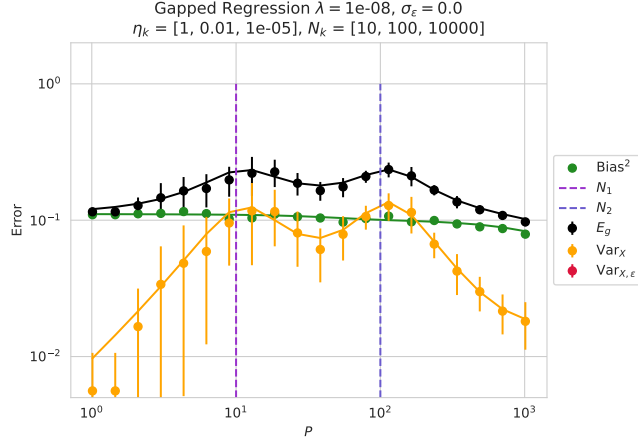


FIG. 6 Double descent without label noise in a linear regression task. Here, Σ has an eigenspectrum with eigenvalues η_1, η_2, η_3 that have values $1, 10^{-2}, 10^{-5}$ and multiplicities $10, 10^2, 10^4$ respectively. The dashed line indicates when $P \approx N_k$. The teacher \bar{w} has increasing power in higher modes, given by $1, 10, 10^2$ respectively. The fact that the higher modes are not learnable leads to an effective label-noise like effect that causes this multiple descent phenomenon. We stress that the variance $\text{Var}_{\mathbf{X}, \epsilon} = 0$ since there is no label noise.

This is equivalent to equation (137), namely

$$\kappa \simeq \frac{1}{-g_{\frac{1}{P}} \mathbf{X} \mathbf{X}^\top (-\lambda)} = \frac{1}{\frac{1}{P} \text{Tr} \left[\left(\frac{1}{P} \mathbf{X} \mathbf{X}^\top + \lambda \mathbf{I} \right)^{-1} \right]}. \quad (143)$$

By virtue of $\text{df}_{\Sigma}^1(\lambda) \geq 0$ we have that $S \geq 1$ implying that $\kappa \geq \lambda$ and $E_{out} \geq E_{tr}$.

In summary, given a finite size training set, one can come up with an estimate of \hat{S} of the S transform without full “omniscient” knowledge of the data distribution or data generating process. This is given by $\hat{S} = (1 - q \text{df}_{\Sigma}^1(\lambda))^{-1}$. This in turn gives estimates of the renormalized ridge and out of sample error via:

$$\kappa \simeq \hat{S} \lambda, \quad E_{out} \simeq \hat{S}^2 E_{tr}. \quad (144)$$

F. Double Descent as a Renormalization Effect

We see that E_g explodes when $\gamma \rightarrow 1$. This is the effect that drives the overfitting peak in classical statistical learning. In the overparameterized setting $P > N$, we have that $\lambda \rightarrow 0$ will imply that the renormalized ridge will also go to zero. Since $\gamma = \frac{N}{P} \text{df}_2 \leq \frac{N}{P}$ we get that the variance explodes only when $N \rightarrow P$ and $\lambda \rightarrow 0$. In Section V.H we will do a fine-grained analysis of the sources of this variance explosion.

Because one can write $\gamma = \text{df}_{\frac{1}{P}}^2 \mathbf{X} \mathbf{X}^\top (\kappa) \leq 1$, if κ stays at zero in the overparameterized limit, then $\gamma = 1$ and the model will continue to overfit. One will then get infinite generalization error in this setting.

However, because κ becomes renormalized in equation (128) to be nonzero even when $\lambda = 0$ when $N > P$, one gets that $\text{df}_2 < 1$ in the overparameterized setting. Indeed, in that setting we have $\text{df}_1 = P/N$ so that S_W has a pole at $\lambda = 0$. By Equation (23) we have $\gamma \leq \frac{1}{1 + \kappa/\eta_1}$ where η_1 is the maximal eigenvalue. Moreover, because, κ grows with N in the overparameterized setting, we have that γ shrinks away from 1. The $(1 - \gamma)^{-1}$ divergence is then reduced. In this way, the renormalized ridge captures the **inductive bias** of overparameterization towards simple interpolating solutions that can still generalize well.

G. Multiple Descent without Label Noise

If one assumes that the spectrum is a series of plateaus at value η_k with degeneracy N_k with a large separation of scale between $\eta_k \gg \eta_{k+1}$, one can obtain multiple descents, even in the absence of label noise. This phenomenon was studied in the kernel regression setting by [21; 59; 60; 61; 62] and the linear regression setting by [95]. In the vicinity

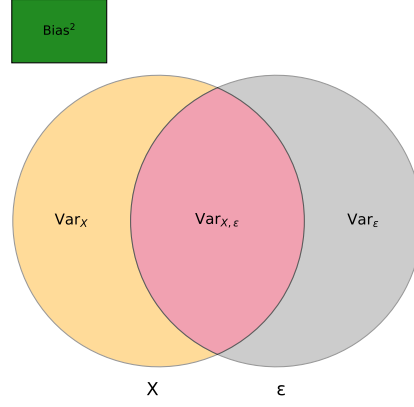


FIG. 7 Schematic of the bias-variance decomposition for linear regression. The color scheme matches the plots in Figures 5, 6 and 9. Grey regions do not contribute to variance.

of each plateau, one can approximately solve the equation for κ by recognizing:

$$\frac{N}{P} \text{df}_1(\kappa) \approx \frac{1}{P} \left[\sum_{k < \ell} N_k + \frac{\eta_\ell N_\ell}{\kappa + \eta_\ell} + \sum_{k > \ell} \frac{N_k \eta_k}{\kappa} \right]. \quad (145)$$

The first term represents all the modes that have been learned. This requires $N_k \ll P$ for each k . Given that finitely many modes have been learned, we can neglect the first term. Then, defining $\tilde{\sigma}_\ell \equiv \frac{1}{P} \sum_k N_k \eta_k$ and $q_\ell \equiv N_\ell/P$ we get:

$$\kappa \left(1 - q_\ell \frac{\eta_\ell}{\eta_\ell + \kappa} - \frac{\tilde{\sigma}_\ell}{\kappa} \right) = \lambda. \quad (146)$$

We recognize this as equivalent to the self-consistent equation for κ given a spectrum of N_ℓ eigenvalues all equal to η_ℓ and ridge equal to $\tilde{\lambda}_\ell = \lambda + \tilde{\sigma}_\ell$. This is given by the solution to isotropic linear regression. Explicitly:

$$\kappa = \frac{1}{2} \left(\eta_\ell (q_\ell - 1) + \tilde{\lambda}_\ell + \sqrt{(\eta_\ell (q_\ell - 1) + \tilde{\lambda}_\ell)^2 + 4\eta_\ell \tilde{\lambda}_\ell} \right). \quad (147)$$

Similarly, by evaluating $\text{df}_2 = \partial_\kappa(\kappa \text{df}_1)$ from Equation (145) one gets:

$$\gamma \approx q_\ell \frac{\eta_\ell^2}{(\kappa + \eta_\ell)^2}. \quad (148)$$

We can then write the generalization error as:

$$E_g = \frac{\kappa^2}{1 - \gamma} \frac{N_d \eta_\ell \bar{w}_\ell^2}{(\eta_\ell + \kappa)^2} + \frac{1}{1 - \gamma} \sum_{k > \ell} N_k \eta_k \bar{w}_k^2 + \sigma_\epsilon^2 \frac{\gamma}{1 - \gamma}. \quad (149)$$

We see that even when $\sigma_\epsilon = 0$, the second term (coming from the non-learnable higher modes) acts as an effective source of noise. We can thus get nonmonotonicity in the generalization error when γ increases. We can get the maximum value of γ as a function of q_ℓ and find that it happens when $q = \frac{\eta_\ell + \tilde{\lambda}_\ell}{\eta_\ell}$. This gives a double descent peak without label noise, due solely to the variance over the choice of dataset \mathbf{X} . We give an example plot of this in Figure 6. We define $\text{Var}_\mathbf{X}$ in the subsequent section, Section V.H.

H. Bias-Variance Decomposition

Although one may be tempted to call the two terms in E_g the *bias* and *variance*, the technical definition in of these two terms in statistical learning is different. The *bias* of an estimator $\hat{\mathbf{w}}$ is defined as:

$$\text{Bias}^2 = (\mathbb{E}_\mathcal{D}[\hat{\mathbf{w}}] - \bar{\mathbf{w}})^\top \Sigma (\mathbb{E}_\mathcal{D}[\hat{\mathbf{w}}] - \bar{\mathbf{w}}). \quad (150)$$

Similarly, the variance is given by:

$$\text{Variance} = \mathbb{E}_{\mathcal{D}} [(\hat{\mathbf{w}} - \mathbb{E}_{\mathcal{D}} \hat{\mathbf{w}})^\top \boldsymbol{\Sigma} (\hat{\mathbf{w}} - \mathbb{E}_{\mathcal{D}} \hat{\mathbf{w}})^\top]. \quad (151)$$

The mean squared generalization error is can then be written as

$$\begin{aligned} E_g &= \mathbb{E}_{\mathcal{D}} [(\hat{\mathbf{w}} - \bar{\mathbf{w}})^\top \boldsymbol{\Sigma} (\hat{\mathbf{w}} - \bar{\mathbf{w}})] \\ &= \underbrace{\mathbb{E}_{\mathcal{D}} [(\bar{\mathbf{w}} - \mathbb{E}_{\mathcal{D}}[\hat{\mathbf{w}}])^\top \boldsymbol{\Sigma} (\bar{\mathbf{w}} - \mathbb{E}_{\mathcal{D}}[\hat{\mathbf{w}}])]}_{\text{Bias}^2} + \underbrace{\mathbb{E}_{\mathcal{D}} [(\hat{\mathbf{w}} - \mathbb{E}_{\mathcal{D}}[\hat{\mathbf{w}}])^\top \boldsymbol{\Sigma} (\hat{\mathbf{w}} - \mathbb{E}_{\mathcal{D}}[\hat{\mathbf{w}}])]}_{\text{Variance}}. \end{aligned} \quad (152)$$

Using RMT one can easily calculate the averaged weights by applying deterministic equivalence:

$$\mathbb{E}_{\mathcal{D}} \hat{\mathbf{w}} = \mathbb{E}_{\mathbf{X}, \epsilon} \left[(\hat{\boldsymbol{\Sigma}} + \lambda)^{-1} (\hat{\boldsymbol{\Sigma}} \bar{\mathbf{w}} + \frac{1}{P} \mathbf{X}^\top \boldsymbol{\epsilon}) \right] = \boldsymbol{\Sigma} (\boldsymbol{\Sigma} + \kappa)^{-1} \bar{\mathbf{w}}. \quad (153)$$

This implies that the Bias² term is:

$$\bar{\mathbf{w}}^\top (\mathbf{I} - \boldsymbol{\Sigma} (\boldsymbol{\Sigma} + \kappa)^{-1}) \boldsymbol{\Sigma} (\mathbf{I} - \boldsymbol{\Sigma} (\boldsymbol{\Sigma} + \kappa)^{-1}) \bar{\mathbf{w}} = \kappa^2 \bar{\mathbf{w}}^\top \boldsymbol{\Sigma} (\boldsymbol{\Sigma} + \kappa)^{-2} \bar{\mathbf{w}}. \quad (154)$$

Given that we know the total generalization error, the correct bias-variance decomposition over \mathcal{D} is:

$$E_g = \underbrace{\kappa^2 \bar{\mathbf{w}}^\top \boldsymbol{\Sigma} (\boldsymbol{\Sigma} + \kappa)^{-2} \bar{\mathbf{w}}}_{\text{Bias}^2} + \underbrace{\frac{\gamma}{1-\gamma} [\kappa^2 \bar{\mathbf{w}}^\top \boldsymbol{\Sigma} (\boldsymbol{\Sigma} + \kappa)^{-2} \bar{\mathbf{w}} + \sigma_\epsilon^2]}_{\text{Variance}}. \quad (155)$$

Assume we have B different datasets all of size P with estimators given by $\hat{\mathbf{w}}_b$. We can **bag** by taking our final learned weights to be

$$\hat{\mathbf{w}}_B = \frac{1}{B} \sum_{b=1}^B \hat{\mathbf{w}}_b. \quad (156)$$

We note that by linearity of expectation $\mathbb{E}[\hat{\mathbf{w}}_B] = \mathbb{E}[\hat{\mathbf{w}}_b]$ for each b . Thus the bias term remains the same, while the variance is reduced by $1/B$. This means that bagging corresponds to keeping κ fixed but performing an effective rescaling

$$\frac{\gamma}{1-\gamma} \rightarrow \frac{1}{B} \frac{\gamma}{1-\gamma}. \quad (157)$$

The variance term can in fact be further decomposed, as in [40], into the variance due to the choice of training set $\text{Var}_{\mathbf{X}}$, the variance due to the label noise Var_{ϵ} , and the joint variance due to their interaction $\text{Var}_{\mathbf{X}, \epsilon}$. We can remove the latter two without affecting the former by averaging over label noise holding training set fixed. We get that:

$$\mathbb{E}_{\epsilon} \hat{\mathbf{w}} = (\hat{\boldsymbol{\Sigma}} + \lambda) \hat{\boldsymbol{\Sigma}} \bar{\mathbf{w}}. \quad (158)$$

For this estimator, we see that the respective generalization error and variance (over \mathbf{X}) are

$$E_g(\mathbb{E}_{\epsilon} \hat{\mathbf{w}}) = \frac{\kappa^2}{1-\gamma} \bar{\mathbf{w}}^\top \boldsymbol{\Sigma} (\boldsymbol{\Sigma} + \kappa)^{-2} \bar{\mathbf{w}}, \quad (159)$$

$$\text{Var}_{\mathbf{X}} = \text{Var}[\mathbb{E}_{\epsilon} \hat{\mathbf{w}}] = \frac{\kappa^2 \gamma}{1-\gamma} \bar{\mathbf{w}}^\top \boldsymbol{\Sigma} (\boldsymbol{\Sigma} + \kappa)^{-2} \bar{\mathbf{w}}. \quad (160)$$

This gives an interpretation of γ as the fraction of the test error due to the variance induced by the choice of training set \mathbf{X} (after removing the effect of noise):

$$\gamma = \frac{\text{Var}[\mathbb{E}_{\epsilon} \hat{\mathbf{w}}]}{E_g(\mathbb{E}_{\epsilon} \hat{\mathbf{w}})} = \frac{\text{Var}_{\mathbf{X}}}{\text{Bias}^2 + \text{Var}_{\mathbf{X}}}. \quad (161)$$

Because averaging over \mathbf{X} at a fixed noise level σ_ϵ also removes the label noise term, we get that $\text{Var}_{\epsilon} = 0$ and

$$\text{Var}_{\mathbf{X}, \epsilon} = \frac{\sigma_\epsilon^2 \gamma}{1-\gamma}. \quad (162)$$

That is, the variance due to noise always enters through its interaction with the variance due to the finite choice of training set. Inspired by the work of Adlam and Pennington [40], we visualize this decomposition as a Venn diagram in Figure 7. We will do the same in the next section as well, in Figure 11.

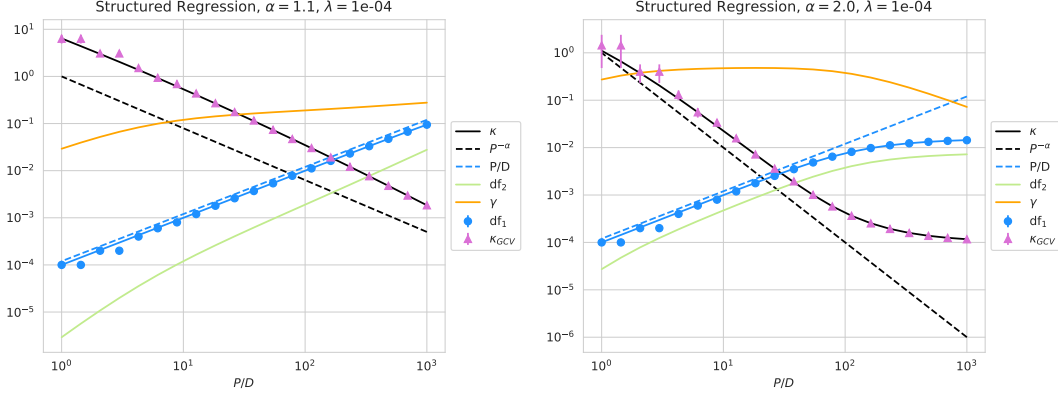


FIG. 8 Left: Scaling of various relevant parameters for power-law structured data. The analytic solution for κ is plotted (solid black), as well as its GCV estimate from the data given by $S(-df_{\Sigma}^1(\lambda))\lambda$ (orchid triangles). The scaling law $P^{-\alpha}$ is also plotted (dashed black), showing excellent agreement. We also plot $df_{\Sigma}^1(\kappa)$ (solid blue) and its empirical estimate $df_{\Sigma}^1(\lambda)$ (blue circles), finding excellent agreement. We also plot the scaling law P/N (dashed blue). Finally, we plot df_2 and $\gamma = \frac{P}{N}df_2$ (dashed green and yellow respectively). We see that γ is relatively constant across P . For faster decays it would be more constant still. Right: The same, with faster spectral decay. We find agreement until $\kappa \sim \lambda$, where we enter the ridge-dominated scaling regime highlighted in Equation (169).

I. Scaling Laws in P

1. Normalizable Spectra

For completeness, we include the derivation of the power law exponents presented in [20; 22]. We take the spectrum of the kernel to scale as $\eta_k \sim k^{-\alpha}$. Here α is known as the **capacity** exponent as in [63; 96; 99; 100; 111]. The task decomposes into the eigenspaces also as a power law with $\tilde{w}_k^2 \eta_k \sim k^{-(1+2\alpha r)}$. Here r is the **source** exponent. The exponent $2\alpha r$ determines how much of \mathbf{w} remains above eigenmode k as measured by $\mathbf{w}^T \Sigma \mathbf{w}$. That is, $\sum_{k' > k} w_{k'}^2 \eta_{k'} \sim k^{-2\alpha r}$.

Interpreting the input space as the reproducing kernel Hilbert space of a kernel with eigenspectrum given by η_k , then α controls the spectral decay of the kernel. Smaller α lead to more expressive but jagged functions while larger α lead to a stronger prior towards smoothness.

The self-consistent equation for κ is approximated by:

$$\kappa \approx \frac{\lambda}{1 - \frac{1}{P} \int_1^{\infty} \frac{k^{-\alpha}}{k^{-\alpha} + \kappa} dk}. \quad (163)$$

Making the change of variables $u = k\kappa^{1/\alpha}$ then gives

$$\kappa \approx \frac{\lambda}{1 - \frac{\kappa^{-1/\alpha}}{P} \int_{\kappa^{1/\alpha}}^{\infty} \frac{1}{1+u^\alpha} du} = \frac{\lambda}{1 - \frac{\kappa^{-1/\alpha}}{P} F(\alpha, \kappa)} \quad (164)$$

for a function F that depends on α, κ . Let's consider first the ridgeless limit $\lambda \rightarrow 0$. Then in order to get a nonzero value of κ , we need

$$\kappa^{-1/\alpha} F(\alpha, \kappa) \sim P. \quad (165)$$

Note as $\kappa \rightarrow 0$, F tends to a constant and so we get the scaling $\kappa \sim P^{-\alpha}$. In the other case, when λ is large, namely $\lambda \gg P^{-\alpha}$ we get that $\kappa \sim \lambda$.

Similarly for γ one gets the approximation:

$$\gamma \approx \frac{1}{P} \int_1^{\infty} \left(\frac{k^{-\alpha}}{k^{-\alpha} + \kappa} \right)^2 dk = \frac{\kappa^{-1/\alpha}}{P} \int_{\kappa^{1/\alpha}}^{\infty} \frac{1}{(1+u^\alpha)^2} du. \quad (166)$$

Taking $\kappa \sim P^{-\alpha}$ we see that γ remains constant as P increases. If $\kappa \sim \lambda$ one gets that $\gamma \sim \lambda^{-1/\alpha}/P \rightarrow 0$ as P increases. In all cases $1/(1-\gamma)$ tends to a constant. Thus, in all cases we can write the generalization error scaling as:

$$E_g \approx \int_1^{\infty} \frac{k^{-(1+2\alpha r)}}{(1+k^{-\alpha}/\kappa)^2} dk = P^{-2\alpha r} \int_{1/P}^{\infty} \frac{u^{-(1+2\alpha r)}}{(1+u^{-\alpha})^2} du, \quad u = k/P. \quad (167)$$

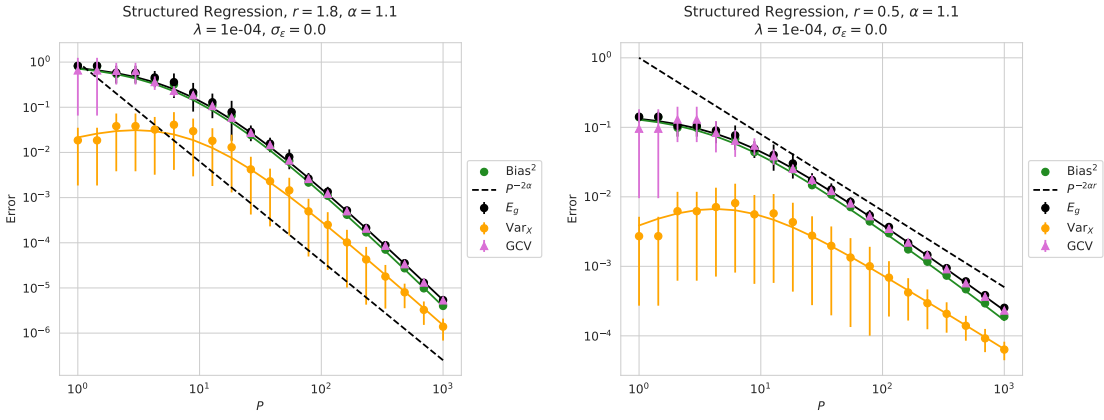


FIG. 9 Generalization error (solid black) for two different teacher decay constants. We see that $\min(1, r)$ determines the whether the scaling law is due solely to the capacity or if the source also plays a role. The bias (solid green) variance over the dataset (solid orange) follow identical scaling laws. The results of empirical simulations are plotted in solid dots, showing excellent agreement. The GCV estimate from the training error is given by orchid triangles. Here, $N = 10000$, and the spectral decay makes the final result insensitive to N .

We can split this integral into a part near $u \sim 1/P$ and a part away from that. The part near $1/P$ will scale as $(1/P)^{-2\alpha r + 2\alpha}$ and thus give a contribution scaling as $P^{-2\alpha}$. The part away from that is P -independent and thus its contribution scales as $P^{-2\alpha r}$.

When $\kappa \sim \lambda$ we can similarly change variables taking $u = k\lambda^{1/\alpha}$ and track the λ dependence:

$$E_g \approx \lambda^{2r} \int_{\lambda^{1/\alpha}}^{\infty} \frac{u^{-(1+2\alpha r)}}{(1+u^{-\alpha})^2} du. \quad (168)$$

The contributions of this integral can again be broken up into the part near $\lambda^{1/\alpha}$ and the part away from it, which is λ independent. The two contributions then scale as λ^2 and λ^{2r} respectively.

This altogether gives the scaling laws:

$$E_g \sim \begin{cases} P^{-2\alpha \min(r,1)}, & P \ll \lambda^{-1/\alpha} \\ \lambda^{2 \min(r,1)}, & P \gg \lambda^{-1/\alpha} \end{cases}. \quad (169)$$

After redefining $\lambda \rightarrow \lambda/P$, one obtains the scaling laws of [20]. Given that $\alpha > 1$ for the spectrum to be normalizable, we get that in the noiseless setting, adding explicit regularization will hurt generalization. Further, we see that faster spectral decays will improve performance, as will having more of the task's power in the top eigenmodes. Either effect can bottleneck the other, hence the min in the exponents.

One can also average over teachers. This corresponds to taking $\bar{\mathbf{w}}_k$ to be constant, or equivalently $1 + 2\alpha r = \alpha$. This sets $r = \frac{1}{2} \frac{\alpha-1}{\alpha}$. In the ridgeless limit this gives the scaling $E_g \sim P^{-2(\alpha-1)}$

In the case where λ itself scales as P^{-l} for some value l as in [63], one gets:

$$E_g \sim P^{-2 \min(\alpha, l) \min(r,1)}. \quad (170)$$

Using this scaling and adding in label noise. In that case, using the fact that γ is a constant in the first case and $\gamma \sim \lambda^{-1/\alpha}/P$ in the second case of Equation (169), we find four scaling regimes:

$$E_g \sim \begin{cases} P^{-2\alpha \min(r,1)} + \sigma_\epsilon^2, & \alpha \ll l \\ P^{-2l \min(r,1)} + \sigma_\epsilon^2 P^{-(\alpha-l)/\alpha}, & l \ll \alpha \end{cases} \quad (171)$$

$$\sim \begin{cases} P^{-2\alpha \min(r,1)}, & l > \alpha, \sigma_\epsilon \ll P^{-\alpha \min(r,1)}, & \text{Signal dominated} \\ \sigma_\epsilon^2 P^0, & l > \alpha, \sigma_\epsilon \gg P^{-\alpha \min(r,1)}, & \text{Noise dominated} \\ P^{-2l \min(r,1)}, & l < \alpha, l < \frac{\alpha}{1+2\alpha \min(r,1)}, & \text{Ridge dominated} \\ \sigma_\epsilon^2 P^{-(\alpha-l)/\alpha}, & l < \alpha, l \geq \frac{\alpha}{1+2\alpha \min(r,1)}, & \text{Noise mitigated} \end{cases}$$

This recovers the four scaling regimes studied in [63]. These four regimes yield the different possible resolution-limited scalings of wide neural networks in the kernel setting trained on power-law data. The first two are effectively ridgeless, whereas one requires a explicit ridge to achieve the second two scaling laws.

2. Non-Normalizable Spectra

If the spectrum has $\alpha \leq 1$, then the final scaling laws will depend on the value of N . We study the regime where $P \ll N$. In this case, in the ridgeless limit the following term must be order 1. The integral is dominated by the large N limit:

$$\frac{N}{P} \text{df}_1 = \frac{1}{P} \int_1^N \frac{dk}{1 + \kappa k^\alpha} \sim \frac{N^{1-\alpha}}{P\kappa} \Rightarrow \kappa \sim \frac{N^{1-\alpha}}{P}. \quad (172)$$

When $\alpha = 0$ this reproduces the leading order in N scaling of isotropic linear regression, where $\kappa = q - 1$. Further, we get that γ has a nontrivial P scaling:

$$\gamma = \frac{1}{P} \int_1^N \frac{dk}{(1 + \kappa k^\alpha)^2} \sim \left(\frac{P}{N}\right)^{\min(1, \frac{1-\alpha}{\alpha})}. \quad (173)$$

The former scaling occurs when $\alpha < 1/2$, leading to the upper limit dominating, while the latter happens when $\alpha > 1/2$. In this setting, when $P \rightarrow N$ we get that $\gamma \rightarrow 1$ and the generalization error explodes. We thus see how a slowly decaying spectrum can lead to non-monotonicity in the generalization error.

VI. LINEAR RANDOM FEATURES

In this section, we will make extensive use of the **push-through identity** [129]:

$$\mathbf{A}(\mathbf{B}\mathbf{A} + \lambda)^{-1} = (\mathbf{A}\mathbf{B} + \lambda)^{-1}\mathbf{A}. \quad (174)$$

A. Setup and Motivation

We consider a general class of linear random feature models of the form

$$f(\mathbf{x}) = \mathbf{x}^\top \mathbf{F}\mathbf{v}, \quad (175)$$

where $\mathbf{F} \in \mathbb{R}^{D \times N}$ is not trainable and maps the data from \mathbb{R}^D to an N -dimensional **feature space**. Here, $\mathbf{v} \in \mathbb{R}^N$ is a vector of trainable parameters. Our statistical assumptions on the training data are the same as in §V: we take $\mathbf{X} \in \mathbb{R}^{P \times N}$ with rows distributed as $\mathbf{x}_\mu \sim \mathcal{N}(\mathbf{0}, \boldsymbol{\Sigma})$, and generate labels as $y_\mu = \bar{\mathbf{w}} \cdot \mathbf{x}_\mu + \epsilon_\mu$ with each $\epsilon_\mu \sim \mathcal{N}(0, \sigma_\epsilon^2)$.

This is the simplest solvable model where the notion of parameters N can enter on a different footing from the input dimension. This model is very limited when viewed literally as a neural network learning functions from a D -dimensional input space, since it can only learn linear functions. However, an alternative perspective put forth in [34] considers that with $D \gg N, P$, one can instead view the D -dimensional space as an abstract feature space. This space can be viewed e.g. as the Hilbert space of functions that are square-integrable with respect to the Gaussian data distribution, or the Hilbert space induced by the NTK of some infinitely wide network. From this space, we are taking an N -dimensional random feature projection corresponding to the N parameters of some model. Similar motivation is given in [39; 71] where the input space is viewed as an analogue of the infinite-width NTK's kernel Hilbert space.

We minimize the same MSE objective as in Equation (4). This gives the following learned weights $\hat{\mathbf{v}}$:

$$\hat{\mathbf{v}} = (\mathbf{F}^\top \mathbf{X}^\top \mathbf{X} \mathbf{F} + P\lambda \mathbf{I})^{-1} \mathbf{F}^\top \mathbf{X}^\top \mathbf{y}. \quad (176)$$

The corresponding learned weights in \mathbb{R}^D are $\hat{\mathbf{w}} = \mathbf{F}\hat{\mathbf{v}} \in \mathbb{R}^D$. Then, taking $\hat{\boldsymbol{\Sigma}} = \frac{1}{P} \mathbf{X}^\top \mathbf{X}$ and applying the pushthrough identity (174):

$$\bar{\mathbf{w}} - \hat{\mathbf{w}} = \lambda(\mathbf{F}\mathbf{F}^\top \hat{\boldsymbol{\Sigma}} + \lambda \mathbf{I})^{-1} \bar{\mathbf{w}} - (\mathbf{F}\mathbf{F}^\top \hat{\boldsymbol{\Sigma}} + \lambda \mathbf{I})^{-1} \mathbf{F}\mathbf{F}^\top \frac{\mathbf{X}^\top \boldsymbol{\epsilon}}{P}. \quad (177)$$

The generalization error is $E_g = (\bar{\mathbf{w}} - \hat{\mathbf{w}})^\top \boldsymbol{\Sigma} (\bar{\mathbf{w}} - \hat{\mathbf{w}})$ and just as in Equation (118) in the linear regression setting, it can be decomposed into signal and noise components. After expanding and applying (174) again, the noise component can be written as:

$$\begin{aligned} \text{Noise} &= \frac{\sigma_\epsilon^2}{P} \text{Tr}[\hat{\boldsymbol{\Sigma}} \mathbf{F}\mathbf{F}^\top (\hat{\boldsymbol{\Sigma}} \mathbf{F}\mathbf{F}^\top + \lambda \mathbf{I})^{-1} \boldsymbol{\Sigma} \mathbf{F}\mathbf{F}^\top (\hat{\boldsymbol{\Sigma}} \mathbf{F}\mathbf{F}^\top + \lambda \mathbf{I})^{-1}] \\ &= -\frac{\sigma_\epsilon^2}{P} \partial_\lambda \left[\lambda \text{Tr}[\boldsymbol{\Sigma} \mathbf{F}\mathbf{F}^\top (\hat{\boldsymbol{\Sigma}} \mathbf{F}\mathbf{F}^\top + \lambda \mathbf{I})^{-1}] \right]. \end{aligned} \quad (178)$$

For now, we will assume that $\mathbf{F}\mathbf{F}^\top$ is invertible. Then, the signal component is:

$$\begin{aligned} \text{Signal} &= \lambda^2 \bar{\mathbf{w}}^\top (\hat{\boldsymbol{\Sigma}} \mathbf{F}\mathbf{F}^\top + \lambda \mathbf{I})^{-1} \boldsymbol{\Sigma} (\mathbf{F}\mathbf{F}^\top \hat{\boldsymbol{\Sigma}} + \lambda \mathbf{I})^{-1} \bar{\mathbf{w}} \\ &= \lambda^2 \bar{\mathbf{w}}^\top (\hat{\boldsymbol{\Sigma}} \mathbf{F}\mathbf{F}^\top + \lambda \mathbf{I})^{-1} \boldsymbol{\Sigma} \mathbf{F}\mathbf{F}^\top (\hat{\boldsymbol{\Sigma}} \mathbf{F}\mathbf{F}^\top + \lambda \mathbf{I})^{-1} (\mathbf{F}\mathbf{F}^\top)^{-1} \bar{\mathbf{w}} \\ &= -\lambda^2 \partial_J|_{J=0} \left[\bar{\mathbf{w}}^\top \left[(\hat{\boldsymbol{\Sigma}} + J\boldsymbol{\Sigma}) \mathbf{F}\mathbf{F}^\top + \lambda \right]^{-1} (\mathbf{F}\mathbf{F}^\top)^{-1} \bar{\mathbf{w}} \right]. \end{aligned} \quad (179)$$

Here, we have applied the push-through identity (174) and used the same differentiation trick as in Section V.B.

B. Averaging Over Data

We will now perform an \mathbf{X} average, viewing \mathbf{F} as fixed. Then, applying the subordination relation Equation (42), we have the following deterministic equivalence:

$$\begin{aligned}\hat{\Sigma}\mathbf{F}\mathbf{F}^\top(\hat{\Sigma}\mathbf{F}\mathbf{F}^\top + \lambda\mathbf{I})^{-1} &\simeq \mathbf{F}\mathbf{F}^\top(\mathbf{F}\mathbf{F}^\top + \lambda S_\Sigma S_{\mathbf{W}}\mathbf{I})^{-1} \\ &\simeq \Sigma\mathbf{F}\mathbf{F}^\top(\Sigma\mathbf{F}\mathbf{F}^\top + \kappa_1\mathbf{I})^{-1},\end{aligned}\tag{180}$$

$$\Rightarrow \lambda(\hat{\Sigma}\mathbf{F}\mathbf{F}^\top + \lambda\mathbf{I})^{-1} \simeq \kappa_1(\Sigma\mathbf{F}\mathbf{F}^\top + \kappa_1\mathbf{I})^{-1},\tag{181}$$

$$\kappa_1 \equiv \lambda S_{\mathbf{W}} = \frac{\lambda}{1 - \frac{D}{P} \text{df}_{\Sigma\mathbf{F}\mathbf{F}^\top}^1(\kappa_1)}.\tag{182}$$

Here \mathbf{W} is a white Wishart with $q = D/P$. Defining $\Sigma_{\mathbf{F}} \equiv \Sigma^{1/2}\mathbf{F}\mathbf{F}^\top\Sigma^{1/2}$, we see that because this shares the same nonzero eigenvalues as $\Sigma\mathbf{F}\mathbf{F}^\top$ that $\text{df}_{\Sigma\mathbf{F}\mathbf{F}^\top}^1(\kappa_1) = \text{df}_{\Sigma_{\mathbf{F}}}^1(\kappa_1)$. Then,

$$\frac{d\kappa_1}{d\lambda} = \frac{1}{1 - \gamma_1}, \quad \gamma_1 \equiv \frac{D}{P} \text{df}_{\Sigma_{\mathbf{F}}}^2(\kappa_1).\tag{183}$$

Applying (181) to (178), the \mathbf{X} -averaged noise term becomes:

$$\begin{aligned}\text{Noise} &\simeq -\sigma_\epsilon^2 \frac{D}{P} \partial_\lambda [\kappa_1 \text{df}_{\Sigma_{\mathbf{F}}}^1(\kappa_1)] \\ &= \sigma_\epsilon^2 \frac{d\kappa_1}{d\lambda} \frac{D}{P} \text{df}_{\Sigma_{\mathbf{F}}}^2(\kappa_1) = \sigma_\epsilon^2 \frac{\gamma_1}{1 - \gamma_1}.\end{aligned}\tag{184}$$

Here, we have used Equation (20). Here we have used the fact that all quantities concentrate over \mathbf{F} to drop the expectation.

The signal term (179) can be obtained using the exact same argument as in Equations (125) and (126). This gives

$$\begin{aligned}\text{Signal} &\simeq \frac{\kappa_1^2}{1 - \gamma_1} \bar{\mathbf{w}}^\top \Sigma\mathbf{F}\mathbf{F}^\top (\Sigma\mathbf{F}\mathbf{F}^\top + \kappa_1\mathbf{I})^{-2} (\mathbf{F}\mathbf{F}^\top)^{-1} \bar{\mathbf{w}} \\ &= \frac{\kappa_1^2}{1 - \gamma_1} \bar{\mathbf{w}}^\top \Sigma^{1/2} (\Sigma_{\mathbf{F}} + \kappa_1\mathbf{I})^{-2} \Sigma^{1/2} \bar{\mathbf{w}}.\end{aligned}\tag{185}$$

We can thus write the full generalization compactly as:

$$E_g^{\mathbf{F}} \simeq -\frac{\kappa_1^2}{1 - \gamma_1} \partial_{\kappa_1} \tilde{\text{tf}}_1(\kappa_1) + \sigma_\epsilon^2 \frac{\gamma_1}{1 - \gamma_1}.\tag{186}$$

Here, we have defined the function

$$\tilde{\text{tf}}_1(\kappa_1) \equiv \bar{\mathbf{w}}^\top \Sigma^{1/2} (\Sigma_{\mathbf{F}} + \kappa_1\mathbf{I})^{-1} \Sigma^{1/2}.\tag{187}$$

We add a tilde to highlight that $\tilde{\text{tf}}_1(\kappa_1)$ depends on both Σ and \mathbf{F} .

Importantly, observe that these asymptotic results are continuous in \mathbf{F} , even when $\mathbf{F}\mathbf{F}^\top$ is not invertible. To extend this argument to the regime in which $\mathbf{F}\mathbf{F}^\top$ is singular, we infinitesimally regularize $\mathbf{F}\mathbf{F}^\top$ as $\mathbf{F}\mathbf{F}^\top + \tau\mathbf{I}_D$, and then let τ tend to zero after averaging over \mathbf{X} . The validity of this interchange of limits can be justified using dominated convergence. An alternative proof of this fact would follow from high-probability bounds on the deviation of the non-averaged generalization error from the deterministic limit, in a similar spirit to the bounds given in [17].

C. Averaging Over Features

We can now perform the \mathbf{F} average in the above equations. Again applying Equation (42), we have the deterministic equivalence:

$$\Sigma_{\mathbf{F}}(\Sigma_{\mathbf{F}} + \kappa_1\mathbf{I})^{-1} = \Sigma(\Sigma + \kappa_1 S_{\mathbf{F}\mathbf{F}^\top}\mathbf{I})^{-1}.\tag{188}$$

We thus have that κ_1 will be further renormalized to

$$\boxed{\kappa_2 \equiv \kappa_1 S_{\mathbf{F}\mathbf{F}^\top}(-\text{df}_1) = \lambda S_{\mathbf{W}}(-\text{df}_1) S_{\mathbf{F}\mathbf{F}^\top}(-\text{df}_1)}. \quad (189)$$

We adopt the shorthand $\text{df}_1 \equiv \text{df}_{\hat{\Sigma}}^1(\kappa_2) \simeq \text{df}_{\hat{\Sigma}_{\mathbf{F}}}^1(\kappa_1) \simeq \text{df}_{\hat{\Sigma}_{\mathbf{F}\mathbf{F}^\top}}^1(\lambda)$, $\text{df}_2 \equiv \text{df}_{\hat{\Sigma}}^2(\kappa_2)$. This is a different renormalization effect, due to the fluctuations not in the data, but in the features. It is equivalent to the effect studied in [97; 103]. Then, we have

$$\begin{aligned} \gamma_1 &= \frac{D}{P} \text{df}_{\hat{\Sigma}_{\mathbf{F}}}^1(\kappa_1) \left(1 + \frac{\kappa_1}{\text{df}_{\hat{\Sigma}_{\mathbf{F}}}^1(\kappa_1)} \partial_{\kappa_1} \text{df}_{\hat{\Sigma}_{\mathbf{F}}}^1(\kappa_1) \right) \\ &\simeq \frac{D}{P} \text{df}_1 \left(1 + \frac{\kappa_1}{\text{df}_1} \frac{d\kappa_2}{d\kappa_1} \partial_{\kappa_2} \text{df}_1 \right). \end{aligned} \quad (190)$$

Applying Equation (22) gives:

$$\boxed{\gamma_1 = \frac{D}{P} \text{df}_1 \left(1 - \frac{\text{df}_1 - \text{df}_2}{\text{df}_1} \frac{d \log \kappa_2}{d \log \kappa_1} \right)}. \quad (191)$$

Next, we can apply Equation (188) to the signal term in Equation (186) and get:

$$\text{Signal} = -\frac{\kappa_1^2}{1 - \gamma_1} \partial_{\kappa_1} \left[\frac{\kappa_2}{\kappa_1} \text{tf}_{\hat{\Sigma}}^1(\kappa_2) \right] = -\frac{\kappa_2^2 \text{tf}'_1}{1 - \gamma_1} \frac{d \log \kappa_2}{d \log \kappa_1} + \frac{\kappa_2 \text{tf}_1}{1 - \gamma_1} \left[1 - \frac{d \log \kappa_2}{d \log \kappa_1} \right], \quad (192)$$

where again we have used shorthand $\text{tf}_1 = \text{tf}_{\hat{\Sigma}, \mathbf{w}}(\kappa_2)$. Together with Equations (189) and (191), this gives the final result:

$$\boxed{E_g = -\frac{\kappa_2^2 \text{tf}'_1}{1 - \gamma_1} \frac{d \log \kappa_2}{d \log \kappa_1} + \frac{\kappa_2 \text{tf}_1}{1 - \gamma_1} \left[1 - \frac{d \log \kappa_2}{d \log \kappa_1} \right] + \sigma_\epsilon^2 \frac{\gamma_1}{1 - \gamma_1}}. \quad (193)$$

This equation recovers and extends the generalization error formulas of all linear random feature models in the literature. We will give explicit examples in Section VI.E.

D. Ridgeless Limits

In the limit of $\lambda \rightarrow 0$, we see that nonzero values of κ_2 will correspond to df taking a value so that it lands on of the poles of one of the S -transforms. In this way, we see that poles in the S -transform determine the different regimes of the ridgeless limit. In what follows, let N_ℓ be the rank of $\mathbf{F}\mathbf{F}^\top$. N_ℓ will correspond to the narrowest width in the random feature model in the subsequent examples. There are three possible behaviors as $\lambda \rightarrow 0$:

1. κ_2 stays zero. This happens when $\text{rank}(\hat{\Sigma}\mathbf{F}\mathbf{F}^\top) = \text{rank}(\hat{\Sigma}\mathbf{F}\mathbf{F}^\top) = \text{rank}(\hat{\Sigma})$. All matrices are full rank, which constrains $D \leq N_\ell, P$. This is the **underparameterized** setting.

Here, because $\text{tf}_1(\kappa_2)$ is analytic as $\kappa_2 \rightarrow 0$, we get that the signal term vanishes completely. Further, because $\text{df}_1 = \text{df}_2 = 1$ at $\kappa_2 = 0$, we have that $\gamma = D/P$. Altogether this gives a generalization error of

$$E_g = \frac{D/P}{1 - D/P} \sigma_\epsilon^2. \quad (194)$$

This is independent of any details of the structure of the features \mathbf{F} .

2. κ_1 stays zero but κ_2 is nonzero. This happens when $\text{rank}(\hat{\Sigma}\mathbf{F}\mathbf{F}^\top) = \text{rank}(\hat{\Sigma}\mathbf{F}\mathbf{F}^\top) < \text{rank}(\hat{\Sigma})$. This means that $\mathbf{F}\mathbf{F}^\top$ is no longer full rank. We have $N_\ell < D, P$. This is the **bottlenecked** setting.

Here, we get that $\text{df}_1 = \text{df}_{\hat{\Sigma}}^{(1)}(\kappa_2) \rightarrow \text{df}_{\hat{\Sigma}}^{(1)}(0) = \frac{N_\ell}{D}$ since $\hat{\Sigma}$ has rank N_ℓ instead of D . We also get $\frac{d \log \kappa_2}{d \log \kappa_1} = \frac{\kappa_1}{\kappa_2} \frac{d\kappa_2}{d\kappa_1} \rightarrow 0$ as $\kappa_1 \rightarrow 0$. Consequently $\gamma_1 = N_\ell/P$. This gives:

$$E_g = \frac{\kappa_2 \text{tf}_1}{1 - N_\ell/P} + \frac{N_\ell/P}{1 - N_\ell/P} \sigma_\epsilon^2. \quad (195)$$

The structure of the features \mathbf{F} only effects the signal term. The noise term is universal and depends only on the narrowest width N_ℓ .

3. Both κ_1 and κ_2 are nonzero. This happens when $\text{rank}(\hat{\Sigma}\mathbf{F}\mathbf{F}^\top) < \text{rank}(\hat{\Sigma}\mathbf{F}\mathbf{F}^\top) \leq \text{rank}(\Sigma)$. This means that $\hat{\Sigma}$ has rank less than $\mathbf{F}\mathbf{F}^\top$. We have $P < D, N_\ell$. This is the **overparameterized** setting.

In order for κ_1 to be nonzero we must have a pole in $S_{\mathbf{W}}(t)$, so $\text{df}_1 = P/D$. This implies

$$\frac{\gamma_1}{1 - \gamma_1} = \frac{\text{df}_1}{\text{df}_1 - \text{df}_2} \frac{d \log \kappa_1}{d \log \kappa_2} - 1 = \frac{\text{df}_2}{\text{df}_1 - \text{df}_2} + \frac{\text{df}_1}{\text{df}_1 - \text{df}_2} \left(\frac{d \log \kappa_1}{d \log \kappa_2} - 1 \right). \quad (196)$$

Using equation (189) and (22) we can write:

$$\frac{d \log \kappa_1}{d \log \kappa_2} = 1 - \frac{d \log S_{\mathbf{F}\mathbf{F}^\top}(-\text{df}_1(\kappa_2))}{d \log \kappa_2} = 1 + \frac{\text{df}_1 - \text{df}_2}{\text{df}_1} \frac{d \log S_{\mathbf{F}\mathbf{F}^\top}(-\text{df}_1)}{d \log \text{df}_1}. \quad (197)$$

Defining $\gamma_2 \equiv \frac{D}{P} \text{df}_2(\kappa_2)$ and using shorthand $S = S_{\mathbf{F}\mathbf{F}^\top}(-\text{df}_1)$ yields:

$$E_g = -\frac{\kappa_2^2 \text{tf}'_1(\kappa_2)}{1 - \gamma_2} + \kappa_2 \text{tf}_1 \frac{d \log S}{d \log \text{df}_1} + \sigma_\epsilon^2 \left[\frac{\gamma_2}{1 - \gamma_2} + \frac{d \log S}{d \log \text{df}_1} \right]. \quad (198)$$

E. Examples

In this subsection we will apply the formulas (194), (195), and (198) to obtain the generalization error of many of the linear random feature models studied in the literature. We will consider both shallow and deep random feature models with varying amounts of structure in the data and features.

1. 1-Layer White Random Feature Model

We consider the simple case of $\Sigma = \mathbf{I}$ and unstructured features \mathbf{F} . That is, $\mathbf{F}^\top \mathbf{F}$ is distributed as a white Wishart. We then have that $\Sigma_{\mathbf{F}}^D = \mathbf{F}\mathbf{F}^\top$. The S -transform was computed in Equation (97) and is given by

$$S_{\mathbf{F}\mathbf{F}^\top} = \frac{1}{\frac{N}{D} - \text{df}_1}. \quad (199)$$

As a consequence we get:

$$\text{df}_{\Sigma_{\mathbf{F}}}^1(\kappa_1) = \text{df}_{\Sigma}^1(\kappa_2) = \frac{1}{1 + \kappa_2}, \quad (200)$$

$$\kappa_2 = \frac{\kappa_1}{\frac{N}{D} - \frac{1}{1 + \kappa_2}} = \frac{\lambda}{\left(\frac{N}{D} - \frac{1}{1 + \kappa_2}\right) \left(1 - \frac{P}{N} \frac{1}{1 + \kappa_2}\right)}, \quad (201)$$

$$\frac{d \log S}{d \log \text{df}_1} = \frac{\text{df}_1}{N/D - \text{df}_1}. \quad (202)$$

We see that at finite ridge, solving for κ_2 in terms of λ will involve solving a cubic equation, as noted by Rocks and Mehta [130].

We now consider the generalization performance in the ridgeless limit $\lambda \rightarrow 0$. When we take this limit, we see that either $\kappa_2 \rightarrow 0$ or κ_2 lands on one of the poles of equation (201). The possible values of κ_1, κ_2 as $\lambda \rightarrow 0$ are:

1. Underparameterized regime: $\lambda = \kappa_1 = \kappa_2 = 0$, $\text{df}_1 = 1$.
2. Bottlenecked regime: $\lambda = \kappa_1 = 0$, $\kappa_2 = \frac{D}{N} - 1$, $\text{df}_1 = N/D$.
3. Overparameterized regime: $\lambda = 0$, $\kappa_1 \neq 0$, $\kappa_2 = \frac{D}{P} - 1$, $\text{df}_1 = P/D$, $\text{df}_2 = (P/D)^2$.

Further, because of the isotropy of the problem, we see that $\text{tf}_1 = \text{df}_1$ for any value of $\bar{\mathbf{w}}$. This gives a generalization error of

$$E_g = \begin{cases} \frac{D/P}{1 - D/P} \sigma_\epsilon^2, & P > D, N \\ \frac{1 - N/D}{1 - N/P} + \frac{N/P}{1 - N/P} \sigma_\epsilon^2, & N < \min(P, D) \\ \left(1 - \frac{P}{D}\right) \left(1 + \frac{P/N}{1 - P/N}\right) + \left(\frac{P/D}{1 - P/D} + \frac{P/N}{1 - P/N}\right) \sigma_\epsilon^2, & P < D, N. \end{cases} \quad (203)$$

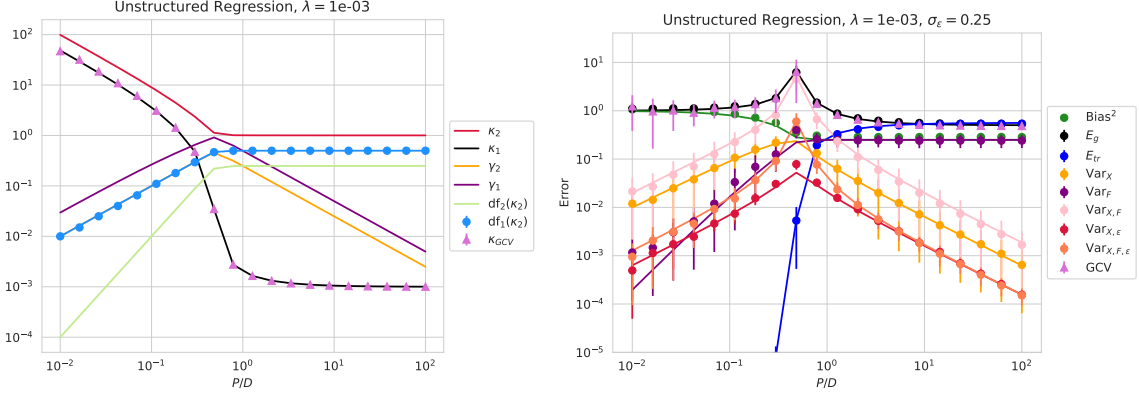


FIG. 10 1-layer linear random features with unstructured covariates, i.e. $\Sigma = \mathbf{I}$. Left: We plot theory (solid lines) for the various quantities of interest: $\kappa_1, \kappa_2, \gamma_1, \gamma_2$ as well as $\text{df}_{\Sigma}^1(\kappa_2), \text{df}_{\Sigma}^2(\kappa_2)$. We also plot the estimate of κ_1 using the training set and find excellent agreement. Right: We plot the training and generalization (blue, black respectively) as well as the bias (green) and variances (orange, purple, pink, red, coral) due to all relevant quantities in the regression. Dots and error bars indicate empirical simulations over 25 seeds over training set and 25 seeds over random feature initializations. Solid curves show theory. We see strong agreement for all relevant quantities. The GCV estimator is plotted as orchid triangles and again we find excellent agreement with the generalization error.

2. Deep White Random Feature Model

We now consider the setting where the random features \mathbf{F} consist of a composition of L layers of random unstructured linear transformations. Regression with this model is analogous to regression with the final layer weights of a deep linear network at initialization. Writing $D = N_0$, we will take things to be normalized so that

$$\mathbf{F}^\top \mathbf{F} = \mathbf{F}_1^\top \cdots \mathbf{F}_L^\top \mathbf{F}_L \cdots \mathbf{F}_1, \quad \mathbb{E} [\mathbf{F}_\ell^\top \mathbf{F}_\ell] = \mathbf{I}. \quad (204)$$

This is exactly an element of the deep product Wishart ensemble. We calculated the S -transform of $\mathbf{F}^\top \mathbf{F}$ and $\mathbf{F} \mathbf{F}^\top$ in Equations (105) and (107) of Section IV.H. The latter will be more useful to us:

$$S_{\mathbf{F} \mathbf{F}^\top} = \prod_{\ell=1}^L \frac{1}{\frac{N_\ell}{D} - \text{df}_1}. \quad (205)$$

This directly yields the self-consistent equation for κ_2 :

$$\text{df}_{\Sigma_{\mathbf{F}}}^1(\kappa_1) = \text{df}_{\Sigma}^2(\kappa_2) = \frac{1}{1 + \kappa_2}, \quad (206)$$

$$\kappa_2 \prod_{\ell=1}^L \left(\frac{N_\ell}{D} - \frac{1}{1 + \kappa_2} \right) = \kappa_1, \quad (207)$$

$$\frac{d \log S}{d \log \text{df}_1} = \sum_{\ell=1}^L \frac{\text{df}_1}{N_\ell/D - \text{df}_1}. \quad (208)$$

Now as $\lambda = 0$ we see that the number of poles expands to one at every layer of the random features. Writing $N_0 = D$, the final generalization error is then:

$$E_g = \begin{cases} \frac{D/P}{1 - D/P} \sigma_\epsilon^2, & P > D, N_\ell \forall \ell \\ \frac{1 - N_\ell/D}{1 - N_\ell/P} + \frac{N_\ell/P}{1 - N_\ell/P} \sigma_\epsilon^2, & N_\ell < \min(P, D) \\ \left(1 - \frac{P}{D}\right) \left(1 + \sum_{\ell=1}^L \frac{P/N_\ell}{1 - P/N_\ell}\right) + \sum_{\ell=0}^L \frac{P/N_\ell}{1 - P/N_\ell} \sigma_\epsilon^2, & P < D, N_\ell \forall \ell. \end{cases} \quad (209)$$

This recovers the results obtained in prior works by the second and third authors using the replica trick [31; 88].

3. 1-Layer Structured Random Feature Model

We now consider the setting where \mathbf{F} are still unstructured and shallow so that $\mathbf{F}^\top \mathbf{F}$ is distributed as a white Wishart, but now the inputs \mathbf{x}_μ are drawn from a structured distribution with covariance Σ .

We return to the shorthand $df_1 = df_{\Sigma}^1(\kappa_2) \simeq df_{\Sigma_F}^1(\kappa_1)$, $df_2 = df_{\Sigma}^2(\kappa_2)$. Then:

$$\kappa_2 = \frac{\kappa_1}{\frac{N}{D} - df_1} = \frac{\lambda}{\left(\frac{N}{D} - df_1\right)(1 - df_1)}, \quad (210)$$

$$\frac{d \log S}{d \log df_1} = \frac{df_1}{N/D - df_1}. \quad (211)$$

Applying Equations (194), (195), and (198) gives the generalization error in terms of the degrees of freedom of Σ .

$$E_g = \begin{cases} \frac{D/P}{1 - D/P} \sigma_\epsilon^2, & D < P, N \\ \frac{\kappa_2 tf_1}{1 - N/P} + \frac{N/P}{1 - N/P} \sigma_\epsilon^2, & N < P, D \\ -\frac{\kappa_2^2 tf'}{1 - \frac{D}{P} df_2} + \frac{\kappa_2 tf_1 P/N}{1 - P/N} + \sigma_\epsilon^2 \left[\frac{\frac{D}{P} df_2}{1 - \frac{D}{P} df_2} + \frac{P/N}{1 - P/N} \right], & P < D, N. \end{cases} \quad (212)$$

These are the same equations as obtained in [35]. When averaging over $\bar{\mathbf{w}}$ we recover the equations of [34].

4. Orthogonal Projections of Structured Covariates

We now let \mathbf{x}_μ be taken from a structured distribution with covariance Σ . We take \mathbf{F} to be a projection to an N dimensional space with $N < D$ so that $\mathbf{F}\mathbf{F}^\top = \mathbf{P} \in \mathbb{R}^{D \times D}$ is a square projection. Then, using the S -transform for square projections calculated in Equation (82), we have

$$\kappa_2 = \kappa_1 \frac{1 - df_1}{\frac{N}{D} - df_1}, \quad (213)$$

$$\frac{d \log S}{d \log df_1} = \frac{df_1}{\frac{N}{D} - df_1} - \frac{df_1}{1 - df_1}. \quad (214)$$

Note that κ_2 is not renormalized as strongly as in the case of a Wishart. Intuitively, a matrix with random Gaussian entries projecting down to $N < D$ dimensions not only projects, but also adds noise. This leads to a larger renormalization relative to the case of a simple projection.

We now evaluate the ridgeless limit. There is no underparameterized case. Applying Equations (195), and (198) gives:

$$E_g = \begin{cases} \frac{\kappa_2 tf_1}{1 - N/P} + \frac{N/P}{1 - N/P} \sigma_\epsilon^2, & N < P, D \\ -\frac{\kappa_2^2 tf'}{1 - \frac{D}{P} df_2} + \kappa_2 tf_1 \frac{1 - N/D}{1 - P/D} \frac{P/N}{1 - P/N} \\ \quad + \sigma_\epsilon^2 \left[\frac{\frac{D}{P} df_2}{1 - \frac{D}{P} df_2} + \frac{1 - N/D}{1 - P/D} \frac{P/N}{1 - P/N} \right] & P < N, D. \end{cases} \quad (215)$$

When $N = D$ this recovers the results for linear regression. To our knowledge, this result has not been explicitly obtained in past works.

5. Deep Structured Random Feature Model

We now generalize the previous example to the case of several layers of random features, each of which has nontrivial structure in its covariance. That is, we take

$$\mathbf{F}^\top \mathbf{F} = \mathbf{F}_1^\top \cdots \mathbf{F}_L^\top \mathbf{F}_L \cdots \mathbf{F}_1, \quad \mathbb{E}[\mathbf{F}_\ell^\top \mathbf{F}_\ell] = \boldsymbol{\Sigma}_\ell. \quad (216)$$

The S -transform we will need is that evaluated for the Gram matrix of a deep structured Wishart product. This has been computed in Equation (112) of Section IV.I. Taking the shorthand $\text{df}_1 = \text{df}_{\boldsymbol{\Sigma}_1}^1$, $\text{df}_2 = \text{df}_{\boldsymbol{\Sigma}_2}^2$, we again have:

$$\text{df}_{\boldsymbol{\Sigma}_F^1}^1(\kappa_1) = \text{df}_1(\kappa_2), \quad (217)$$

$$\kappa_2 \prod_{\ell=1}^L (-\text{df}_1) \zeta_{\boldsymbol{\Sigma}_\ell} \left(-\frac{D}{N_\ell} \text{df}_1 \right) = \kappa_1, \quad (218)$$

$$\begin{aligned} \frac{d \log S}{d \log \text{df}_1} &= \sum_{\ell} \left(-1 + \frac{D}{N_\ell} \text{df}_1 \frac{\zeta'_{\boldsymbol{\Sigma}_\ell}(-\frac{D}{N_\ell} \text{df}_1)}{\zeta_{\boldsymbol{\Sigma}_\ell}(-\frac{D}{N_\ell} \text{df}_1)} \right) \\ &= \sum_{\ell} \left(-1 - \frac{\frac{D}{N_\ell} \text{df}_1}{\kappa_\ell \text{df}_{\boldsymbol{\Sigma}_\ell}^1(\kappa_\ell)} \right), \quad \kappa_\ell \equiv -\zeta_{\boldsymbol{\Sigma}_\ell}(-\frac{D}{N_\ell} \text{df}_1) \\ &= \sum_{\ell=1}^L \frac{\text{df}_{\boldsymbol{\Sigma}_\ell}^2(\kappa_\ell)}{\text{df}_{\boldsymbol{\Sigma}_\ell}^1(\kappa_\ell) - \text{df}_{\boldsymbol{\Sigma}_\ell}^2(\kappa_\ell)}. \end{aligned} \quad (219)$$

In the last line we have used the fact that $\text{df}_{\boldsymbol{\Sigma}_\ell}^1(\kappa_\ell) = \frac{D}{N_\ell} \text{df}_1$ and applied Equation (21). In the ridgeless limit $\text{df}_{\boldsymbol{\Sigma}_\ell}^1 = P/N_\ell$. Adopting the notation $\gamma^{(\ell)} \equiv \frac{N_\ell}{P} \text{df}_{\boldsymbol{\Sigma}_\ell}^2$, $\gamma^{(0)} \equiv \frac{D}{P} \text{df}_2 = \gamma_2$ gives the formula for the generalization error:

$$E_g = \begin{cases} \frac{D/P}{1 - D/P} \sigma_\epsilon^2, & P > D, \{N_\ell\}_{\ell=1}^L \\ \frac{\kappa_2 \text{tf}_1}{1 - N_\ell/P} + \sigma_\epsilon^2 \frac{N_\ell/P}{1 - N_\ell/P} & N_\ell < D, P, \{N'_\ell\}_{\ell' \neq \ell} \\ -\frac{\kappa_2^2 \text{tf}'_1}{1 - \gamma^{(0)}} + \kappa_2 \text{tf}_1 \sum_{\ell=1}^L \frac{\gamma^{(\ell)}}{1 - \gamma^{(\ell)}} + \sigma_\epsilon^2 \sum_{\ell=0}^L \frac{\gamma^{(\ell)}}{1 - \gamma^{(\ell)}} & P < D, \{N_\ell\}_{\ell=1}^L. \end{cases} \quad (220)$$

This is the same result as obtained in [31] using replica theory. Lastly, taking Equation (218) and (219) plugging in to Equation (193) gives the finite ridge result for quoted in [31].

F. Training Error

One can also compute the training error as in Section V.E, yielding

$$\begin{aligned} E_{tr} &= \frac{\lambda^2}{P} \bar{\mathbf{w}}^\top \mathbf{X}^\top \left(\frac{1}{P} \mathbf{X} \mathbf{F} \mathbf{F}^\top \mathbf{X}^\top + \lambda \right)^{-2} \mathbf{X} \bar{\mathbf{w}} + \sigma_\epsilon^2 \lambda^2 \text{tr} \left[\left(\frac{1}{P} \mathbf{X} \mathbf{F} \mathbf{F}^\top \mathbf{X}^\top + \lambda \right)^{-2} \right] \\ &= -\lambda^2 \partial_\lambda \bar{\mathbf{w}}^\top \hat{\boldsymbol{\Sigma}} (\mathbf{F} \mathbf{F}^\top \hat{\boldsymbol{\Sigma}} + \lambda)^{-1} \bar{\mathbf{w}} - \sigma_\epsilon^2 \lambda^2 \partial_\lambda \underbrace{\left[\frac{1 - \frac{D}{P} \text{df}_{\boldsymbol{\Sigma}_F^1}^1(\kappa_1)}{\lambda} \right]}_{1/\kappa_1} \\ &\simeq -\frac{\lambda^2}{1 - \gamma_1} \text{tf}'_1(\kappa_1) + \frac{\sigma_\epsilon^2 \lambda^2 / \kappa_1^2}{1 - \gamma_1} = \frac{\lambda^2}{\kappa_1^2} (E_g + \sigma_\epsilon^2). \end{aligned} \quad (221)$$

Thus we see that the analogue of the KARE (i.e., the GCV estimator) is given by multiplying the training error by $S_{\mathbf{W}}(-\text{df}_1)^2$. This is also asymptotically equal to $S_{\mathbf{W}}(-\text{df}_{\hat{\boldsymbol{\Sigma}}_F}(\lambda))^2$, which can be calculated from the training data alone.

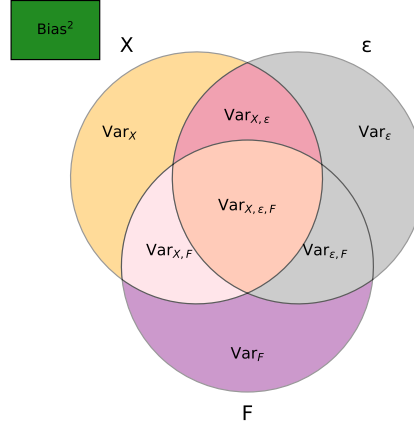


FIG. 11 Schematic of the bias-variance decomposition for linear random features, as in [40]. The color scheme matches the plots in Figures 10 and 12. Grey regions do not contribute to variance.

G. Implicit Regularization of Ensembles

Consider the taking E different sets of random features \mathbf{F}_e all drawn from the same distribution. On each independent ensemble, one runs regression with ridge λ and obtains $\hat{\mathbf{w}}_e$. Taking the average of all of these gives the **ensembled** predictor:

$$\hat{\mathbf{w}}_E = \frac{1}{E} \sum_e \hat{\mathbf{w}}_e. \quad (222)$$

Similar to how in Section V.H we saw that bagging reduces the variance over \mathbf{X}, ϵ by a factor of $1/B$, ensembling reduces the variance over the features \mathbf{F} by $1/E$. For a large ensemble of models, we can ask what $\lim_{E \rightarrow \infty} \hat{\mathbf{w}}_E$ converges to. Applying deterministic equivalence to the features, this becomes:

$$\begin{aligned} \mathbb{E}_{\mathbf{F}} \hat{\mathbf{w}} &= \mathbb{E}_{\mathbf{F}} (\mathbf{F}\mathbf{F}^\top \mathbf{X}^\top \mathbf{X} + P\lambda\mathbf{I})^{-1} \mathbf{F}\mathbf{F}^\top \mathbf{X}^\top \mathbf{y} \\ &\simeq (\mathbf{X}^\top \mathbf{X} + P\lambda S_{\mathbf{F}\mathbf{F}^\top} \mathbf{I})^{-1} \mathbf{X}^\top \mathbf{y}. \end{aligned} \quad (223)$$

This is just ridge regression in the original input space \mathbb{R}^D but with the ridge λ renormalized to $\lambda S_{\mathbf{F}\mathbf{F}^\top} = \lambda \kappa_2 / \kappa_1$. In the case where $\mathbf{F}\mathbf{F}^\top$ is a projection, this was obtained in [101; 102; 103]. Our results hold for any features \mathbf{F} so that $\mathbf{F}\mathbf{F}^\top$ is free of $\hat{\Sigma}$, as in [103].

H. Fine-Grained Bias-Variance Decomposition

Extending the results of Sections V.H and VI.G, we consider averaging the learned weights $\hat{\mathbf{w}}$ over three sources of variance for a general feature map \mathbf{F} . The three sources are the choice of training set \mathbf{X} , the label noise ϵ , and the random features \mathbf{F} . We have

$$\begin{aligned} \mathbb{E}_{\mathbf{X}, \epsilon, \mathbf{F}} \hat{\mathbf{w}} &= \mathbb{E}_{\mathbf{X}, \mathbf{F}} \mathbf{F} (\mathbf{F}^\top \mathbf{X}^\top \mathbf{X} \mathbf{F} + P\lambda\mathbf{I})^{-1} \mathbf{F}^\top \mathbf{X}^\top \mathbf{X} \bar{\mathbf{w}} \\ &= \mathbb{E}_{\mathbf{F}} \mathbf{F}\mathbf{F}^\top (\Sigma \mathbf{F}\mathbf{F}^\top + \kappa_1 \mathbf{I})^{-1} \Sigma \bar{\mathbf{w}} \\ &= \Sigma (\Sigma + \kappa_2 \mathbf{I})^{-1} \bar{\mathbf{w}}. \end{aligned} \quad (224)$$

This yields that:

$$\text{Bias}^2 = E_g(\mathbb{E}_{\mathbf{X}, \epsilon, \mathbf{F}} \hat{\mathbf{w}}) = \kappa_2^2 \bar{\mathbf{w}}^\top \Sigma (\Sigma + \kappa_2 \mathbf{I})^{-2} \bar{\mathbf{w}} = -\kappa_2^2 \text{tf}'_1. \quad (225)$$

The variance term is similarly decomposable into contributions from the various combinations of \mathbf{X}, ϵ , and \mathbf{F} as in the work of Adlam and Pennington [40]. We sketch this in Figure 11. We can explicitly get $\text{Var}_{\mathbf{X}}, \text{Var}_{\mathbf{X}, \epsilon}, \text{Var}_{\epsilon}$ by considering $\mathbb{E}_{\mathbf{F}} \hat{\mathbf{w}}$. This was seen to be equivalent to ridge regression with a rescaled ridge $\lambda S_{\mathbf{F}\mathbf{F}^\top}$ in Equation (223).

This ridge will be further renormalized to κ_2 in the final deterministic expression for the generalization error. Thus, the bias-variance results of Section V.H apply with $\kappa = \kappa_2, \gamma = \gamma_2$ and we get:

$$\text{Var}_{\mathbf{X}} = -\frac{\gamma_2}{1-\gamma_2} \kappa_2^2 \text{tf}'_1, \quad \text{Var}_{\mathbf{X}, \epsilon} = \frac{\gamma_2}{1-\gamma_2} \sigma_\epsilon^2, \quad \text{Var}_\epsilon = 0. \quad (226)$$

One can similarly compute $\text{Var}_{\mathbf{F}}, \text{Var}_{\mathbf{F}, \epsilon}$ by instead averaging the estimator $\hat{\mathbf{w}}$ over \mathbf{X} :

$$\begin{aligned} \mathbb{E}_{\mathbf{X}} \hat{\mathbf{w}} &= \mathbb{E}_{\mathbf{X}} \mathbf{F} (\mathbf{F}^\top \mathbf{X}^\top \mathbf{X} \mathbf{F} + P\lambda \mathbf{I})^{-1} \mathbf{F}^\top \mathbf{X}^\top (\mathbf{X} \bar{\mathbf{w}} + \epsilon) \\ &= \mathbf{F} \mathbf{F}^\top \Sigma (\mathbf{F} \mathbf{F}^\top \Sigma + \kappa_1 \mathbf{I})^{-1} \bar{\mathbf{w}}. \end{aligned} \quad (227)$$

This gives that $\text{Var}_{\mathbf{F}, \epsilon} = 0$. The generalization error is then averaged over \mathbf{F} to yield:

$$E_g(\mathbb{E}_{\mathbf{X}} \hat{\mathbf{w}}) = (\bar{\mathbf{w}} - \mathbb{E}_{\mathbf{X}} \hat{\mathbf{w}})^\top \Sigma (\bar{\mathbf{w}} - \mathbb{E}_{\mathbf{X}} \hat{\mathbf{w}}) = \kappa_1^2 \bar{\mathbf{w}}^\top \Sigma^{1/2} (\Sigma_{\mathbf{F}} + \kappa_1 \mathbf{I})^{-2} \Sigma^{1/2} \bar{\mathbf{w}}. \quad (228)$$

This gives $\text{Var}_{\mathbf{F}}$ via:

$$\text{Bias}^2 + \text{Var}_{\mathbf{F}} = E_g(\mathbb{E}_{\mathbf{X}} \hat{\mathbf{w}}) = -\kappa_1^2 \partial_{\kappa_1} \tilde{\text{tf}}_1(\kappa_1) \Rightarrow \text{Var}_{\mathbf{F}} = \left(1 - \frac{d \log \kappa_2}{d \log \kappa_1}\right) \kappa_2 \text{tf}_2(\kappa_2). \quad (229)$$

The joint variance $\text{Var}_{\mathbf{X}, \mathbf{F}}$ is then given by the subtraction.

$$\text{Var}_{\mathbf{X}, \mathbf{F}} = \frac{\gamma_1}{1-\gamma_1} [-\kappa_1^2 \tilde{\text{tf}}'_1(\kappa_1)] - \frac{\gamma_2}{1-\gamma_2} [-\kappa_2^2 \text{tf}'_1(\kappa_2)] \quad (230)$$

Finally, we get that all the variance due to ϵ is in $\text{Var}_{\mathbf{X}, \epsilon}, \text{Var}_{\mathbf{X}, \mathbf{F}, \epsilon}$, with:

$$\text{Var}_{\mathbf{X}, \mathbf{F}, \epsilon} = \sigma_\epsilon^2 \left[\frac{\gamma_1}{1-\gamma_1} - \frac{\gamma_2}{1-\gamma_2} \right]. \quad (231)$$

All these terms are graphically presented in Figure 11. The expressions are consistent with what [40] find in the setting of random feature models on isotropic data.

1. Overparameterized Case

We can decompose the full deep structured random feature model generalization error into bias and variance terms as follows:

$$\underbrace{-\kappa_2^2 \text{tf}'_1}_{\text{Bias}^2} - \underbrace{\kappa_2^2 \text{tf}'_1 \frac{\gamma^{(0)}}{1-\gamma^{(0)}}}_{\text{Var}_{\mathbf{X}}} + \underbrace{\kappa_2 \text{tf}_1 \sum_{\ell=1}^L \frac{\gamma^{(\ell)}}{1-\gamma^{(\ell)}}}_{\text{Var}_{\mathbf{F}} + \text{Var}_{\mathbf{X}, \mathbf{F}}} + \underbrace{\frac{\gamma^{(0)}}{1-\gamma^{(0)}}}_{\text{Var}_{\mathbf{X}, \epsilon}} + \underbrace{\sigma_\epsilon^2 \sum_{\ell=1}^L \frac{\gamma^{(\ell)}}{1-\gamma^{(\ell)}}}_{\text{Var}_{\mathbf{X}, \mathbf{F}, \epsilon}}. \quad (232)$$

$$\text{Var}_{\mathbf{F}} = \kappa_2 \text{tf}_2 \frac{1}{1 + \sum_{\ell=0}^L \frac{\gamma^{(\ell)}}{1-\gamma^{(\ell)}}}. \quad (233)$$

The remaining term is:

$$\text{Var}_{\mathbf{X}, \mathbf{F}} = \kappa_2 \text{tf}_1 \sum_{\ell=1}^L \frac{\gamma^{(\ell)}}{1-\gamma^{(\ell)}} - \frac{\kappa_2 \text{tf}_2}{1 + \sum_{\ell=0}^L \frac{\gamma^{(\ell)}}{1-\gamma^{(\ell)}}}. \quad (234)$$

Note that the model-wise double descent peak that occurs when any of the $\gamma^\ell = 1$ for $\ell \geq 1$ is due entirely to the variances $\text{Var}_{\mathbf{X}, \epsilon}, \text{Var}_{\mathbf{X}, \mathbf{F}, \epsilon}$. The sample-wise double descent peak on the other hand is due to only to $\text{Var}_{\mathbf{X}}, \text{Var}_{\mathbf{X}, \epsilon}$.

2. Bottlenecked Case

Noting $\frac{d \log \kappa_2}{d \log \kappa_1} = 0$, we get:

$$\text{Bias}^2 = -\kappa_2^2 \text{tf}'_1 \quad \text{Var}_{\mathbf{X}} = \frac{\gamma^{(\ell)}}{1 - \gamma^{(\ell)}} [-\kappa_2^2 \text{tf}'_1], \quad \text{Var}_{\mathbf{F}} = \kappa_2 \text{tf}_2. \quad (235)$$

Here $\gamma^{(\ell)} = N_\ell/P$. The remaining term in the variance is then

$$\text{Var}_{\mathbf{X}, \mathbf{F}} = \frac{\gamma^{(\ell)}}{1 - \gamma^{(\ell)}} \kappa_2 \text{tf}_2. \quad (236)$$

3. Underparameterized Case

Because E_g depends only on σ_ϵ^2 we have that all of $\text{Var}_{\mathbf{X}}, \text{Var}_{\mathbf{F}}, \text{Var}_{\mathbf{X}, \mathbf{F}}$ vanish. The only nontrivial variance is the noise term, $\text{Var}_{\mathbf{X}, \epsilon}$.

I. Scaling Laws in P and N

As in the kernel setting, we take $\sigma_\epsilon^2 = 0$ and study the generalization performance for power-law distributed data $\eta_k \sim k^{-\alpha}$. In Section VI.I.1 we will average over teachers, connecting to results of [34] and reproducing phenomena observed in [30]. In section VI.I.2 we do not average over $\bar{\mathbf{w}}$ and instead take $\bar{w}_k^2 \eta_k \sim k^{-(1+2r\alpha)}$. We get a refinement of the scaling laws and observe different exponents in the overparameterized and underparameterized regime. As in Section V.I, α, r are the capacity and source exponents respectively.

In Section VI.I.3, we find a new scaling law in the overparameterized regime where finite width effects change the leading order scaling behavior and hurt generalization without fully bottlenecking the model. This is related to the variance-dominated behavior studied by the first and second authors with colleagues in [39].

1. Target Averaged Results

We can reproduce the results of [34] for general random feature models. There, the teacher vector $\bar{\mathbf{w}}$ was averaged over. In this case, using that $\mathbb{E}_{\mathbf{w}} \text{tf}_1 = \text{df}_1$, we get that in the zero noise limit of Equation (220):

$$E_g \simeq \begin{cases} 0, & P > D, N \\ \frac{\kappa_2 \text{df}_1}{1 - N_\ell/P} & N < D, P \\ \kappa_2 \text{df}_1 \left(1 + \sum_{\ell=1}^L \frac{\gamma^{(\ell)}}{1 - \gamma^{(\ell)}} \right) & P < D, N. \end{cases} \quad (237)$$

Unsurprisingly, in the underparameterized setting with no noise, there is no scaling law since $\bar{\mathbf{w}}$ is recovered exactly. In order to study the scaling properties of the bottlenecked and overparameterized settings, we need to know how κ_2 scales with N, P respectively. Again, this can be easily seen through Equation (189) defining the renormalized ridge κ_2 .

In the ridgeless limit, we either have a pole in $S_{\mathbf{F}\mathbf{F}^\top}(-\text{df}_1)$ (bottlenecked) or in $S_{\mathbf{W}}(-\text{df}_1)$ (overparameterized). Even in the most general case of deep structured random features, this happens only when $D\text{df}_1(\kappa_2)$ scales either as P or N , respectively. On the other hand, from Section V.I, we know that

$$D\text{df}_1(\kappa_2) = \int_1^\infty \frac{k^{-\alpha}}{\kappa_2 + k^{-\alpha}} dk \sim \kappa_2^{-1/\alpha}. \quad (238)$$

Thus, in order for the S -transforms to have a pole, we need $\kappa_2 \sim N^{-\alpha}, P^{-\alpha}$ in the bottlenecked and overparameterized settings respectively. Then $\text{df}_1 = N/D, P/D$ in these respective cases, giving:

$$E_g \sim \begin{cases} N^{1-\alpha} \frac{1}{1 - N_\ell/P} & \text{bottlenecked} \\ P^{1-\alpha} \left(1 + \sum_{\ell=1}^L \frac{\gamma^{(\ell)}}{1 - \gamma^{(\ell)}} \right) & \text{overparameterized} \end{cases} \quad (239)$$

In the case where the covariances of the features are white, we get $\gamma^{(\ell)} = P/N_\ell$. At $L = 1$, this formula then simplifies to

$$E_g \sim \begin{cases} N^{1-\alpha} \frac{1}{1 - N_\ell/P} & \text{bottlenecked} \\ P^{1-\alpha} \frac{1}{1 - P/N_\ell} & \text{overparameterized,} \end{cases} \quad (240)$$

which reproduces the main scalings found in [34]. One can see both resolution-limited and variance-limited scaling exponents in these expressions [30]. The parameter that is the bottleneck (N, P respectively) has a nontrivial scaling exponent, and scaling it up will continue decreasing the loss until a double descent peak is hit. This is the resolution-limited scaling. The non-bottleneck parameter enters only with trivial exponent, and scales only the subleading terms in the expansion of the generalization error. This is the variance-limited scaling.

We now consider the case where the weights of layer ℓ are drawn from an anisotropic distribution with covariance Σ_ℓ having eigenvalues decaying like $\eta_k \sim k^{-\alpha_\ell}$. This setting was studied in section VI.E.5. In the overparameterized ridgeless limit given by Equation (220), we have by definition of κ_ℓ that $\text{df}_{\Sigma_\ell}^1(\kappa_\ell) = P/N_\ell$, which gives that $\kappa_\ell \sim P^{-\alpha_\ell}$ assuming $\alpha_\ell > 1$ in a normalizable spectrum. This then gives $\gamma^{(\ell)} = \frac{N_\ell}{P} \text{df}_{\Sigma_\ell}^2 \sim O_P(1)$ independent of P . In the case where the spectrum of the weight matrices is not normalizable we get $\kappa_\ell \sim N_\ell^{1-\alpha_\ell}/P, \gamma^{(\ell)} \sim (P/N_\ell)^{\min(1, (1-\alpha_\ell)/\alpha_\ell)}$ as in Section V.I.2. In the window of $1/2 < \alpha < 1$, we get that the N_ℓ enters with nontrivial exponent. That is, the variance-limited exponents become nontrivial if the weight spectrum is non-normalizable, contrasting with previous works that have only considered the case of normalizable or isotropic weight spectra [31; 34]. Previous empirical works on feature-learning neural networks have encountered nontrivial scaling in N_ℓ [131; 132]. However, it is not clear whether this arises due through the mechanism described here or through data-dependent correlations between the weights at different layers. Products of strongly-correlated matrices are not amenable to easy treatment using the tools of free probability.

2. General Targets

We can extend this scaling analysis to general power-law structured $\bar{\mathbf{w}}$ with coefficients decaying as $\eta_k \bar{w}_k^2 = k^{-(1+2\alpha r)}$ with source exponent r , rather than averaging over the target weights. As noted in the prior section, in the ridgeless limit we have that $\kappa_2 \sim \min(P, N)^{-\alpha}$. This yields:

$$\begin{aligned} \kappa_2 \text{tf}_1(\kappa_2) &\sim \int_1^\infty \frac{k^{-(1+2\alpha r)}}{1 + k^{-\alpha}/\kappa_2} \sim \min(P, N)^{-2\alpha \min(r, 1/2)}, \\ -\kappa_2^2 \text{tf}'_1(\kappa_2) &\sim \int_1^\infty \frac{k^{-(1+2\alpha r)}}{(1 + k^{-\alpha}/\kappa_2)^2} \sim \min(P, N)^{-2\alpha \min(r, 1)}. \end{aligned} \quad (241)$$

This gives the following scalings in the bottlenecked and overparameterized regimes:

$$E_g \sim \begin{cases} N^{-2\alpha \min(r, 1/2)} \frac{1}{1 - N/P} + \sigma_\epsilon^2 \frac{N/P}{1 - N/P} \\ P^{-2\alpha \min(r, 1)} + P^{-2\alpha \min(r, 1/2)} \sum_{\ell=1}^L \frac{\gamma^{(\ell)}}{1 - \gamma^{(\ell)}} + \sigma_\epsilon^2 \sum_{\ell=0}^L \frac{\gamma^{(\ell)}}{1 - \gamma^{(\ell)}}. \end{cases} \quad (242)$$

The teacher-averaged results correspond to setting $1 + 2\alpha r = \alpha$, or equivalently $r = \frac{1}{2} \frac{\alpha-1}{\alpha}$. We see that in this setting $r < 1/2$. This uniquely determines the scalings and recovers the results of Section VI.I.1. We consider the general non-ridgeless case with label noise in Section VI.I.5.

3. Variance-Dominated Scaling

Several papers have found both theoretically and empirically that the leading order corrections of finite width in the overparameterized regime is to introduce an initialization-dependent variance that strictly hurts generalization [39; 83; 86; 88; 89]. By definition, this variance can be removed by ensembling networks over different initializations. The authors in [39] also highlight that finite-width networks in the lazy regime can exhibit a large separation of scales in the overparameterized regime between the size of P where this initialization-dependent variance begins to inhibit

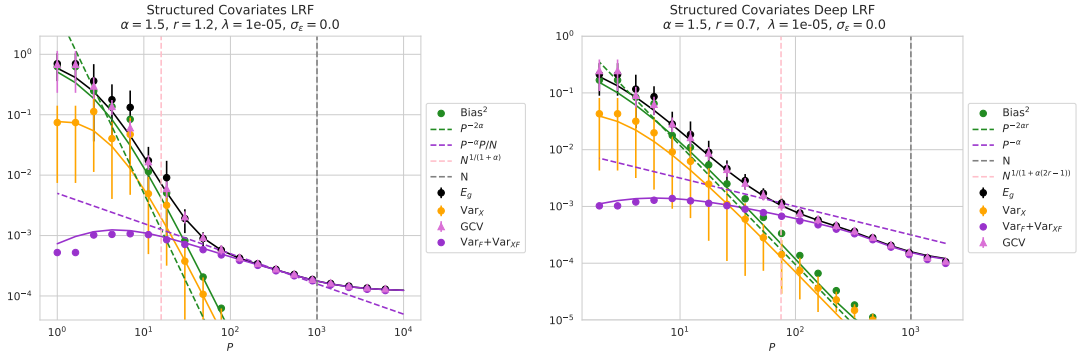


FIG. 12 Left: Linear random feature model with input dimension $D = 10000$ and hidden width $N = 1000$ with unstructured weights but structured input. Right: Deep linear random feature model with input dimension 2000 and two hidden layers of widths $N = 1000$ and unstructured weights. The input dimension is $D = 2000$. In both cases, the source exponent puts us in the regime where variance-dominated behavior can occur. Past a certain point (dashed pink), most of the limiting behavior of performance is due to variance over initializations (solid purple) which can thus be removed by ensembling. The ridge has been chosen to eliminate the double descent peak. We bag over 20 data seeds and ensemble over 20 initialization seeds.

generalization and the interpolation threshold at $P = N$. In that work, they studied a special type of nonlinear model to reproduce the behavior. Here, we show that this can happen also in linear random feature models.

Using Equation (232), one can compute the following two terms in the overparameterized ridgeless setting:

$$\begin{aligned} \text{Bias}^2 + \text{Var}_{\mathbf{X}} &\sim P^{-2\alpha \min(r,1)}, \\ \text{Var}_{\mathbf{F}} + \text{Var}_{\mathbf{F},\mathbf{X}} &\sim P^{-2\alpha \min(r,1/2)} \sum_{\ell=1}^L \frac{\gamma^{(\ell)}}{1 - \gamma^{(\ell)}}. \end{aligned} \quad (243)$$

When $\sigma_\epsilon^2 = 0$, the sum of these two terms gives the generalization error E_g . When over half of the generalization error is due to the variance term, we say that the scaling is **variance-dominated**. We will denote the value of P where the scaling becomes variance-dominated by $P_{\mathbf{F}}$. In the above, if $r \leq 1/2$, then the scaling exponents of the P factors in front agree. Assume for now that the features are isotropic. We have that $\gamma^{(\ell)} = P/N_\ell$. Consequently, we get that $P_{\mathbf{F}} \sim \frac{N}{1+L}$. Thus, for deep random feature models, the depth gives a linear separation between $P = P_{\mathbf{F}}$ and the interpolation threshold $P = N_\ell$. Unless L is immense, this doesn't lead to a genuine scaling law.

We must therefore have $r > 1/2$ in order to have $\text{Var}_{\mathbf{F}} + \text{Var}_{\mathbf{F},\mathbf{X}}$ dominate $\text{Bias}^2 + \text{Var}_{\mathbf{X}}$ over an extended range of scales. The value of P where this new scaling enters is at:

$$P_{\mathbf{F}}^{-2\alpha \min(r,1)} \sim \frac{P_{\mathbf{F}}^{-(\alpha-1)}}{N} \Rightarrow P_{\mathbf{F}} \sim N^{\frac{1}{1+2\alpha \min(r-1/2,1/2)}}. \quad (244)$$

This crossover determines when variance-dominated behavior emerges.

The condition $r > 1/2$ has a clear interpretation in terms of the theory of kernels. Consider the D dimensional input space as the reproducing kernel Hilbert space (RKHS) \mathcal{H} of some kernel with eigenspectrum given by the eigenvalues η_k of Σ . Having the target function $f(\mathbf{x}) = \bar{\mathbf{w}} \cdot \mathbf{x}$ be a normalizable element of \mathcal{H} is equivalent to the two-norm $\|\mathbf{w}\|^2$ being finite. This in turn is equivalent to $r > 1/2$. Thus, if the target function is finite-norm in the original space, passing through random features can substantially hurt the scaling properties of E_g .

Remaining in the overparameterized setting $P < N$, consider the case where a given Σ_ℓ is anisotropic, with power law structure. That is, the eigenvalues of Σ_ℓ decay as $k^{-\alpha_\ell}$. Then by the same analysis as in Section V.I.2, we have that $\gamma^{(\ell)}$ scales as $(P/N_\ell)^{c_\ell}$ where $c_\ell = \max(0, \min(1, \frac{1-\alpha_\ell}{\alpha_\ell}))$. There, as long as $r > 1/2$,

$$P_{\mathbf{F}} \sim N^{\frac{c}{c+2\alpha \min(r-1/2,1/2)}}. \quad (245)$$

In particular when $r > 1/2$ and $\alpha_\ell \geq 1$ we get that this term always dominates.

4. Effects of Weight Structure

In [31], the second and third authors analyzed deep linear random feature models with structured Gaussian weights, showing that adding structure to weights generally hurts generalization. There, using the fact that each structured

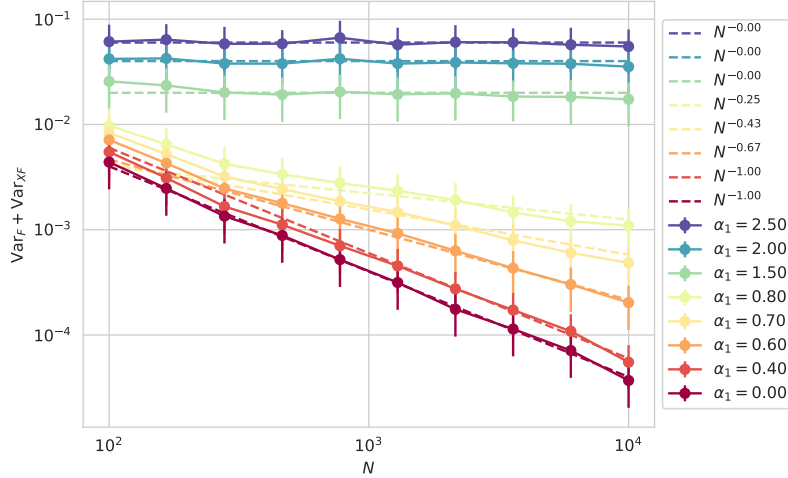


FIG. 13 Scaling of finite N corrections to a shallow linear random feature model when $P = 10, D = 10000$. Dashed lines are pure power laws. For $0.5 < \alpha_\ell < 1$ one observes nontrivial scaling laws with the width. For $\alpha_\ell > 1$ one observes a constant scaling, and taking the infinite width limit does not get rid of $\text{Var}_{\mathbf{F}}$. For $\alpha_\ell > 1$ the finite asymptotic values scale as $\alpha_\ell - 1$, and are shown as dashed lines.

Gaussian can be interpreted as a product of an unstructured Gaussian matrix with the fixed weight covariance, this effect was interpreted in terms of the rotation-invariance of the unstructured Gaussian factors: there are no preferred directions into which variance in the weights should be shunted, so structure should not be beneficial. When studying scaling properties, [31] only considered the case of normalizable weight spectra $\alpha_\ell > 1$.

Here, we offer a refined interpretation of why weight structure is harmful in terms of source-capacity conditions. Large exponents α_ℓ yield rapidly-decaying weight spectra. This reduces the effective dimensionality of the hidden layers and limits the ability of signals to propagate through this channel. This induces a variance over initializations that becomes stronger as α_ℓ is increased. For $\alpha_\ell > 1$, $\text{Var}_{\mathbf{F}} + \text{Var}_{\mathbf{X}_{\mathbf{F}}}$ remains finite even as the hidden layer sizes go to infinity. This residual variance at infinite width can be seen from the approximation $\gamma^{(\ell)}/(1 - \gamma^{(\ell)}) \approx \alpha_\ell - 1 + 1/(N_\ell/P - 1)$ with normalizable spectrum used in [31] and based on earlier results of [34]. We illustrate this effect in Figure (13).

The capacity-limiting effect of structured weights is related to the rotation-invariance of linear random feature models noted in [31]: even if the task is low-dimensional, meaning that only a low-dimensional signal needs to be propagated through the network, the lack of correlations between the layers means that this signal cannot be preserved through selective routing along large-variance dimensions. As a result, we suggest that the ability to coordinate signal propagation across layers is an important characteristic of feature learning in fully-trained deep networks. It would also be interesting to explore the connections between weight decay exponents and the exponents of finite- N corrections in wide feature-learning networks.

We can also extend our analysis beyond the $\alpha_\ell > 1$ case. As in Section (V.I.2), when $1/2\alpha_\ell < 1$, we have that $\gamma^{(\ell)}$ scales nontrivially with N_ℓ as $(N_\ell/P)^c$, with $c = (1 - \alpha_\ell)/\alpha_\ell$. In the language of Bahri *et al.* [30], this gives an example of nontrivial variance-limited scaling, that is, there is nontrivial scaling with respect to the bottleneck parameter N_ℓ .

5. Characterization of All Scaling Regimes

We now consider the scaling regimes in the case of general $\lambda, \sigma_\epsilon^2$ in the case of a deep structured linear random feature model, as considered in Section V.I.E.5. We will take the spectrum of Σ to be normalizable. At finite ridge we need $\lambda > \min(P, N)^{-\alpha}$ so that $\kappa_2 \sim \lambda$, otherwise κ_2 will go as $\min(P, N)^{-\alpha}$ and the situation becomes equivalent to the ridgeless setting. If λ exceeds this threshold, we have

$$\begin{aligned}
 -\kappa_2^2 \text{tf}'_1 &\sim \lambda^{2 \min(r, 1)}, & \kappa_2 \text{tf}_1 &\sim \lambda^{2 \min(r, 1/2)} \\
 D \text{df}_1 &\sim D \text{df}_2 \sim \lambda^{-1/\alpha}, & \gamma_2 &\sim \frac{\lambda^{-1/\alpha}}{P}.
 \end{aligned} \tag{246}$$

Then for general structured random features from Equation (197)

$$\frac{d \log \kappa_1}{d \log \kappa_2} = 1 + \frac{df_1 - df_2}{df_1} \sum_{\ell=1}^L \frac{df_{\Sigma_\ell}^2(\kappa_\ell)}{df_{\Sigma_\ell}^1(\kappa_\ell) - df_{\Sigma_\ell}^2(\kappa_\ell)}. \quad (247)$$

We have by definition of κ_ℓ that $df_{\Sigma_\ell}^1(\kappa_\ell) = \frac{D}{N_\ell} df_1 \sim \lambda^{-1/\alpha}/N_\ell$. Assuming Σ_ℓ has a power law spectrum with exponent α_ℓ , let c_ℓ be $\min(\max(\frac{1-\alpha_\ell}{\alpha_\ell}, 1), 0)$. Then, taking $N = \min(\{N_\ell\}_{\ell=1}^L)$ to be the smallest width and c the corresponding c_ℓ :

$$\begin{aligned} \frac{d \log S}{d \log df_1} &\sim \left(\frac{\lambda^{-1/\alpha}}{N} \right)^c, \\ \frac{d \log \kappa_2}{d \log \kappa_1} &\sim 1, \quad 1 - \frac{d \log \kappa_2}{d \log \kappa_1} \sim \left(\frac{\lambda^{-1/\alpha}}{N} \right)^c. \end{aligned} \quad (248)$$

We have used the fact that $df_1 \sim df_2$ when Σ has normalizable spectrum. Finally from Equation (191) we have $\gamma_1 \sim \lambda^{-1/\alpha}/P$. Together this gives:

$$E_g \sim \lambda^{2 \min(r,1)} + \lambda^{2 \min(r,1/2)} \left(\frac{\lambda^{-1/\alpha}}{N} \right)^c + \sigma_\epsilon^2 \frac{\lambda^{-1/\alpha}}{P}. \quad (249)$$

If we take the ridge to scale as $\lambda \sim P^{-l} + N^{-l}$ then in the overparameterized regime this is effectively P^{-l} and in the bottlenecked regime this is effectively N^{-l} . As $N \rightarrow \infty$ this recovers the ridge scaling considered in Section V.I. If $l < \alpha$ then $\kappa_2 \sim \min(P, N)^{-l}$. If $l > \alpha$ then we achieve the ridgeless scaling limit $\kappa_2 \sim \min(P, N)^{-\alpha}$.

Using Equations (241), in the bottlenecked regime, $N < P$ we get

$$E_g \sim \frac{N^{-2 \min(\alpha, l) \min(r, 1/2)}}{1 - N/P} + \sigma_\epsilon^2 \frac{N^{\min(1, \alpha/l)}}{P}. \quad (250)$$

This gives the following scaling regimes in N (resolution limited) and P (variance limited):

$$E_g \sim \begin{cases} \frac{N^{-2\alpha \min(r, 1/2)}}{1 - N/P}, & \alpha < l; N^{-2\alpha \min(r, 1/2)} \gg \sigma_\epsilon^2 N/P & \text{Signal dominated} \\ \frac{N^{-2l \min(r, 1/2)}}{1 - N/P}, & l < \alpha; N^{-2l \min(r, 1/2)} \gg \sigma_\epsilon^2 N^{l/\alpha}/P & \text{Ridge dominated} \\ \sigma_\epsilon^2 \frac{N}{P} & \alpha < l; N^{-2 \min(\alpha, l) \min(r, 1/2)} \ll \sigma_\epsilon^2 N/P & \text{Noise dominated} \\ \sigma_\epsilon^2 N^{l/\alpha}/P & l < \alpha; N^{-2 \min(\alpha, l) \min(r, 1/2)} \ll \sigma_\epsilon^2 N^{l/\alpha}/P & \text{Noise mitigated} \end{cases} \quad (251)$$

The resolution-limited exponents are similar but not identical to those in the linear regression setting (171). The variance-limited exponents in P are always trivial.

In the overparameterized regime, $P < N$ we have

$$E_g \sim P^{-2 \min(\alpha, l) \min(r, 1)} + P^{-2 \min(\alpha, l) \min(r, 1/2)} \left(\frac{P}{N} P^{-\min(\frac{\alpha-l}{\alpha}, 0)} \right)^c + \sigma_\epsilon^2 P^{-\min(\frac{\alpha-l}{\alpha}, 0)}. \quad (252)$$

This gives the following scaling regimes:

$$E_g \sim \begin{cases} P^{-2\alpha \min(r, 1)}, & \alpha < l; P \ll P_\epsilon; r \leq 1/2 \text{ or } P \ll P_{\mathbf{F}} & \text{Signal dominated} \\ P^{-\alpha} \left(\frac{P}{N} \right)^c, & \alpha < l; P \ll P_\epsilon; r > 1/2; P \gg P_{\mathbf{F}} & \text{Var}_{\mathbf{F}} \text{ dominated} \\ P^{-2l \min(r, 1)}, & l < \alpha; P \ll P_\epsilon; r \leq 1/2 \text{ or } P \ll P_{\mathbf{F}} & \text{Ridge dominated} \\ P^{-l} \left(\frac{P^{l/\alpha}}{N} \right)^c, & l < \alpha; P \ll P_\epsilon; r > 1/2; P \gg P_{\mathbf{F}} & \text{Ridge \& Var}_{\mathbf{F}} \text{ dominated} \\ \sigma_\epsilon^2 P^0, & \alpha < l; P \gg P_\epsilon, & \text{Noise dominated} \\ \sigma_\epsilon^2 P^{-\frac{\alpha-l}{\alpha}}, & l < \alpha; P \gg P_\epsilon & \text{Noise mitigated} \end{cases} \quad (253)$$

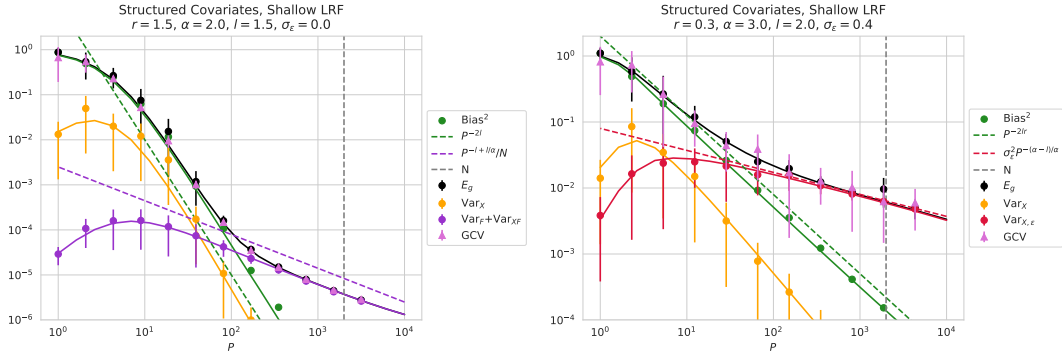


FIG. 14 Shallow linear random feature model with $D = 10000$, $N = 2000$ and isotropic weights exhibiting multiple scaling regimes. Dashed lines are exact power laws for reference. Left: exhibiting the transition from ridge dominated to joint variance and ridge dominated scaling. Solid curves are theory and dots are empirical results. Right: Shallow linear random feature model exhibiting the transition from ridge dominated to noise mitigating behavior. Relevant variances are plotted. In both cases, the double descent peak at $P = N$ is eliminated.

Here,

$$P_{\mathbf{F}} \sim N^{\frac{\epsilon}{c+2 \min(\alpha, l) \min(r-1/2, 1/2)}} \quad (254)$$

and P_{ϵ} is defined to be the value of P where either of the last two scalings become comparable in size to the first four:

$$\min(P_{\epsilon}^{-2 \min(\alpha, l) \min(r, 1)}, P_{\epsilon}^{-2 \min(\alpha, l) \min(r, 1/2)} P_{\epsilon}^{c \max(1, l/\alpha)} / N) = \sigma_{\epsilon}^2 P_{\epsilon}^{-\min(0, \frac{\alpha-l}{\alpha})}. \quad (255)$$

VII. MODELS WITH ADDITIVE FEATURE NOISE

A. Setup and Motivation

In this section, we turn our attention to a model in which the true latent features are not only randomly projected, but also corrupted by additive noise. Concretely, we consider a model where the targets are generated as

$$y_\mu = \bar{\mathbf{w}} \cdot \mathbf{x}_\mu + \epsilon_\mu, \quad (256)$$

while the student has access only to features that are both projected by a matrix $\mathbf{F} \in \mathbb{R}^{D \times N}$ and corrupted by additive noise $\boldsymbol{\xi} \in \mathbb{R}^N$ that is independent and identically distributed for each sample. As before, the entries in \mathbf{F} have variance $1/D$ while the entries in $\boldsymbol{\xi}$ are order 1. Using the same setup as in Equation (175), we have

$$f(\mathbf{x}) = (\mathbf{x}^\top \mathbf{F} + \boldsymbol{\xi}^\top) \mathbf{v}. \quad (257)$$

Here \mathbf{v} are the trainable weights. We take the latent features and additive noise to be jointly Gaussian and independent:

$$\begin{pmatrix} \mathbf{x} \\ \boldsymbol{\xi} \end{pmatrix} \sim \mathcal{N} \left(\mathbf{0}_{D+N}, \begin{pmatrix} \boldsymbol{\Sigma} & \mathbf{0} \\ \mathbf{0} & \boldsymbol{\Sigma}_\xi \end{pmatrix} \right). \quad (258)$$

This model has been prominently studied in several prior works. It was first explicitly solved by Mei & Montanari [26]. There, the authors considered a random feature model $f(\mathbf{x}) = \sigma(\mathbf{x}^\top \mathbf{F}) \mathbf{v}$ where σ is a nonlinearity applied element-wise and \mathbf{v} is trainable. \mathbf{F} has random entries with mean zero and variance $1/D$. Mei & Montanari highlighted that for a random feature model where features \mathbf{F} are mapped through a nonlinearity σ with

$$\mu_0 = \mathbb{E}_{x \sim \mathcal{N}(0,1)}[\sigma(x)], \quad \mu_1 = \mathbb{E}_{x \sim \mathcal{N}(0,1)}[x\sigma(x)], \quad \mu_\star = \mathbb{E}_{x \sim \mathcal{N}(0,1)}[\sigma(x)^2] - \mu_0^2 - \mu_1^2 \quad (259)$$

the asymptotic generalization error is equal to that for a Gaussian equivalent model. The Gaussian equivalent makes the replacement

$$\sigma(\mathbf{x}^\top \mathbf{F}) \simeq \mu_0 \mathbf{1} + \mu_1 \mathbf{x}^\top \mathbf{F} + \boldsymbol{\xi}, \quad \boldsymbol{\xi} \sim \mathcal{N}(0, \mu_\star \mathbf{I}). \quad (260)$$

Here $\mathbf{1}$ is the vector of ones. Taking $\mu_0 = 0, \mu_1 = 1$ we recover Equation (257) in the case where the elements of $\boldsymbol{\xi}$ are independent and normally distributed for each sample. Equivalences of random features passed through nonlinearities in the proportional limit have also been studied in [32; 33; 64]. Scalings beyond the linear regime have been studied in [133; 134].

An alternative reason to study random features corrupted by additive noise is an extension of the perspective taken in [34] for linear random features. There, one takes $D \gg N, P$. The D -dimensional space can be viewed as an analogue of the infinite-width NTK features, while N is viewed as the number of parameters. A linear random feature model is thus similar to doing regression with a random feature approximation to the NTK. This is similar to the finite-width NTK (also known as the **empirical neural tangent kernel** or eNTK). However, it is known that the entries of the finite-width eNTK also have initialization-dependent variance going as $1/n$, where n is the width of the network [84].¹² This enters at a different scale than the number of parameters N . The authors in [39] use this additive noise to model eNTK fluctuations. This leads to a performance decrease, driven primarily by initialization variance at relatively small values of P .

B. Averaging Over Data

Let $\mathbf{X} \in \mathbb{R}^{P \times D}$ be the design matrix on the train set, with $\mathbf{X}_{\mu i} = [\mathbf{x}_\mu]_i$. Let $\boldsymbol{\Xi} \in \mathbb{R}^{P \times N}$ be the feature noise matrix on the train set, with $\boldsymbol{\Xi}_{\mu i} = [\boldsymbol{\xi}_\mu]_i$. Define the matrices $\bar{\mathbf{X}}$ and $\bar{\mathbf{F}}$ to be

$$\bar{\mathbf{X}} \equiv (\mathbf{Z}_1 \quad \mathbf{Z}_2) \in \mathbb{R}^{P \times (D+N)}, \quad \bar{\mathbf{F}} \equiv \begin{pmatrix} \boldsymbol{\Sigma}^{1/2} \mathbf{F} \\ \boldsymbol{\Sigma}_\xi^{1/2} \end{pmatrix} \in \mathbb{R}^{(D+N) \times N}. \quad (261)$$

¹² This is distinct from N in the random feature model, which we have also been calling width.

Here $\mathbf{Z}_1, \mathbf{Z}_2$ are both unstructured Gaussian matrices. All structure is added by the features $\overline{\mathbf{F}}$. Then $\overline{\mathbf{X}}, \overline{\mathbf{F}}$ are free of one another and we can apply deterministic equivalence. Moreover, $f(\mathbf{X}) = \overline{\mathbf{X}} \overline{\mathbf{F}} \mathbf{v}$ corresponds to a linear random feature model, as studied in the previous section. We also define the extended teacher vector:

$$\overline{\mathbf{w}}_{D+N} \equiv \begin{pmatrix} \boldsymbol{\Sigma}^{1/2} \overline{\mathbf{w}} \\ \mathbf{0}_N \end{pmatrix} \in \mathbb{R}^{D+N}. \quad (262)$$

This accounts for the fact that the target labels do not depend on the noise $\boldsymbol{\xi}$.

We can now directly apply the formulas for E_g in the linear random feature case from the prior section.

$$E_g = -\frac{\kappa_1^2}{1-\gamma_1} \partial_{\kappa_1} \overline{\mathbf{w}}_{D+N}^\top (\overline{\mathbf{F}} \overline{\mathbf{F}}^\top + \kappa_1 \mathbf{I})^{-1} \overline{\mathbf{w}}_{D+N} + \sigma_\epsilon^2 \frac{\gamma_1}{1-\gamma_1}, \quad (263)$$

$$\kappa_1 = \frac{\lambda}{1 - \frac{N}{P} \text{df}_{\overline{\mathbf{F}}^\top \overline{\mathbf{F}}}^1(\kappa_1)}, \quad \gamma_1 = \frac{N}{P} \text{df}_{\overline{\mathbf{F}}^\top \overline{\mathbf{F}}}^2(\kappa_1), \quad (264)$$

$$\overline{\mathbf{F}}^\top \overline{\mathbf{F}} = \mathbf{F}^\top \boldsymbol{\Sigma} \mathbf{F} + \boldsymbol{\Sigma}_\xi \quad (265)$$

$$\overline{\mathbf{F}} \overline{\mathbf{F}}^\top = \begin{pmatrix} \boldsymbol{\Sigma}^{1/2} \mathbf{F} \mathbf{F}^\top \boldsymbol{\Sigma}^{1/2} & \boldsymbol{\Sigma}^{1/2} \mathbf{F} \boldsymbol{\Sigma}_\xi^{1/2} \\ \boldsymbol{\Sigma}_\xi^{1/2} \mathbf{F}^\top \boldsymbol{\Sigma}^{1/2} & \boldsymbol{\Sigma}_\xi \end{pmatrix}. \quad (266)$$

Because of the structure of $\overline{\mathbf{w}}_{D+N}$, we care only about the top left block in:

$$(\overline{\mathbf{F}} \overline{\mathbf{F}}^\top + \kappa_1 \mathbf{I})^{-1} = \begin{pmatrix} \kappa_1 \mathbf{I} + \boldsymbol{\Sigma}^{1/2} \mathbf{F} \mathbf{F}^\top \boldsymbol{\Sigma}^{1/2} & \boldsymbol{\Sigma}^{1/2} \mathbf{F} \boldsymbol{\Sigma}_\xi^{1/2} \\ \boldsymbol{\Sigma}_\xi^{1/2} \mathbf{F}^\top \boldsymbol{\Sigma}^{1/2} & \kappa_1 \mathbf{I} + \boldsymbol{\Sigma}_\xi \end{pmatrix}^{-1} \equiv \begin{pmatrix} M_{11} & M_{12} \\ M_{12}^\top & M_{22} \end{pmatrix}. \quad (267)$$

By applying the Schur complement formula [129], this can be written compactly as:

$$M_{11} = \left[\kappa_1 \mathbf{I}_D + \kappa_1 \frac{1}{D} \boldsymbol{\Sigma}^{1/2} \mathbf{F} (\boldsymbol{\Sigma}_\xi + \kappa_1 \mathbf{I}_N)^{-1} \mathbf{F}^\top \boldsymbol{\Sigma}^{1/2} \right]^{-1} \quad (268)$$

$$= \frac{1}{\kappa_1} \left[\mathbf{I}_D - \boldsymbol{\Sigma}^{1/2} \mathbf{F} (\kappa_1 \mathbf{I}_N + \boldsymbol{\Sigma}_\xi + \mathbf{F}^\top \boldsymbol{\Sigma} \mathbf{F})^{-1} \mathbf{F}^\top \boldsymbol{\Sigma}^{1/2} \right]. \quad (269)$$

In the last line we have used the Woodbury matrix inversion identity [129]. Upon taking the appropriate κ_1 derivatives, the signal term reproduces the formula for the model studied in [39]. This is also equivalent to the very general Gaussian model studied in [24].

At this point, we will specialize to the case of isotropic noise $\boldsymbol{\Sigma}_\xi = \sigma_\xi^2 \mathbf{I}$. This further simplifies the signal term to:

$$-\frac{\kappa_1^2}{1-\gamma_1} \partial_{\kappa_1} \left[\frac{\kappa_1 + \sigma_\xi^2}{\kappa_1} \overline{\mathbf{w}}^\top \boldsymbol{\Sigma}^{1/2} (\boldsymbol{\Sigma}^{1/2} \mathbf{F} \mathbf{F}^\top \boldsymbol{\Sigma}^{1/2} + (\kappa_1 + \sigma_\xi^2) \mathbf{I})^{-1} \boldsymbol{\Sigma}^{1/2} \overline{\mathbf{w}} \right]. \quad (270)$$

C. Averaging Over Isotropic Features

Under the assumption that $\mathbf{F}^\top \mathbf{F}$ is distributed as a white Wishart matrix, we get:

$$\kappa_2 = \frac{\kappa_1 + \sigma_\xi^2}{\frac{N}{D} - \text{df}_{\boldsymbol{\Sigma}}^1} \Rightarrow \kappa_2 \left(\frac{N}{D} - \text{df}_{\boldsymbol{\Sigma}}^1 - \frac{\sigma_\xi^2}{\kappa_2} \right) = \kappa_1. \quad (271)$$

Because of the additive shift, $\text{df}_{\overline{\mathbf{F}}^\top \overline{\mathbf{F}}}^1 = \text{df}_{\mathbf{F}^\top \boldsymbol{\Sigma} \mathbf{F} + \sigma_\xi^2}$ is related to $\text{df}_{\boldsymbol{\Sigma}}^1$ as follows:

$$\begin{aligned} \text{df}_{\mathbf{F}^\top \boldsymbol{\Sigma} \mathbf{F} + \sigma_\xi^2}^1(\kappa_1) &= \text{df}_{\mathbf{F}^\top \boldsymbol{\Sigma} \mathbf{F}}^1(\kappa_1 + \sigma_\xi^2) + \sigma_\xi^2 \frac{1 - \text{df}_{\boldsymbol{\Sigma} \mathbf{F}^\top \boldsymbol{\Sigma} \mathbf{F}}^1(\kappa_1 + \sigma_\xi^2)}{\kappa_1 + \sigma_\xi^2} \\ &= \frac{D}{N} \text{df}_{\boldsymbol{\Sigma}}^1(\kappa_2) + \sigma_\xi^2 \frac{1 - \frac{D}{N} \text{df}_{\boldsymbol{\Sigma}}^1(\kappa_2)}{\kappa_1 + \sigma_\xi^2} \\ &= \frac{D}{N} \underbrace{\left[\text{df}_{\boldsymbol{\Sigma}}^1(\kappa_2) + \frac{\sigma_\xi^2}{\kappa_2} \right]}_{\overline{\text{df}}_1}. \end{aligned} \quad (272)$$

Here we have defined $\overline{\text{df}}_1$. The final expressions simplify dramatically in terms of this quantity. Then:

$$\overline{\text{df}}_2 = \partial_{\kappa_2}[\kappa_2 \overline{\text{df}}_1] = \text{df}_2 \quad (273)$$

$$\gamma_1 = \frac{N}{P} \frac{d}{d\kappa_1} [\kappa_1 \text{df}_{\mathbf{F}^\top \mathbf{F}}^1(\kappa_1)] = \frac{N}{P} \overline{\text{df}}_1 \left[1 - \frac{d \log \kappa_2}{d \log \kappa_1} \frac{\overline{\text{df}}_1 - \text{df}_2}{\overline{\text{df}}_1} \right], \quad (274)$$

$$\frac{d \log \kappa_1}{d \log \kappa_2} = 1 + \frac{1}{N/D - \overline{\text{df}}_1} (\overline{\text{df}}_1 - \text{df}_2). \quad (275)$$

Writing $\text{tf}_1 = \text{tf}_{\Sigma}^1$, the generalization error then takes an identical form to the linear random feature case, with the only difference being the replacement $\text{df}_1 \rightarrow \overline{\text{df}}_1$ in the consistency equation for κ_2 :

$$E_g = -\frac{\kappa_2^2 \text{tf}_1'}{1 - \gamma_1} \frac{d \log \kappa_2}{d \log \kappa_1} + \frac{\kappa_2 \text{tf}_1}{1 - \gamma_1} \left[1 - \frac{d \log \kappa_2}{d \log \kappa_1} \right] + \frac{\gamma_1}{1 - \gamma_1} \sigma_\epsilon^2. \quad (276)$$

In the ridgeless limit, we have two behaviors depending on whether $\kappa_1 = 0$ or $\kappa_1 \neq 0$. Note that κ_2 always stays nonzero in this setting. This highlights that the input dimension D drops out from determining whether the model is overparameterized or underparameterized. The relevant quantities to compare are N and P . We have:

- $N < P$, underparameterized:

Then $\kappa_1 = 0$ and $\overline{\text{df}}_1 \rightarrow 1$, giving $\gamma_1 = N/P$. Our final formula simplifies to

$$E_g = \frac{\kappa_2 \text{tf}_1}{1 - N/P} + \sigma_\epsilon^2 \frac{N/P}{1 - N/P}. \quad (277)$$

Here, κ_2 satisfies the equation

$$\frac{N}{D} = \overline{\text{df}}_1 = \text{df}_{\Sigma}^1(\kappa_2) + \frac{\sigma_\xi^2}{\kappa_2}. \quad (278)$$

- $P < N$, overparameterized:

Then $\overline{\text{df}}_1 \rightarrow P/D$ and we get:

$$E_g = -\frac{\kappa_2^2 \text{tf}_1'(\kappa_2)}{1 - \frac{D}{P} \text{df}_2} + \frac{\kappa_2 \text{tf}_1 P/N}{1 - P/N} + \sigma_\epsilon^2 \left[\frac{\frac{D}{P} \text{df}_2}{1 - \frac{D}{P} \text{df}_2} + \frac{P/N}{1 - P/N} \right]. \quad (279)$$

Here, κ_2 satisfies the equation

$$\frac{P}{D} = \overline{\text{df}}_1 = \text{df}_{\Sigma}^1(\kappa_2) + \frac{\sigma_\xi^2}{\kappa_2}. \quad (280)$$

In both cases, these appear identical to the forms of the linear random feature model. Moreover, these expressions recover the results of [39; 94]. We leave the extensions of this analysis to deep nonlinear random features with structured weights to future work.

D. An Interesting Equivalence

We have seen that we can safely replace $N \text{df}_{\mathbf{F}^\top \Sigma \mathbf{F} + \sigma_\xi^2}(\kappa_1)$ with $D \overline{\text{df}}_1(\kappa_2)$. Moreover, similar to Equation (146), we can interpret $D \overline{\text{df}}_1 = \text{Tr}[\tilde{\Sigma}(\tilde{\Sigma} + \kappa_2)]$. Here $\tilde{\Sigma}$ is a covariance matrix having the same spectrum as Σ with an additional \tilde{N} eigenvalues with value $\tilde{\sigma}_\xi^2 \equiv \sigma_\xi^2 / \tilde{N}$ and $\tilde{N} \rightarrow \infty$. Then, $\tilde{\sigma}_\xi^2 (\tilde{\sigma}_\xi^2 + \kappa_2)^{-1} \rightarrow \tilde{\sigma}_\xi^2 / \kappa_2$. Since there are \tilde{N} of them, the total contribution will yield σ_ξ^2 / κ_2 . These eigenvalues will always remain below the level of resolution given by κ_2 and thus be un-learnable. Thus, when they are passed through the linear random feature matrix, they act as additive feature noise. This is analogous to how the higher-order unlearned modes in Section V.G act as effective noise.

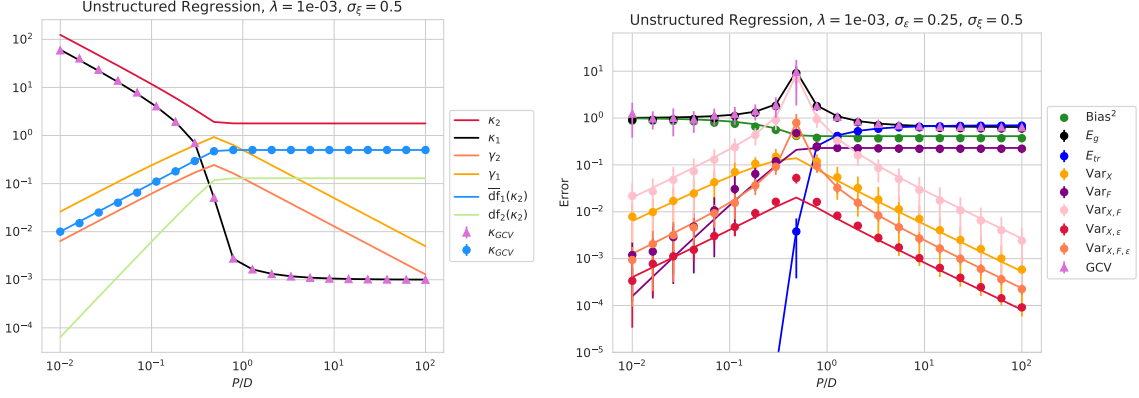


FIG. 15 1-layer nonlinear linear random features with unstructured covariates, i.e. $\Sigma = \mathbf{I}$. Left: We plot theory (solid lines) for the various quantities of interest: $\kappa_1, \kappa_2, \gamma_1, \gamma_2$ as well as $\bar{df}_1(\kappa_2), df_2(\kappa_2)$. We also plot the estimate of κ_1 using the training set and find excellent agreement. Right: We plot the training and generalization (blue, black respectively) as well as the bias (green) and variances (orange, purple, pink, red, coral) due to all relevant quantities in the regression. Dots and error bars indicate empirical simulations over 40 seeds over training set and 40 seeds over random feature initializations. Solid curves show theory. We see strong agreement for all relevant quantities. The GCV estimator is plotted as orchid triangles and again we find excellent agreement with the generalization error.

E. Example: Nonlinear Random Features with Isotropic Covariates

Specializing to the case where $\Sigma = \mathbf{I}$ we can obtain the results for the random feature model studied in [26; 40]:

$$\kappa_2 = \frac{\lambda}{\left(\frac{N}{D} - \bar{df}_1\right)\left(1 - \frac{D}{P}\bar{df}_1\right)}, \quad \bar{df}_1 = \frac{1}{1 + \kappa_2} + \frac{\sigma_\xi^2}{\kappa_2}. \quad (281)$$

One can solve these equations self-consistently for κ_2 . In the ridgeless limit, this gives:

$$\kappa_2 = \frac{1 + \sigma_\xi^2 - \psi - \sqrt{(1 + \sigma_\xi^2 - \psi)^2 + 4\psi\sigma_\xi^2}}{2\psi}, \quad (282)$$

where $\psi = \min(P, N)/D$. Using that $tf_1 = df_1 = (1 + \kappa_2)^{-1}$ and $df_2 = (1 + \kappa_2)^{-2}$ we recover the ridgeless expressions in [26; 40]:

- Underparameterized

$$E_g = \frac{1 - \frac{N}{D} - \sigma_\xi^2 + \sqrt{\left(1 - \frac{N}{D} + \sigma_\xi^2\right)^2 + 4\frac{N}{D}\sigma_\xi^2}}{2(1 - N/P)} + \sigma_\epsilon^2 \frac{N/P}{1 - N/P}. \quad (283)$$

- Overparameterized

$$E_g = \frac{1 - \frac{P}{D} - \sigma_\xi^2 + \sqrt{\left(1 - \frac{P}{D} + \sigma_\xi^2\right)^2 + 4\frac{P}{D}\sigma_\xi^2}}{2(1 - P/N)} + (\sigma_\epsilon^2 - \sigma_\xi^2) \left[\frac{1 + \frac{P}{D} + \sigma_\xi^2 - \sqrt{\left(1 - \frac{P}{D} + \sigma_\xi^2\right)^2 + 4\frac{P}{D}\sigma_\xi^2}}{2\sqrt{\left(1 - \frac{P}{D} + \sigma_\xi^2\right)^2 + 4\frac{P}{D}\sigma_\xi^2}} \right] + \sigma_\epsilon^2 \frac{P/N}{1 - P/N}. \quad (284)$$

We illustrate these solutions in Figure 15.

F. Fine-Grained Bias-Variance Decomposition

We conclude with a fine-grained bias-variance decomposition of nonlinear random feature models in the case of isotropic features and feature noise, and structured input data. This extends work by Adlam & Pennington [40], who

derived this decomposition for isotropic input data. Again, using the technology we've developed so far, these can be derived in a few lines of algebra, and straightforwardly interpreted.

Averaging over the dataset involves an average over both \mathbf{X} and Ξ . This is the same as averaging $\overline{\mathbf{X}}$ in the linear random feature description. Thus, the equations of the prior section apply. For a test point prediction, one has

$$\begin{aligned}\mathbb{E}_{\overline{\mathbf{X}}, \overline{\mathbf{F}}, \xi} \hat{y} &= \mathbb{E}_{\overline{\mathbf{X}}, \overline{\mathbf{F}}, \xi} (\mathbf{x}^\top \mathbf{F} + \xi^\top) \hat{\mathbf{v}} = \mathbb{E}_{\overline{\mathbf{X}}, \overline{\mathbf{F}}} \mathbf{x}^\top \mathbf{F} \hat{\mathbf{v}} \\ &= \mathbb{E}_{\overline{\mathbf{X}}, \overline{\mathbf{F}}} \mathbf{x}^\top \mathbf{F} (\overline{\mathbf{F}}^\top \overline{\mathbf{X}}^\top \overline{\mathbf{X}} \overline{\mathbf{F}} + \lambda \mathbf{I})^{-1} \overline{\mathbf{F}}^\top \overline{\mathbf{X}}^\top (\mathbf{X} \mathbf{w} + \epsilon) \\ &= \mathbb{E}_{\overline{\mathbf{F}}} \mathbf{x}^\top \mathbf{F} (\mathbf{F}^\top \Sigma \mathbf{F} + \sigma_\xi^2 \mathbf{I} + \kappa_1 \mathbf{I})^{-1} \mathbf{F}^\top \Sigma \bar{\mathbf{w}} \\ &= \mathbf{x}^\top (\Sigma + \kappa_2 \mathbf{I})^{-1} \Sigma \bar{\mathbf{w}}.\end{aligned}\tag{285}$$

This gives us as before:

$$\text{Bias}^2 = -\kappa_2^2 \text{tf}'_1(\kappa_2).\tag{286}$$

Similarly, one can average over just the data. This is an average over both \mathbf{X} and Ξ as Ξ carries a data index. This gives

$$\begin{aligned}\mathbb{E}_{\mathbf{X}, \Xi} \hat{y} &= \mathbb{E}_{\mathbf{X}, \Xi} (\mathbf{x}^\top \mathbf{F} + \xi^\top) \hat{\mathbf{v}} \\ &= \mathbb{E}_{\overline{\mathbf{X}}} \bar{\mathbf{x}}^\top \overline{\mathbf{F}} (\overline{\mathbf{F}}^\top \overline{\mathbf{X}}^\top \overline{\mathbf{X}} \overline{\mathbf{F}} + \lambda \mathbf{I})^{-1} \overline{\mathbf{F}}^\top \overline{\mathbf{X}}^\top (\overline{\mathbf{X}} \bar{\mathbf{w}}_{D+N} + \epsilon) \\ &= \bar{\mathbf{x}}^\top \overline{\mathbf{F}} \overline{\mathbf{F}}^\top (\overline{\mathbf{F}} \overline{\mathbf{F}}^\top + \kappa_1 \mathbf{I})^{-1} \bar{\mathbf{w}}_{D+N}.\end{aligned}\tag{287}$$

We note that the noise drops out as before, so $\text{Var}_{\mathbf{F}, \epsilon} = 0$. We thus get:

$$\begin{aligned}\text{Bias}^2 + \text{Var}_{\mathbf{X}} &= \kappa_1^2 \bar{\mathbf{w}}_{D+N}^\top (\overline{\mathbf{F}} \overline{\mathbf{F}}^\top + \kappa_1 \mathbf{I})^{-2} \bar{\mathbf{w}}_{D+N} \\ &= -\kappa_1^2 \partial_{\kappa_1} \left[\frac{\kappa_1 + \sigma_\xi^2}{\kappa_1} \bar{\mathbf{w}}^\top \Sigma^{1/2} (\mathbf{F}^\top \Sigma \mathbf{F} + \kappa_1 \mathbf{I} + \sigma_\xi^2 \mathbf{I})^{-1} \Sigma^{1/2} \bar{\mathbf{w}} \right] \\ &= -\kappa_1^2 \partial_{\kappa_1} \left[\frac{\kappa_2}{\kappa_1} \text{tf}_1(\kappa_2) \right].\end{aligned}\tag{288}$$

This is as before and thus yields:

$$\text{Var}_{\mathbf{F}} = \left(1 - \frac{d \log \kappa_2}{d \log \kappa_1} \right) \kappa_2 \text{tf}_2(\kappa_2).\tag{289}$$

Averaging over features is more subtle, since both the \mathbf{F} and Ξ matrices are averaged over. It is better to write:

$$\overline{\mathbf{X}} = \begin{pmatrix} \mathbf{X} & \Sigma^{1/2} \end{pmatrix}, \quad \overline{\mathbf{F}} = \begin{pmatrix} \mathbf{F} \\ \mathbf{Z} \end{pmatrix} \sim \mathcal{N}(0, \mathbf{I}_{N+P}).\tag{290}$$

In this case we still have $\hat{\mathbf{v}} = (\overline{\mathbf{F}}^\top \overline{\mathbf{X}}^\top \overline{\mathbf{X}} \overline{\mathbf{F}} + \lambda \mathbf{I})^{-1} \overline{\mathbf{F}}^\top \overline{\mathbf{X}}^\top \mathbf{X} \mathbf{w}$. One can then evaluate the feature-averaged test set prediction as follows:

$$\begin{aligned}\mathbb{E}_{\overline{\mathbf{F}}, \xi} \hat{y} &= \mathbb{E}_{\overline{\mathbf{F}}, \xi} [\mathbf{x}^\top \mathbf{F} + \xi^\top] \hat{\mathbf{v}} = \mathbb{E}_{\overline{\mathbf{F}}} \mathbf{x}^\top \mathbf{F} \hat{\mathbf{v}} \\ &= \mathbb{E}_{\overline{\mathbf{F}}} \Pi_D \overline{\mathbf{F}} (\overline{\mathbf{F}}^\top \overline{\mathbf{X}}^\top \overline{\mathbf{X}} \overline{\mathbf{F}} + \lambda \mathbf{I})^{-1} \overline{\mathbf{F}}^\top \overline{\mathbf{X}}^\top (\mathbf{X} \bar{\mathbf{w}} + \epsilon) \\ &= \Pi_D (\overline{\mathbf{X}}^\top \overline{\mathbf{X}} + \kappa_{\mathbf{F}} \mathbf{I})^{-1} \overline{\mathbf{X}}^\top (\mathbf{X} \bar{\mathbf{w}} + \epsilon), \quad \kappa_{\mathbf{F}} = \lambda S_{\mathbf{F} \mathbf{F}^\top} \\ &= (\mathbf{X}^\top \mathbf{X} + \sigma_\xi^2 \mathbf{I} + \kappa_{\mathbf{F}} \mathbf{I})^{-1} \mathbf{X}^\top (\mathbf{X} \bar{\mathbf{w}} + \epsilon).\end{aligned}\tag{291}$$

Here, in the second line we have written $\mathbf{F} = \Pi_D \overline{\mathbf{F}}$ as the projection onto the first D components of $\overline{\mathbf{F}}$. This is again just ridge regression without random features and with ridge parameter $\kappa_{\mathbf{F}} + \sigma_\xi^2$. As before, after averaging over \mathbf{X} this ridge will get renormalized to κ_2 . We thus get:

$$\text{Var}_{\mathbf{X}} = \frac{\gamma_2}{1 - \gamma_2} [-\kappa_2^2 \text{tf}'_1], \quad \text{Var}_{\mathbf{X}, \epsilon} = \frac{\gamma_2}{1 - \gamma_2} \sigma_\epsilon^2.\tag{292}$$

This consequently gives:

$$\text{Var}_{\mathbf{X}, \epsilon} = \left[\frac{\gamma_1}{1 - \gamma_1} - \frac{\gamma_2}{1 - \gamma_2} \right] \sigma_\epsilon^2.\tag{293}$$

We thus recover the exact same form of the decomposition as in the linear random feature model setting. See Figure 11 for a schematic illustration.

G. Scaling Laws in P and N

As in prior scaling law subsections, we consider Σ to have eigenvalues decaying as $\eta_k \sim k^{-\alpha}$, with α the capacity exponent. We consider the scaling of κ_2 as a function of P, N in the ridgeless limit $\lambda \rightarrow 0$. Because

$$\kappa_2 = \frac{\lambda}{\left(\frac{N}{D} - \overline{\text{df}}_1\right)\left(\frac{P}{D} - \overline{\text{df}}_1\right)}, \quad (294)$$

we must have that $\overline{\text{df}}_1 \rightarrow \frac{\min(P, N)}{D}$. This implies

$$\frac{\min(P, N)}{D} = \text{df}_{\Sigma}(\kappa_2) + \frac{\sigma_{\xi}^2}{\kappa_2}. \quad (295)$$

If σ_{ξ}^2 is negligible, we have that $\overline{\text{df}}_1 \approx \text{df}_{\Sigma}^1$, giving $\kappa_2 \sim \min(P, N)^{-\alpha}$ as in Section VI.I.5. Then, all of the results of that Section apply. On the other hand, if the second term dominates, then $\kappa_2 \sim \frac{D}{\min(P, N)} \sigma_{\xi}^2$. Schematically, the transition from one behavior to the other will occur when:

$$\frac{\sigma_{\xi}^2}{\kappa_2} \sim \frac{\min(P, N)}{D} \Rightarrow \min(P, N) \gg (\sigma_{\xi}^2 D)^{-1/(\alpha-1)}. \quad (296)$$

One can consider scaling σ_{ξ} with D so that $\tilde{\sigma}_{\xi}^2 \equiv \sigma_{\xi}^2 D$ is a constant. Under this scaling, when condition (296) is met, we get that $\kappa_2 \sim \min(P, N)^{-1} \tilde{\sigma}_{\xi}^2$.

This then gives the following scalings in the underparameterized regime $N < P$:

$$E_g \sim \begin{cases} \frac{(N/\tilde{\sigma}_{\xi}^2)^{-2\min(r, 1/2)}}{1 - N/P}, & (N/\tilde{\sigma}_{\xi}^2)^{-2\min(r, 1/2)} \gg \sigma_{\epsilon}^2 (N/\tilde{\sigma}_{\xi}^2)^{1/\alpha} / P \quad \boldsymbol{\xi} \text{ dominated} \\ \sigma_{\epsilon}^2 (N/\tilde{\sigma}_{\xi}^2)^{1/\alpha} / P & (N/\tilde{\sigma}_{\xi}^2)^{-2\min(r, 1/2)} \ll \sigma_{\epsilon}^2 (N/\tilde{\sigma}_{\xi}^2)^{1/\alpha} / P \quad \text{Noise } \boldsymbol{\xi}\text{-mitigated} \end{cases} \quad (297)$$

Similarly, in the overparameterized $P > N$ regime we have:

$$E_g \sim \begin{cases} \left(\frac{P}{\tilde{\sigma}_{\xi}^2}\right)^{-2\min(r, 1)}, & P \ll P_{\epsilon}; r \leq 1/2 \text{ or } P \ll P_{\mathbf{F}} \quad \boldsymbol{\xi} \text{ dominated} \\ P^0 / (N\tilde{\sigma}_{\xi}^2), & P \ll P_{\epsilon}; r > 1/2; P \gg P_{\mathbf{F}} \quad \text{Joint } \boldsymbol{\xi}, \text{Var}_{\mathbf{F}} \text{ dominated} \\ \sigma_{\epsilon}^2 \left(\frac{P}{\tilde{\sigma}_{\xi}^2}\right)^{-\frac{\alpha-1}{\alpha}}, & P \gg P_{\epsilon} \quad \text{Noise } \boldsymbol{\xi}\text{-mitigated} \end{cases} \quad (298)$$

We demonstrate examples of these scalings in Figure 16.

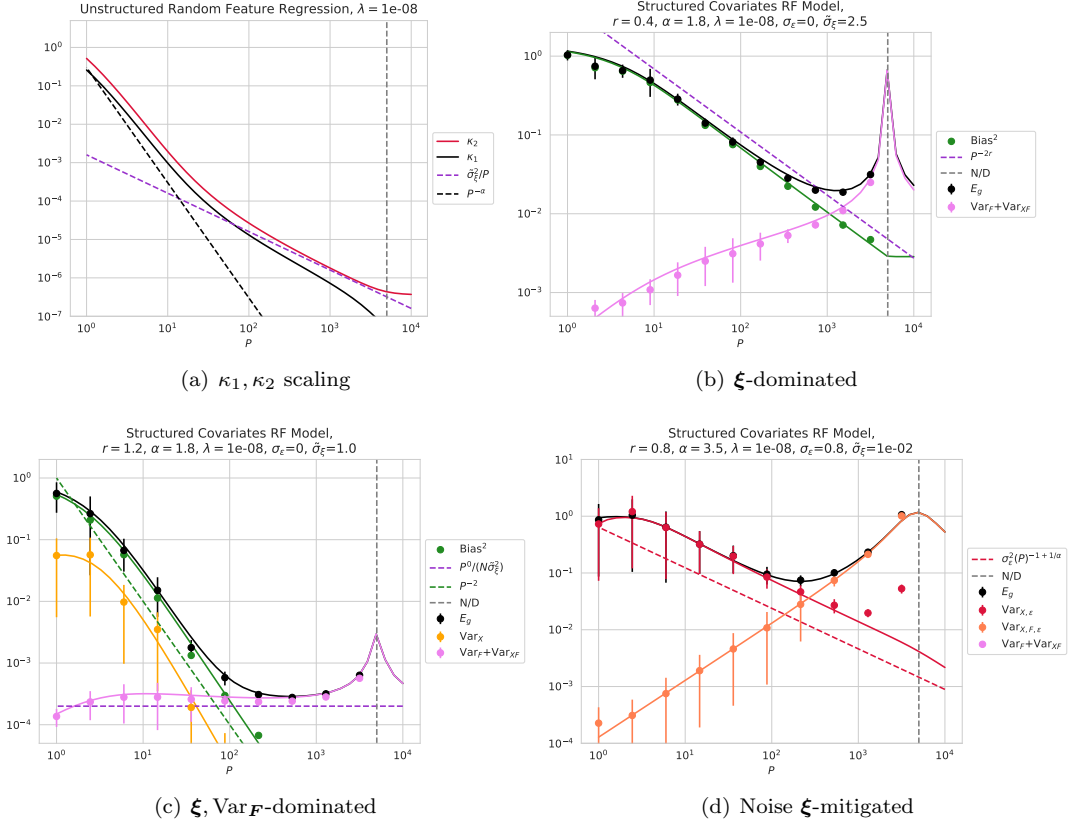


FIG. 16 a) The transition between $\kappa_2 \sim P^{-\alpha}$ and $\kappa_2 \sim \tilde{\sigma}_\xi^2/P$ in the overparameterized regime. b) Illustration of ξ -dominated scaling. The dashed purple line is the power law exponent prediction. c) The transition from ξ -dominated to joint $\xi, \text{Var}_{\mathbf{F}}$ -dominated scaling when $r > 1/2$. We see a plateau, with an estimate given by the dashed purple line from scaling arguments. This is identical to the plateau studied in the model in [82]. d) The feature noise ξ can act as an effective ridge $\lambda \sim 1/P$ and thus mitigate the effect of noise. This gives a nontrivial scaling with P in the presence of noise rather than a plateau. However, in the absence of explicit ridge, there is also a subsequent double descent peak. Our fine-grained bias-variance decomposition shows that this is due explicitly to the joint variance, $\text{Var}_{\mathbf{X}\mathbf{F}\epsilon}$. Near the double descent peak the empirics are less numerically stable, leading to slight deviation from theory curves. In all cases we take a width $N = 5000$ random feature model and bag over 25 datasets and ensemble over 25 initializations.

VIII. CONCLUSION

By using S -transform subordination relations, we have given compact derivations for the generalization error, training error, and fine-grained bias-variance decomposition across a variety of high-dimensional regression models. These include linear regression, kernel methods, linear random feature models, and nonlinear random feature models. We also studied the scaling properties of these models in the setting where the input covariates and target weights had power law structure. We derived novel formulas for the generalization error of a very generic class of random feature models and for all the sources of variance in that setting. Using these formulas, we are able to interpret a novel scaling regime found in overparameterized random feature models as due to the limiting behavior of parameter variance. We characterized all scaling regimes for power-law structured random feature models. We extended this analysis to shallow nonlinear random feature models with structured input data.

The multiplicative property of the S -transform makes it a particularly powerful tool for analyzing the structure of covariances given by passing data through layers of features. It allows for most formulae in the random features literature to be succinctly derived. Beyond the proportional regime, or in a feature-learning regime where features in all layers become correlated with themselves and with the data, the free probability assumptions necessary to apply the S transform likely break down. It will be interesting to investigate to what extent methods in random matrix theory and free probability can still be adapted to this setting, and what additional technology will need to be developed to study scaling laws in the feature learning regime.

ACKNOWLEDGMENTS

We thank Blake Bordelon, Hamza Chaudhry, and Paul Masset for inspiring conversations. We also thank Blake Bordelon, Benjamin Ruben, and Sabarish Sainathan for helpful comments on earlier versions of this manuscript. ABA is grateful to Bruno Loureiro, Alex Maloney, and Jamie Simon for helpful discussions on random matrices, deterministic equivalence, and diagrammatics at the Aspen Center for Theoretical Physics Winter Program on Theoretical Physics for Machine Learning. ABA also thanks Nina Anikeeva for useful discussions on bias-variance decompositions.

ABA is supported by the Professor Yaser S. Abu-Mostafa Fellowship from the Fannie and John Hertz Foundation. JAZV and CP were supported by NSF Award DMS-2134157 and NSF CAREER Award IIS-2239780. CP is further supported by a Sloan Research Fellowship. This work has been made possible in part by a gift from the Chan Zuckerberg Initiative Foundation to establish the Kempner Institute for the Study of Natural and Artificial Intelligence. This research was supported in part by grants NSF PHY-1748958 and PHY-2309135 to the Kavli Institute for Theoretical Physics (KITP), through the authors' participation in the Fall 2023 program "Deep Learning from the Perspective of Physics and Neuroscience."

REFERENCES

- [1] J. Hestness, S. Narang, N. Ardalani, G. Diamos, H. Jun, H. Kianinejad, M. M. A. Patwary, Y. Yang, and Y. Zhou, arXiv preprint arXiv:1712.00409 (2017).
- [2] J. Kaplan, S. McCandlish, T. Henighan, T. B. Brown, B. Chess, R. Child, S. Gray, A. Radford, J. Wu, and D. Amodei, arXiv preprint arXiv:2001.08361 (2020).
- [3] G. Bachmann, S. Anagnostidis, and T. Hofmann, *Advances in Neural Information Processing Systems* **36** (2024).
- [4] J. Hoffmann, S. Borgeaud, A. Mensch, E. Buchatskaya, T. Cai, E. Rutherford, D. d. L. Casas, L. A. Hendricks, J. Welbl, A. Clark, *et al.*, arXiv preprint arXiv:2203.15556 (2022).
- [5] B. Widom, *The Journal of Chemical Physics* **43**, 3898 (1965).
- [6] L. P. Kadanoff, *Physics Physique Fizika* **2**, 263 (1966).
- [7] L. P. Kadanoff, W. Götze, D. Hamblen, R. Hecht, E. Lewis, V. V. Palciauskas, M. Rayl, J. Swift, D. Aspnes, and J. Kane, *Reviews of Modern Physics* **39**, 395 (1967).
- [8] K. G. Wilson, *Physical review B* **4**, 3174 (1971).
- [9] K. G. Wilson, *Physical Review B* **4**, 3184 (1971).
- [10] K. G. Wilson and J. Kogut, *Physics reports* **12**, 75 (1974).
- [11] J. Cardy, *Scaling and renormalization in statistical physics*, Vol. 5 (Cambridge university press, 1996).
- [12] A. Krogh and J. A. Hertz, *Journal of Physics A: Mathematical and General* **25**, 1135 (1992).
- [13] L. H. Dicker, *Bernoulli* **22**, 1 (2016).
- [14] E. Dobriban and S. Wager, *The Annals of Statistics* **46**, 247 (2018).
- [15] P. Nakkiran, arXiv preprint arXiv:1912.07242 (2019).
- [16] M. S. Advani, A. M. Saxe, and H. Sompolinsky, *Neural Networks* **132**, 428 (2020).
- [17] T. Hastie, A. Montanari, S. Rosset, and R. J. Tibshirani, *The Annals of Statistics* **50**, 949 (2022).
- [18] P. Sollich, *Advances in neural information processing systems* **11** (1998).
- [19] P. Sollich and A. Hales, *Neural computation* **14**, 1393 (2002).
- [20] B. Bordelon, A. Canatar, and C. Pehlevan, in *International Conference on Machine Learning* (PMLR, 2020) pp. 1024–1034.
- [21] A. Canatar, B. Bordelon, and C. Pehlevan, *Nature communications* **12**, 2914 (2021).
- [22] S. Spigler, M. Geiger, and M. Wyart, *Journal of Statistical Mechanics: Theory and Experiment* **2020**, 124001 (2020).
- [23] J. B. Simon, M. Dickens, D. Karkada, and M. Dewese, *Transactions on Machine Learning Research* (2023).
- [24] B. Loureiro, C. Gerbelot, H. Cui, S. Goldt, F. Krzakala, M. Mezard, and L. Zdeborová, *Advances in Neural Information Processing Systems* **34**, 18137 (2021).
- [25] C. Louart, Z. Liao, and R. Couillet, *The Annals of Applied Probability* **28**, 1190 (2018).
- [26] S. Mei and A. Montanari, *Communications on Pure and Applied Mathematics* **75**, 667 (2022).
- [27] B. Adlam and J. Pennington, in *International Conference on Machine Learning* (PMLR, 2020) pp. 74–84.
- [28] S. d’Ascoli, M. Refinetti, G. Biroli, and F. Krzakala, in *International Conference on Machine Learning* (PMLR, 2020) pp. 2280–2290.
- [29] S. d’Ascoli, L. Sagun, and G. Biroli, *Advances in Neural Information Processing Systems* **33**, 3058 (2020).
- [30] Y. Bahri, E. Dyer, J. Kaplan, J. Lee, and U. Sharma, arXiv preprint arXiv:2102.06701 (2021).
- [31] J. A. Zavatone-Veth and C. Pehlevan, in *Advances in Neural Information Processing Systems* (2023).
- [32] O. Dhifallah and Y. M. Lu, arXiv preprint arXiv:2008.11904 (2020).
- [33] H. Hu and Y. M. Lu, *IEEE Transactions on Information Theory* **69**, 1932 (2022).
- [34] A. Maloney, D. A. Roberts, and J. Sully, arXiv preprint arXiv:2210.16859 (2022).
- [35] F. Bach, *SIAM Journal on Mathematics of Data Science* **6**, 26 (2024).
- [36] D. V. Voiculescu, K. J. Dykema, and A. Nica, *Free random variables* (American Mathematical Society, 1992).
- [37] M. Belkin, D. Hsu, S. Ma, and S. Mandal, *Proceedings of the National Academy of Sciences* **116**, 15849 (2019).
- [38] P. Nakkiran, G. Kaplun, Y. Bansal, T. Yang, B. Barak, and I. Sutskever, *Journal of Statistical Mechanics: Theory and Experiment* **2021**, 124003 (2021).
- [39] A. Atanasov, B. Bordelon, S. Sainathan, and C. Pehlevan, in *The Eleventh International Conference on Learning Representations* (2022).
- [40] B. Adlam and J. Pennington, *Advances in neural information processing systems* **33**, 11022 (2020).
- [41] U. Anwar, A. Saparov, J. Rando, D. Paleka, M. Turpin, P. Hase, E. S. Lubana, E. Jenner, S. Casper, O. Sourbut, *et al.*, arXiv preprint arXiv:2404.09932 (2024).
- [42] J. S. Rosenfeld, A. Rosenfeld, Y. Belinkov, and N. Shavit, in *International Conference on Learning Representations* (2019).
- [43] S. Ahmad and G. Tesauro, *Advances in neural information processing systems* **1** (1988).
- [44] T. Besiroglu, E. Erdil, M. Barnett, and J. You, arXiv preprint arXiv:2404.10102 (2024).
- [45] B. Ghorbani, O. Firat, M. Freitag, A. Bapna, M. Krikun, X. Garcia, C. Chelba, and C. Cherry, arXiv preprint arXiv:2109.07740 (2021).
- [46] D. Hernandez, J. Kaplan, T. Henighan, and S. McCandlish, arXiv preprint arXiv:2102.01293 (2021).
- [47] D. Hernandez, T. Brown, T. Conerly, N. DasSarma, D. Drain, S. El-Showk, N. Elhage, Z. Hatfield-Dodds, T. Henighan, T. Hume, *et al.*, arXiv preprint arXiv:2205.10487 (2022).
- [48] M. A. Gordon, K. Duh, and J. Kaplan, in *Proceedings of the 2021 Conference on Empirical Methods in Natural Language Processing* (2021) pp. 5915–5922.
- [49] N. Muennighoff, A. Rush, B. Barak, T. Le Scao, N. Tazi, A. Piktus, S. Pyysalo, T. Wolf, and C. A. Raffel, *Advances in*

- Neural Information Processing Systems **36** (2024).
- [50] X. Zhai, A. Kolesnikov, N. Houlsby, and L. Beyer, in *Proceedings of the IEEE/CVF conference on computer vision and pattern recognition* (2022) pp. 12104–12113.
- [51] I. M. Alabdulmohsin, X. Zhai, A. Kolesnikov, and L. Beyer, *Advances in Neural Information Processing Systems* **36** (2024).
- [52] E. Caballero, K. Gupta, I. Rish, and D. Krueger, in *The Eleventh International Conference on Learning Representations* (2022).
- [53] M. Hutter, arXiv preprint arXiv:2102.04074 (2021).
- [54] U. Sharma and J. Kaplan, *Journal of Machine Learning Research* **23**, 1 (2022).
- [55] E. Michaud, Z. Liu, U. Girit, and M. Tegmark, *Advances in Neural Information Processing Systems* **36** (2024).
- [56] S. Arora and A. Goyal, arXiv preprint arXiv:2307.15936 (2023).
- [57] R. Dietrich, M. Oppen, and H. Sompolinsky, *Physical review letters* **82**, 2975 (1999).
- [58] S. Mei, T. Misiakiewicz, and A. Montanari, *Applied and Computational Harmonic Analysis* **59**, 3 (2022), special Issue on Harmonic Analysis and Machine Learning.
- [59] L. Xiao, H. Hu, T. Misiakiewicz, Y. Lu, and J. Pennington, in *Advances in Neural Information Processing Systems*, Vol. 35, edited by S. Koyejo, S. Mohamed, A. Agarwal, D. Belgrave, K. Cho, and A. Oh (Curran Associates, Inc., 2022) pp. 4558–4570.
- [60] T. Misiakiewicz, arXiv (2022), arXiv:2204.10425 [math.ST].
- [61] H. Hu and Y. M. Lu, arXiv (2022), arXiv:2205.06798 [cs.LG].
- [62] S. Dubova, Y. M. Lu, B. McKenna, and H.-T. Yau, arXiv (2023), arXiv:2310.18280 [math.PR].
- [63] H. Cui, B. Loureiro, F. Krzakala, and L. Zdeborová, *Advances in Neural Information Processing Systems* **34**, 10131 (2021).
- [64] J. Pennington and P. Worah, *Advances in neural information processing systems* **30** (2017).
- [65] Y. Dandi, L. Stephan, F. Krzakala, B. Loureiro, and L. Zdeborová, in *Advances in Neural Information Processing Systems*, Vol. 36, edited by A. Oh, T. Neumann, A. Globerson, K. Saenko, M. Hardt, and S. Levine (Curran Associates, Inc., 2023) pp. 54754–54768.
- [66] L. Pesce, F. Krzakala, B. Loureiro, and L. Stephan, in *Proceedings of the 40th International Conference on Machine Learning*, Proceedings of Machine Learning Research, Vol. 202, edited by A. Krause, E. Brunskill, K. Cho, B. Engelhardt, S. Sabato, and J. Scarlett (PMLR, 2023) pp. 27680–27708.
- [67] A. Montanari and B. N. Saeed, in *Proceedings of Thirty Fifth Conference on Learning Theory*, Proceedings of Machine Learning Research, Vol. 178, edited by P.-L. Loh and M. Raginsky (PMLR, 2022) pp. 4310–4312.
- [68] D. Schröder, H. Cui, D. Dmitriev, and B. Loureiro, arXiv preprint arXiv:2302.00401 (2023).
- [69] D. Schröder, D. Dmitriev, H. Cui, and B. Loureiro, arXiv preprint arXiv:2402.13999 (2024).
- [70] B. Bordelon and C. Pehlevan, arXiv preprint arXiv:2106.02713 (2021).
- [71] B. Bordelon, A. Atanasov, and C. Pehlevan, arXiv preprint arXiv:2402.01092 (2024).
- [72] A. Jacot, B. Simsek, F. Spadaro, C. Hongler, and F. Gabriel, *Advances in neural information processing systems* **33**, 15568 (2020).
- [73] J. Lee, L. Xiao, S. Schoenholz, Y. Bahri, R. Novak, J. Sohl-Dickstein, and J. Pennington, *Advances in neural information processing systems* **32** (2019).
- [74] T. Misiakiewicz and A. Montanari, arXiv preprint arXiv:2308.13431 (2023).
- [75] B. Schölkopf and A. J. Smola, *Learning with kernels: support vector machines, regularization, optimization, and beyond* (MIT press, 2002).
- [76] C. K. Williams and C. E. Rasmussen, *Gaussian processes for machine learning* (MIT press Cambridge, MA, 2006).
- [77] L. Chizat, E. Oyallon, and F. Bach, *Advances in neural information processing systems* **32** (2019).
- [78] C. Liu, L. Zhu, and M. Belkin, arXiv (2021), arXiv:2010.01092 [cs.LG].
- [79] B. Ghorbani, S. Mei, T. Misiakiewicz, and A. Montanari, *The Annals of Statistics* **49** (2021).
- [80] M. Belkin, S. Ma, and S. Mandal, in *Proceedings of the 35th International Conference on Machine Learning*, Proceedings of Machine Learning Research, Vol. 80, edited by J. Dy and A. Krause (PMLR, 2018) pp. 541–549.
- [81] S. Fort, G. K. Dziugaite, M. Paul, S. Kharaghani, D. M. Roy, and S. Ganguli, *Advances in Neural Information Processing Systems* **33**, 5850 (2020).
- [82] A. Atanasov, B. Bordelon, and C. Pehlevan, in *International Conference on Learning Representations* (2021).
- [83] M. Geiger, A. Jacot, S. Spigler, F. Gabriel, L. Sagun, S. d’Ascoli, G. Biroli, C. Hongler, and M. Wyart, *Journal of Statistical Mechanics: Theory and Experiment* **2020**, 023401 (2020).
- [84] E. Dyer and G. Gur-Ari, arXiv preprint arXiv:1909.11304 (2019).
- [85] D. A. Roberts, S. Yaida, and B. Hanin, *The principles of deep learning theory*, Vol. 46 (Cambridge University Press Cambridge, MA, USA, 2022).
- [86] B. Bordelon and C. Pehlevan, in *Advances in Neural Information Processing Systems*, Vol. 36, edited by A. Oh, T. Neumann, A. Globerson, K. Saenko, M. Hardt, and S. Levine (Curran Associates, Inc., 2023) pp. 9707–9750.
- [87] K. Aitken and G. Gur-Ari, arXiv preprint arXiv:2006.06687 (2020), arXiv:2006.06687.
- [88] J. A. Zavatone-Veth, W. L. Tong, and C. Pehlevan, *Physical Review E* **105**, 064118 (2022).
- [89] J. A. Zavatone-Veth, A. Canatar, B. S. Ruben, and C. Pehlevan, *Journal of Statistical Mechanics: Theory and Experiment* **2022**, 114008 (2022).
- [90] H. Cramér, *Mathematical methods of statistics*, Vol. 26 (Princeton university press, 1999).
- [91] L. Fahrmeir and H. Kaufmann, *The Annals of Statistics* **13**, 342 (1985).
- [92] A. Wei, W. Hu, and J. Steinhardt, in *International Conference on Machine Learning* (PMLR, 2022) pp. 23549–23588.

- [93] S. Mei, A. Montanari, and P.-M. Nguyen, Proceedings of the National Academy of Sciences **115**, E7665 (2018).
- [94] G. Mel and J. Pennington, in *International Conference on Learning Representations* (2021).
- [95] G. Mel and S. Ganguli, in *Proceedings of the 38th International Conference on Machine Learning*, Proceedings of Machine Learning Research, Vol. 139, edited by M. Meila and T. Zhang (PMLR, 2021) pp. 7578–7587.
- [96] H. Cui, B. Loureiro, F. Krzakala, and L. Zdeborová, Machine Learning: Science and Technology **4**, 035033 (2023).
- [97] A. Jacot, B. Simsek, F. Spadaro, C. Hongler, and F. Gabriel, in *International Conference on Machine Learning* (PMLR, 2020) pp. 4631–4640.
- [98] G. H. Golub, M. Heath, and G. Wahba, Technometrics **21**, 215 (1979).
- [99] A. Caponnetto and E. D. Vito, “Fast rates for regularized least-squares algorithm,” Tech. Rep. (Massachusetts Institute of Technology Computer Science and Artificial Intelligence Laboratory, 2005).
- [100] A. Caponnetto and E. De Vito, Foundations of Computational Mathematics **7**, 331 (2007).
- [101] D. LeJeune, H. Javadi, and R. Baraniuk, in *International Conference on Artificial Intelligence and Statistics* (PMLR, 2020) pp. 3525–3535.
- [102] T. Yao, D. LeJeune, H. Javadi, R. G. Baraniuk, and G. I. Allen, in *2021 IEEE International Conference on Big Data and Smart Computing (BigComp)* (2021) pp. 65–68.
- [103] P. Patil and D. LeJeune, in *The Twelfth International Conference on Learning Representations* (2024).
- [104] M. Potters and J.-P. Bouchaud, *A First Course in Random Matrix Theory: For Physicists, Engineers and Data Scientists* (Cambridge University Press, 2020).
- [105] T. Hastie, R. Tibshirani, J. H. Friedman, and J. H. Friedman, *The elements of statistical learning: data mining, inference, and prediction*, Vol. 2 (Springer, 2009).
- [106] H. Neudecker and A. Wesselman, *Linear Algebra and its Applications* **127**, 589 (1990).
- [107] T. Tao, *Topics in random matrix theory*, Vol. 132 (American Mathematical Society, 2023).
- [108] Z. Burda, R. Janik, and M. Nowak, Physical Review E **84**, 061125 (2011).
- [109] D. Kobak, J. Lomond, and B. Sanchez, *Journal of Machine Learning Research* **21**, 1 (2020).
- [110] D. Wu and J. Xu, in *Advances in Neural Information Processing Systems*, Vol. 33, edited by H. Larochelle, M. Ranzato, R. Hadsell, M. Balcan, and H. Lin (Curran Associates, Inc., 2020) pp. 10112–10123.
- [111] I. Steinwart, D. R. Hush, C. Scovel, *et al.*, in *COLT* (2009) pp. 79–93.
- [112] D. V. Voiculescu, *Free probability theory*, Vol. 12 (American Mathematical Soc., 1997).
- [113] A. Nica and R. Speicher, *Lectures on the combinatorics of free probability*, Vol. 13 (Cambridge University Press, 2006).
- [114] J. A. Mingo and R. Speicher, *Free probability and random matrices*, Vol. 35 (Springer, 2017).
- [115] J. Bun, R. Allez, J.-P. Bouchaud, and M. Potters, *IEEE Transactions on Information Theory* **62**, 7475 (2016).
- [116] D. Weingarten, *Journal of Mathematical Physics* **19**, 999 (1978).
- [117] P. Brouwer and C. Beenakker, *Journal of Mathematical Physics* **37**, 4904 (1996).
- [118] B. Collins and S. Matsumoto, *Journal of Mathematical Physics* **50** (2009).
- [119] T. Banica, *Letters in Mathematical Physics* **91**, 105 (2010).
- [120] T. Tao and V. Vu, *Modern Aspects of Random Matrix Theory* **72**, 121 (2014).
- [121] V. A. Marchenko and L. A. Pastur, *Matematicheskii Sbornik* **114**, 507 (1967).
- [122] R. R. Muller, *IEEE Transactions on Information Theory* **48**, 2086 (2002).
- [123] J. A. Zavatone-Veth and C. Pehlevan, *SciPost Physics Core* **6**, 026 (2023).
- [124] Z. Burda, A. Jarosz, G. Livan, M. A. Nowak, and A. Swiech, *Physical Review E* **82**, 061114 (2010).
- [125] P. Craven and G. Wahba, *Numerische mathematik* **31**, 377 (1978).
- [126] C. Cheng and A. Montanari, arXiv preprint arXiv:2210.08571 (2022).
- [127] T. Misiakiewicz and B. Saeed, arXiv preprint arXiv:2403.08938 (2024).
- [128] U. M. Tomasini, A. Sclocchi, and M. Wyart, in *International Conference on Machine Learning* (PMLR, 2022) pp. 21548–21583.
- [129] R. A. Horn and C. R. Johnson, *Matrix Analysis* (Cambridge University Press, 2012).
- [130] J. W. Rocks and P. Mehta, *Physical Review E* **106**, 025304 (2022).
- [131] N. Vyas, A. Atanasov, B. Bordelon, D. Morwani, S. Sainathan, and C. Pehlevan, *Advances in Neural Information Processing Systems* **36** (2024).
- [132] F. Guth, B. Ménard, G. Rochette, and S. Mallat, arXiv preprint arXiv:2305.18512 (2023).
- [133] Y. M. Lu and H.-T. Yau, arXiv preprint arXiv:2205.06308 (2022).
- [134] H. Hu, Y. M. Lu, and T. Misiakiewicz, arXiv (2024), arXiv:2403.08160 [stat.ML].